LUND UNIVERSITY

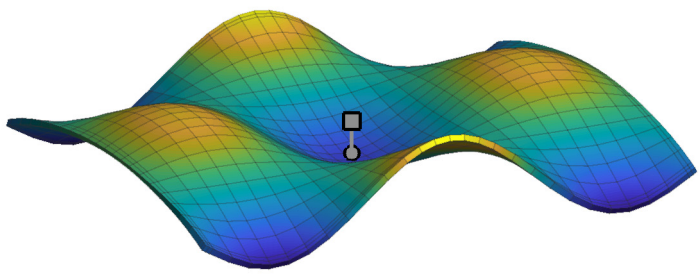

REDUCED ORDER MODELING IN STRUCTURAL DYNAMICS
Consideration of local nonlinearities

LINUS ANDERSSON

Structural Mechanics

Licentiate Dissertation

DEPARTMENT OF CONSTRUCTION SCIENCES
DIVISION OF STRUCTURAL MECHANICS

ISRN LUTVDG/TVSM--21/3082--SE (1-132) | ISSN 0281-6679
ISBN 978-91-7895-909-9 (Print) | 978-91-7895-910-5 (Pdf)
LICENTIATE DISSERTATION

REDUCED ORDER MODELING IN STRUCTURAL DYNAMICS

Consideration of local nonlinearities

LINUS ANDERSSON

Printed by V-husets tryckeri LTH, Lund, Sweden, May 2021 *(Pl)*.

For information, address:
Div. of Structural Mechanics,
Faculty of Engineering LTH, Lund University, Box 118, SE-221 00 Lund, Sweden.
Homepage: www.byggmek.lth.se

Acknowledgements

The work presented in this dissertation was carried out at the Division of Structural Mechanics at the Faculty of Engineering LTH, Lund University.

I would like to express my sincere gratitude towards my main supervisor Prof. Kent Persson and co-supervisors Dr. Peter Persson and Prof. Per-Erik Austrell for their guidance, support and encouragement. Thanks also to Dr. Marcin Kozłowski from Silesian University of Technology for his helpful advice and assistance regarding the experimental studies of soft-body impact tests. Bo Zadig is gratefully acknowledged for his excellent work on many of the illustrations. I would also like to thank the rest of the staff at the Division of Structural Mechanics for providing an inspiring workplace.

I would furthermore like to thank my good friend Jens Malmborg for good company while sharing the office room as well as moral support, valuable advice and encouraging discussions.

Finally, I thank my fiancee Frida and our wonderful children Oskar and Vera for bringing lots of joy to my life and reminding me of what is truly important.

May 2021
Linus Andersson

Abstract

A structural design process may include various load cases for which a sufficient load-bearing capacity must be demonstrated. In addition to static load cases, a verification of dynamic loads, e.g. accidental loads such as blast and impact loading, may be required. To this end, the response may be estimated using a computational model representing an idealized structure. Particularly in the conceptual design phase, a time-efficient and straightforward modeling approach can be of great utility, allowing for an interactive design process where alternative designs may be tested. Furthermore, a dynamic response analysis often requires some form of time (or frequency) discretization and can therefore become computationally expensive compared to the corresponding static analysis. The balance between performance and accuracy as well as the purpose, i.e. the output quantities of interest, are thus important aspects in a dynamic response analysis.

A structural dynamics analysis typically requires a model being accurate as well as computationally efficient. The model accuracy is particularly important in a verification of structures characterized by brittle failure modes, i.e. that do not deform plastically before failure. Furthermore, to avoid a too conservative design and to ensure sufficient accuracy, it can be necessary to consider the nonlinear response of a structure, e.g. due to contact interactions or nonlinear material behavior. However, a nonlinear structural dynamic problem often requires computationally expensive solution methods. Consequently, there is a need for modeling strategies that enable time-efficient, accurate analyses and a straightforward modeling approach, appropriate in a structural design process. To achieve this, a reduced order model can be established providing an accurate prediction of important output quantities.

Dynamic substructuring turns out to be an important aspect in the process of developing reduced order models. By subdivision of the structure into substructures, dynamic substructuring can be employed to effectively adjust the level of accuracy for different parts of the structure. For example, substructures that remain linear elastic can typically be modeled using mode-superposition methods whereas substructures which exhibit a nonlinear behavior can be represented by a refined submodel.

In the dissertation, strategies for reduced order modeling are investigated on the basis of structural engineering applications within two different areas, namely concrete structures subjected to blast loading and glass structures subjected to soft-body impact. Interestingly, however, some of the challenges with regard to the structural dynamics problems are similar. In particular, the response of higher order modes may be of importance and, moreover, an accurate representation of the structural behavior may necessitate a model considering local nonlinearities.

By means of dynamic substructuring, computationally efficient analysis techniques are developed for evaluating concrete structures subjected to blast loading, appropriate for use in a structural design process. In particular, a comparison to commonly used modeling strategies, using equivalent single-degree-of-freedom systems, suggests that the developed models provide an increased accuracy of the shear force. Brittle failure modes such as shear failure are typically critical for concrete structures subjected to blast loading.

Furthermore, reduced order models are established for verification of glass panels subjected to soft-body impact. In particular, a non-linear viscous single-degree-of-freedom system is proposed for reduced modeling of the standardized EN 12600 impactor. Further, the response of higher order modes is considered using a set of load-dependent mode shapes. The developed models are validated by experimental tests of impact on glass panels.

Finally, a review of various reduced order modeling techniques is presented which, in a broader perspective, provide a basis for developing reduced order models in various structural engineering applications.

Contents

Part I

Introduction and Overview

1 Introduction

1.1 BACKGROUND

A structural design process or verification of an existing structure may include various load cases for which a sufficient load-bearing capacity must be demonstrated. The response may then be estimated using a computational model representing an idealized structure. Developing a suitable model by means of modeling abstractions is, thus, an important step in a structural design process—the model should capture the governing structural behavior and provide a sufficiently accurate prediction of important output quantities. Furthermore, particularly in the conceptual design phase, a time-efficient and straightforward modeling approach can be of great utility, allowing for an interactive design process where alternative designs may be tested.

In addition to static load cases, verification of dynamic loads, e.g. accidental loads such as blast and impact loading, may be required. An inherent problem in structural dynamic modeling, however, is the uncertainty related to simplifications and modeling abstractions, which can lead to an overestimation of the response for one load case but an underestimation for another. Therefore, one often seek a "best estimate" model. Hence, to ensure an adequate design and an accurate prediction of the dynamic response the model should be made as simple as possible, but no simpler.

A dynamic response analysis in general requires some form of time (or frequency) discretization and can therefore be expected to be computationally more expensive compared to the corresponding static analysis. The balance between performance and accuracy as well as the purpose, i.e. the output quantities of interest, are thus key aspects in structural dynamic modeling. A detailed analysis, aiming to mimic the response of the real structure, may be useful for analyzing complicated structures and can provide further insight into the structural behavior. In contrast, a simplified, approximate model may be beneficial for analyzing the governing structural behavior or evaluating certain failure modes being known"a priori", e.g. as stated in the applicable design code or based on knowledge acquired from previous analyses of similar structures.

The model accuracy is particularly important in a verification of structures characterized by brittle failure modes, i.e. that do not deform plastically before failure. For example, the re-

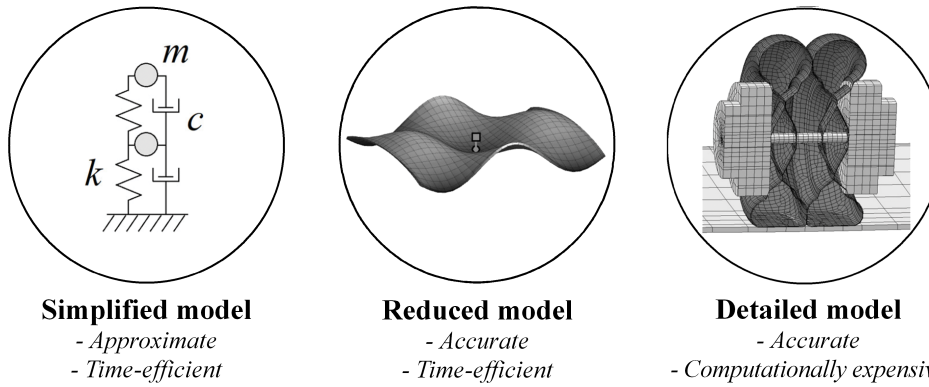

Figure 1.1: Principal differences between various models.

sponse of higher order modes may be of considerable importance. Furthermore, to avoid a too conservative design and to ensure sufficient accuracy, it can be necessary to consider the nonlinear response of a structure, e.g. due to contact interactions or nonlinear material behavior. However, a nonlinear structural dynamic problem often requires computationally expensive solution methods. Hence, there is a need for modeling strategies that enable time-efficient, accurate analyses and a straightforward modeling approach. To this end, a reduced order model may be established, developed to provide an accurate prediction of important output quantities.

The principal idea is illustrated in Figure 1.1. A *simplified model* typically consider the governing structural behavior and provide a rough estimate of the response in a time-efficient manner whereas a *detailed model* provide a "best estimate" representation of the structural behavior of the underlying system. In contrast, using a detailed model as a starting point, a *reduced model* may be formed, providing a sufficiently accurate prediction of important output quantities, while being computationally efficient.

Dynamic substructuring (DS) can be an important aspect in the process of developing reduced order models. By subdivision of the structure into substructures, DS can be employed to effectively adjust the level of accuracy for different parts of the structure. For example, substructures that remain linear elastic can typically be modeled using mode-superposition methods whereas substructures which exhibit a nonlinear behavior can be represented by a refined submodel. An approach being particularly suitable for structures with local nonlinearities.

In the dissertation, strategies for developing reduced order models are investigated on the basis of structural engineering applications within two different areas, namely concrete structures subjected to blast loading and glass structures subjected to soft-body impact. Interestingly, however, some of the challenges with regard to the structural dynamics problems are similar. In particular, the response of higher order modes may be of importance and, moreover, an accurate representation of the structural behavior may necessitate a model considering local nonlinearities.

1.2 AIMS AND OBJECTIVES

The aim of this research is to facilitate a broadened use of interactive structural design processes, where different designs can be tested in a time-efficient and convenient manner. The long-term aim is that methods are available that can be used in accurate and computationally efficient design tools for structural dynamic applications, suitable for such design processes.

The objectives are to develop accurate and computationally efficient modeling strategies appropriate for implementation in such specialized design tools. In particular, various reduced order modeling techniques are evaluated and exemplified on the basis of the aforementioned structural engineering applications. In the broader perspective, a review of the available reduced order modeling methods provide a basis for further investigations. Apart from various numerical studies, the objectives include investigations of experimental methodologies for validating reduced order models employed for analyzing glass structures subjected to soft-body impact.

1.3 LIMITATIONS

In this work, focus is on investigating computationally efficient modeling techniques, appropriate for use in a structural design process. Accordingly, the models are evaluated based on output quantities typically used in a structural verification. However, a detailed investigation with regard to design code requirements, e.g. related to the reinforcement arrangement in concrete structures or allowable stress levels in glass structures, are not within the scope of this dissertation.

On the basis of the aforementioned applications, various reduced order modeling techniques and DS methods are investigated. However, the presented review is by no means exhaustive. In particular, focus is on reduced order modeling techniques in structural dynamics, applied in time domain analyses. Similar methods have been developed in other fields, e.g. system and control, where focus often is on single input–output relations. Here, however, a structural dynamics approach is considered where typically output for the whole structure is of interest.

Numerical models in structural dynamics applications are often established by means of the finite element (FE) method. However, using the methods studied herein, a numerical model is typically the starting point, which is then further modified to obtain a computational efficient reduced model. Therefore, only a brief review of the FE method is presented. Thus, details regarding numerical methods for discretizing continuous systems are not within the scope of this dissertation.

1.4 OUTLINE OF DISSERTATION

This dissertation is divided into two parts:

Part I contains an introduction to reduced order modeling in structural dynamics, dynamic substructuring, and the applications further investigated in the appended papers. Starting with the equations of motion, Chapter 2 introduces various mode-superposition methods. Furthermore, a brief overview of damping models for time domain analyses and dynamic response analysis techniques are presented. In Chapter 3, dynamic substructuring is introduced. In particular, various assembly methods and component mode synthesis methods are discussed. Moreover, a brief overview of interface reduction techniques are presented. In Chapter 4, civil engineering applications using the concepts introduced in Chapter 2 and 3 are discussed. In particular, an overview is presented of reduced order modeling techniques applied to concrete and glass structures subjected to blast and impact loading, respectively.

Part II contains the appended papers. Papers A and B considers concrete structures subjected to blast loading and Paper C considers glass structures subjected to soft-body impact. In Paper A, reduced order models are developed providing an increased response accuracy compared to the simplified models commonly used for design of concrete beams and slabs subjected to blast loading. Paper B presents strategies for analyzing concrete frame structures subjected to blast loading in a computationally efficient manner. In Paper C, reduced order models for verifying glass panels subjected to soft-body impact are presented. In particular, the models are validated using a detailed reference model as well as experimental tests.

2 Reduced order modeling in structural dynamics

A structural dynamics analysis differs from the corresponding static analysis in some important aspects. Firstly, the structure is subjected to a time-varying excitation and, secondly, the accelerations of the structure give rise to inertia forces. Consequently, both the stiffness and mass distribution of the structure affect the structural dynamic behavior. Moreover, the load characteristics, not only the load magnitude, affect the dynamic response.

In a structural verification, the real structure (or design) must be idealized to obtain a suitable analytical model. In general, the analytical model must be discretized in some manner, e.g. by means of the finite element (FE) method or by an assumed-mode approach [1]. In particular, the model should provide a sufficiently accurate response prediction and be computationally efficient, both aspects being particularly important in a structural dynamics problem.

Starting with the equations of motion, this chapter introduces various mode based modeling approaches in structural dynamics. In particular, strategies for reducing the system size by means of subspace projections are investigated. In general, linear elastic systems are considered. In Chapter 3, however, dynamic substructuring is introduced, allowing for a mode based reduced modeling of linear substructures interacting with nonlinear subsystems, expressed in terms of physical displacements.

2.1 EQUATIONS OF MOTION

2.1.1 Single-degree-of-freedom systems

The simplest possible model is a lumped mass system with a massless supporting structure. Such a system can be modeled by a single-degree-of-freedom (SDOF) system having only one system variable, a degree-of-freedom (DOF), representing the movement of the lumped mass. The equation of motion for an SDOF system can be derived from Newton's second law of motion. Hence, the inertia force acting in the opposite direction of the acceleration is

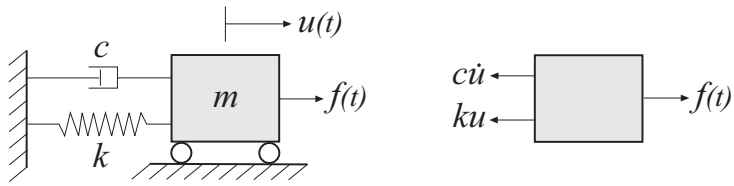

Figure 2.1: Single-degree-of-freedom system.

balanced by the external load and the force imposed by the supporting structure, e.g. expressed as

$$f(t) - f_S(t,u) - f_D(t,\dot{u}) = m\ddot{u}(t) \tag{2.1}$$

where u is the displacement, m is the lumped mass, f is the external force, f_S is the elastic (or inelastic) resisting force and f_D is the damping resisting force (dot notation is used for differentiation with respect to time). If assuming linear elastic behavior and linear viscous damping, Eq. 2.1 can be rewritten to obtain the equation of motion for a linear elastic SDOF system, a second-order differential equation of the form:

$$m\ddot{u}(t) + c\dot{u}(t) + ku(t) = f(t) \tag{2.2}$$

where c is the damping coefficient and k is the linear spring stiffness (see Figure 2.1). Furthermore, in many applications it is convienent to rewrite Eq. 2.2 such that:

$$\ddot{u}(t) + 2\zeta\omega_n\dot{u}(t) + \omega_n^2 u(t) = \frac{f(t)}{m} \tag{2.3}$$

where

$$\omega_n = \sqrt{\frac{k}{m}} \tag{2.4}$$

is the natural frequency, or eigenfrequency, and

$$\zeta = \frac{c}{2m\omega_n} \tag{2.5}$$

is the damping ratio.

Despite its simple form, the SDOF system turns out to be useful in several structural dynamic applications. Apart from a wide range of applications in which the governing structural behavior can be well-represented by an SDOF system it is the basis in response analyses methods based on modal expansion techniques (see further Section 2.2.2).

Furthermore, in some applications, continuous structures may be well-represented by a so-called *generalized* SDOF system. For example, consider a simply supported beam subjected to an external point load, as shown in Figure 2.2a. The vertical displacement at midspan may be considered a degree-of-freedom. A linear spring stiffness representing the load–displacement relation at midspan can readily by derived using standard static load cases found in textbooks

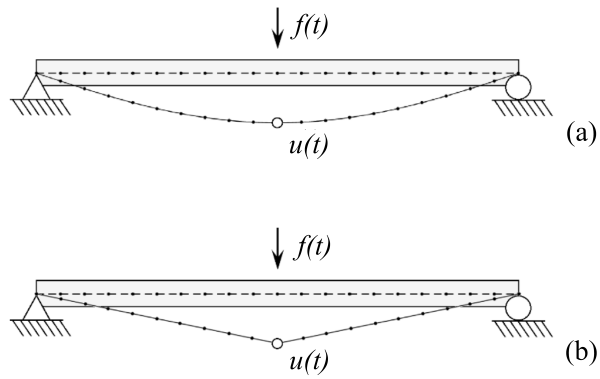

Figure 2.2: Example of approximate, generalized SDOF systems for a elastic (a) and elasto-plastic (b) response. $f(t)$ is the external force and $u(t)$ is the vertical displacement at midspan.

(see e.g. [2]). The mass associated to the vertical displacement may be determined based on the assumed mode shape or, as a rough estimate, say 50% of the beam mass, which is referred to as a lumped mass model. The beam's dynamic response, in terms of the midspan displacement, is thus represented by a generalized SDOF system. More specifically, the SDOF system represents the motion of both the midspan displacement and the amplitude of the mode, corresponding to the static deflection of the external force. It should be emphasized that the mode *shape* is constant whereas the mode amplitude varies through time.

In more general form, the generalized mass and stiffness for a linear elastic beam, assuming small displacements, can be written as:

$$k = \int_0^L EI(\psi'')^2 dx \tag{2.6a}$$

$$m = \int_0^L \rho A \psi^2 dx \tag{2.6b}$$

where L is the beam length, E is Young's modulus, I is the area moment of inertia, ρ is the mass per unit volume, A is the cross-sectional area , and ψ is an *admissible function*, meaning that it is continuous, satisfies geometric boundary conditions, and possesses derivatives of sufficient order [1]. Further, ψ is in general normalized such that a value of one is provided in a suitable position (e.g. at midspan).

In the specific case of a linear elastic simply supported beam, it turns out that a lumped mass model can be employed for a fairly accurate prediction of the fundamental natural frequency. However, the accuracy of this simplified model can be expected to decrease with an increasing forcing frequency, because the response of higher order modes is neglected. Moreover, note that a generalized SDOF system may also be utilized for modeling the nonlinear response of a structure, at least in an approximate manner. Consider, for example, a simply supported beam

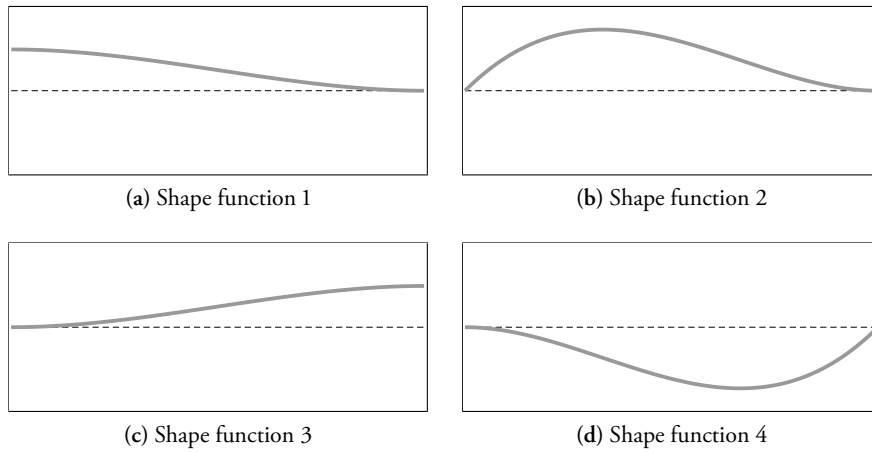

(**a**) Shape function 1 (**b**) Shape function 2

(**c**) Shape function 3 (**d**) Shape function 4

Figure 2.3: Beam element shape functions corresponding to transversal (1 and 3) and rotational (2 and 4) displacements at beam ends.

where a plastic hinge may developed at midspan, modeled by means of the assumed mode shape shown in Figure 2.2b. This model can e.g. be employed for estimating the inelastic dynamic response of a concrete beam—a frequently used approach in blast loading design of concrete structures [3].

2.1.2 Multi-degree-of-freedom systems

To compute the response of complex structures some form of discretization is in general required, e.g. by means of the FE method [4, 5]. The structure is then idealized as an assemblage of elements representing subsystems, e.g. bars, beams, shells or a continuum, for which the stiffness and mass distribution are easier to define. Using the FE method, the displacement field within each element is expressed in terms of generalized coordinates, having a physical meaningful interpretation as the displacements in a set of element DOFs. A global assembly can then be formed by interconnecting the element DOFs in nodal points.

Consider, for instance, a special type of element, namely a linear elastic Bernoulli beam element. Further, let the transverse and rotational motion of the beam ends constitute a set of four DOFs. Then, the transverse displacement of the beam element can be approximated by a superposition of cubical shape functions (see e.g. [1] for further details), thus

$$u(x,t) = \sum_{j=1}^{4} \psi_j(x) u_j(t) \tag{2.7}$$

where ψ_j is a shape function corresponding to a unit displacement/rotation at DOF j while the other DOFs are held fixed (see Figure 2.3).

Moreover, the beam element stiffness matrix can be derived by means of Lagrange's equations [1]. Then, the stiffness matrix entries are given by

$$k_{ij} = \int_0^L EI\psi_i''\psi_j'' dx \tag{2.8}$$

where ψ'' is the second derivative of the shape functions with respect to the beam longitudinal coordinate x. Further, the *consistent mass matrix* is given by

$$m_{ij} = \int_0^L \rho A\psi_i\psi_j dx \tag{2.9}$$

(notice the similarity to Eqs. 2.6a and 2.6b, respectively). In contrast to a lumped mass matrix, which is diagonal, a consistent mass matrix may include coupling terms, e.g. a coupling of the beam element's translational and rotational DOFs.

Other element types may be derived in a similar manner using shape functions representing the displacement within an element due to the displacements in the element DOFs. Note also that the entry k_{ij} is in fact the static reaction force in DOF i due to a unit displacement in DOF j, while the other DOFs are held fixed. Thus, the stiffness matrix for a linear elastic Bernoulli beam element may be established, as an alternative approach, using standard load cases found in textbooks. Furthermore, notice that the linear elastic beam element (assuming small displacements) is a special case being "exact" for static load cases where displacements/rotations are enforced at the beam ends. In general, however, the shape functions constitute an approximation of the displacement field within the element.

The assemblage of element system matrices forms a linear multi-degree-of-freedom (MDOF) system. In matrix form, the linear equations of motion can be expressed as:

$$\mathbf{M}\ddot{\mathbf{u}}(t) + \mathbf{C}\dot{\mathbf{u}}(t) + \mathbf{K}\mathbf{u}(t) = \mathbf{f}(t) \tag{2.10}$$

where $\mathbf{M}$, $\mathbf{C}$ and $\mathbf{K}$ are the $n \times n$ mass, damping and stiffness matrices, n being the number of global DOFs. The damping matrix can be constructed in several ways, as further discussed in Section 2.3. In general, coupling terms are present in the $\mathbf{C}$ and $\mathbf{K}$ matrices whereas $\mathbf{M}$ is diagonal if the mass is lumped to the global DOFs. It should also be noted that, with an appropriate DOF numbering, the system matrices will be narrowly banded, which in turn enables efficient solution methods. This is one reason why the FE method is one of the most important methods in applied mechanics and extensively used in a wide range of applications.

2.2 REDUCED ORDER MODELING USING SUBSPACE PROJECTION

In structural dynamics applications, many of the commonly used modeling techniques for linear elastic continuous structures are based on approximations using some form of shape

functions, also referred to as *mode shapes*. In particular, a set of modes form a basis in which the response, i.e. the mode amplitudes, may be represented by coordinates, often referred to as *generalized coordinates*. Furthermore, a mode-superposition approach can be employed for reducing the number of variables in a system expressed in terms of physical displacements—the system is then said to be projected onto a *reduced basis*. Note that, in contrast to a generalized SDOF system, a mode-superposition method is, in general, only applicable to linear elastic systems.

2.2.1 Rayleigh–Ritz method

As mentioned in Section 2.1.1, a linear elastic continuous system may be represented by an assumed mode shape to form a generalized SDOF system. Using the Rayleigh–Ritz method, this approach can be extended further such that the displacements is approximated by a superposition of k linearly independent mode shapes, satisfying the geometric boundary conditions. Thus, the displacement vector in Eq. 2.10 can be expressed as:

$$\mathbf{u}(t) = \sum_{j=1}^{k} \boldsymbol{\psi}_j q_j(t) \tag{2.11}$$

where q_j is the generalized coordinate corresponding to the amplitude of mode shape ψ_j and k is the number of mode shapes, e.g. generated using a set of assumed load patterns (henceforth, the time dependence of variables is omitted for compactness). Note that the FE method uses a similar technique applied on the element level, where the shape functions are constructed such that the generalized coordinates instead are the displacements of the nodal DOFs. Here, however, the Rayleigh–Ritz method is applied on the global discretized structure, e.g. obtained in a previous stage by means of the FE method.

Further, the relation between the generalized coordinates and the physical DOFs can be expressed as a transformation:

$$\mathbf{u} = \boldsymbol{\Psi}\mathbf{q} \tag{2.12}$$

where $\boldsymbol{\Psi} = \begin{bmatrix} \boldsymbol{\psi}_1 & \boldsymbol{\psi}_2 & \dots & \boldsymbol{\psi}_k \end{bmatrix}$ is a transformation matrix with the corresponding set of generalized coordinates $\mathbf{q} = \begin{bmatrix} q_1 & q_2 & \dots & q_k \end{bmatrix}^\top$.

Furthermore, the Rayleigh–Ritz method, as introduced above, can be employed for reducing the global system size by letting the number of modes be less than the number of physical DOFs, thus, $k \ll n$. By inserting Eq. 2.12 in Eq. 2.10 and pre-multiplying with $\boldsymbol{\Psi}^\top$ the reduced system is given by:

$$\tilde{\mathbf{M}}\ddot{\mathbf{q}} + \tilde{\mathbf{C}}\dot{\mathbf{q}} + \tilde{\mathbf{K}}\mathbf{q} = \tilde{\mathbf{f}} \tag{2.13}$$

where

$$\tilde{\mathbf{M}} = \boldsymbol{\Psi}^\top\mathbf{M}\boldsymbol{\Psi}, \quad \tilde{\mathbf{C}} = \boldsymbol{\Psi}^\top\mathbf{C}\boldsymbol{\Psi}, \quad \tilde{\mathbf{K}} = \boldsymbol{\Psi}^\top\mathbf{K}\boldsymbol{\Psi}, \quad \tilde{\mathbf{f}} = \boldsymbol{\Psi}^\top\mathbf{f}.$$

Here, $\tilde{\mathbf{M}}, \tilde{\mathbf{C}}$ and $\tilde{\mathbf{K}}$ are the $k \times k$ reduced system matrices and $\tilde{\mathbf{f}}$ is a $k \times 1$ reduced load vector. The linearly independent mode shapes form a reduced basis. Hence, the reduction

can be interpreted as a projection of the system equations onto a subspace, thus, the reduction is achieved be means of a *subspace projection*. This principal idea is employed in most of the reduction techniques discussed in this dissertation.

2.2.2 Modal decomposition

The equation of motion for free-vibration of an undamped MDOF system is given by:

$$\mathbf{M}\ddot{\mathbf{u}} + \mathbf{K}\mathbf{u} = \mathbf{0} \tag{2.14}$$

where $\mathbf{M}$ and $\mathbf{K}$ are the $n \times n$ mass and stiffness matrices, respectively, and $\mathbf{u}$ is a $n \times 1$ displacement vector including generalized and/or physical displacement coordinates.

By assuming harmonic motion, $\mathbf{u} = \phi \cos(\omega t - \theta)$, where ϕ is a vector constant through time and θ is the phase angle, and substituting into Eq. 2.14, the following nth-order generalized eigenvalue is obtained [1]:

$$\left(\mathbf{K} - \omega_j^2 \mathbf{M}\right) \boldsymbol{\phi}_j = 0 \quad j = 1, 2, \ldots, n. \tag{2.15}$$

where $\boldsymbol{\phi}_j$ is the eigenvector for mode j and ω_j is the corresponding eigenfrequency.

The amplitudes of the eigenmodes are arbitrary, thus, the modes may be scaled in any convenient manner. For example, in many applications it is convenient to scale the eigenmodes such that the modal mass is one unit of mass, i.e.

$$\boldsymbol{\phi}_j^\top \mathbf{M} \boldsymbol{\phi}_j = 1. \tag{2.16}$$

By pre-multiplying with $\boldsymbol{\phi}_j^\top$ in Eq. 2.15, it follws that the corresponding modal stiffness is given by

$$\boldsymbol{\phi}_j^\top \mathbf{K} \boldsymbol{\phi}_j = \omega_j^2. \tag{2.17}$$

Furthermore, an important property of the eigenmodes is the orthogonality property, namely that

$$\boldsymbol{\phi}_i^\top \mathbf{M} \boldsymbol{\phi}_j = 0 \quad \text{if} \quad i \neq j \tag{2.18}$$

$$\boldsymbol{\phi}_i^\top \mathbf{K} \boldsymbol{\phi}_j = 0 \quad \text{if} \quad i \neq j. \tag{2.19}$$

Similarly to the Rayleigh–Ritz approach described in Section 2.2.1, a transformation can be expressed as:

$$\mathbf{u} = \boldsymbol{\Phi}\mathbf{q} \tag{2.20}$$

where $\boldsymbol{\Phi} = \begin{bmatrix} \boldsymbol{\phi}_1 & \boldsymbol{\phi}_2 & \ldots & \boldsymbol{\phi}_n \end{bmatrix}$ is the *modal matrix* and $\mathbf{q} = \begin{bmatrix} q_1 & q_2 & \ldots & q_n \end{bmatrix}^\top$ is the corresponding set of modal coordinates.

In contrast to a Rayleigh–Ritz approach using assumed mode shapes, however, the orthogonality property of the eigenmodes implies that the *modal mass matrix* and *modal stiffness matrix*

are diagonal. Thus, by setting $\mathbf{\Psi} = \mathbf{\Phi}$ in Eq. 2.13 the modal mass and stiffness matrices are given by:

$$\tilde{\mathbf{M}} = \mathbf{\Phi}^\top \mathbf{M} \mathbf{\Phi} = \mathbf{I} \tag{2.21}$$

$$\tilde{\mathbf{K}} = \mathbf{\Phi}^\top \mathbf{M} \mathbf{\Phi} = \mathbf{\Lambda} = \text{diag}(\omega_1^2, \omega_2^2, \ldots, \omega_n^2). \tag{2.22}$$

Hence, if neglecting damping, a set of n uncoupled second-order differential equations, which can be solved independently, is obtained, e.g. expressed as:

$$\ddot{q}_j + \omega_j^2 q_j = \boldsymbol{\phi}_j^\top \mathbf{f} \quad j = 1, 2, \ldots, n. \tag{2.23}$$

If using a modal basis including all n eigenmodes, a pure transformation from physical to modal coordinates is obtained. Hence, the systems expressed in terms of modal and physical coordinates, respectively, are equivalent. However, a set of n eigenmodes is rarely used in practice. Instead, a reduced system is commonly established using a truncated modal basis. The benefit of using modal coordinates is thus two-fold—the orthogonality property of the modes enables a set of uncoupled differential equations and the number of system variables are decreased.

2.2.3 Krylov-subspace methods

Despite the great utility of modal expansion techniques and the wide range of applications, there are some drawbacks when employed for reducing the number of system variables. Firstly, solving an eigenvalue problem for large structures can be computationally expensive and, secondly, information related to the spatial distribution of the load is not considered. Hence, the modal basis may include eigenmodes that are not important for the specific load case. For example, consider again the simply supported beam in Figure 2.2a. Indeed, anti-symmetric eigenmodes, having zero displacement at midspan, cannot be excited by the external pressure and, consequently, nothing is gained by including these eigenmodes in the reduction basis.

An alternative to a reduction using a modal truncation is the so-called Krylov-subspace methods, which do consider the spatial distribution of the load and, moreover, are computationally efficient. As shown in the derivation below, the basis vectors can be computed by matrix–vector multiplications. In contrast, a eigenvalue problem must be solved when computing the eigenmodes.

In a structural dynamics context, the Krylov-vectors can be interpreted as the displacement due to quasi-static loads and, accordingly, the modes are sometimes referred to as *static correction modes* [6]. As discussed further in Sections 2.2.4 and 2.2.5, this naming convention is also useful in an attempt to demonstrate how the Krylov-subspace methods are related to the static correction method, which is commonly employed in modal analyses to consider the quasi-static response of higher order modes excluded in a modal truncation. In the following, the static correction modes are derived based on the approach presented in [7].

Neglecting damping, the equation of motion can be written as:

$$\mathbf{M}\ddot{\mathbf{u}} + \mathbf{K}\mathbf{u} = \mathbf{f}. \tag{2.24}$$

Further, the displacement can be split into a static and dynamic part:

$$\mathbf{u} = \mathbf{u}_{\text{stat}} + y. \tag{2.25}$$

By setting the acceleration to zero in Eq. 2.24, the static response is given by $\mathbf{u}_{\text{stat}} = \mathbf{K}^{-1}\mathbf{f}$. Further, substituting Eq. 2.25 into Eq. 2.24 an expression similar to Eq. 2.24 is obtained for y, namely

$$\mathbf{M}\ddot{y} + \mathbf{K}y = -\mathbf{M}\mathbf{K}^{-1}\ddot{\mathbf{f}}. \tag{2.26}$$

This procedure can be continued by splitting y into a static and dynamic part z, i.e.

$$\mathbf{y} = \mathbf{y}_{\text{stat}} + z. \tag{2.27}$$

The quasi-static solution is then given by

$$\mathbf{y}_{\text{stat}} = \mathbf{K}^{-1}\left(-\mathbf{M}\mathbf{K}^{-1}\right)\ddot{\mathbf{f}}. \tag{2.28}$$

In a similar manner, substituting Eq. 2.27 into Eq. 2.26 yields:

$$\mathbf{M}\ddot{\mathbf{z}} + \mathbf{K}\mathbf{z} = \left(-\mathbf{M}\mathbf{K}^{-1}\right)^2 \frac{\mathrm{d}^4\mathbf{f}}{\mathrm{d}t^4}. \tag{2.29}$$

Thus, the response is given by a sequence of quasi-static solutions:

$$\mathbf{u} = \mathbf{u}_{\text{stat}} + \mathbf{y}_{\text{stat}} + \mathbf{z}_{\text{stat}} + \dots \tag{2.30}$$

Hence, a recursive procedure is obtained, indicating that the dynamic response can be approximated as

$$\mathbf{u} \approx \sum_{j=1}^{k} \mathbf{K}^{-1}\left(-\mathbf{M}\mathbf{K}^{-1}\right)^{j-1} \frac{\mathrm{d}^{2(j-1)}\mathbf{f}}{\mathrm{d}t^{2(j-1)}} \tag{2.31}$$

where k is the number of static corrections. Furthermore, the higher order derivatives can be treated as separate DOFs. Hence, instead of computing a sequence of static corrections, a dynamic response analysis is conducted by means of generalized coordinates representing the amplitudes of the quasi-static modes. However, for this technique to be meaningful, the spatial variation of the load must be time-independent in some manner. For example, the external load may be decomposed into a set of m spatial load vectors such that

$$\mathbf{f} = \sum_{j=1}^{m} \mathbf{f}_j \alpha_j(t) = \mathbf{F}\alpha(t) \tag{2.32}$$

where $\mathbf{F}$ is a $n \times m$ matrix containing the spatial load vectors and $\alpha(t)$ contains the corresponding time functions. Then, the set of j-th order static correction modes are given by:

$$\mathbf{x}_{\text{cor},j} = \mathbf{K}^{-1}\left(\mathbf{M}\mathbf{K}^{-1}\right)^{j-1}\mathbf{F}. \tag{2.33}$$

(a) 1st static correction mode (b) 2nd static correction mode

Figure 2.4: Example of static correction modes and corresponding load distributions, derived from an uniform external pressure.

Further, the generated correction modes can be collected in a matrix:

$$\boldsymbol{\Psi}_{\text{cor}} = \begin{bmatrix} \mathbf{x}_{\text{cor},1} & \mathbf{x}_{\text{cor},2} & \dots & \mathbf{x}_{\text{cor},k} \end{bmatrix} \tag{2.34}$$

where Ψ_{cor} is a $n \times (k \cdot m)$ matrix including static correction modes. Due to the consideration of the external force in the derivation, the static correction modes are often referred to as load-dependent vectors. Further, by means of mode superposition, the physical displacements are given by:

$$\mathbf{u} = \boldsymbol{\Psi}_{\text{cor}} \eta \tag{2.35}$$

where $\eta = \begin{bmatrix} \eta_1 & \eta_2 & \dots & \eta_k \end{bmatrix}^\top$ are the generalized coordinates, corresponding to the correction mode amplitudes. A reduced system is then obtained by setting $\boldsymbol{\Psi} = \boldsymbol{\Psi}_{\text{cor}}$ in Eq. 2.13. However, to avoid numerical round-off errors, the correction modes may be generated using the modified Gram–Schmidt orthogonalization procedure [8, 9]. Moreover, by solving a small eigenvalue problem, the basis $\boldsymbol{\Psi}_{\text{cor}}$ can be replaced by a corresponding set of mass- and stiffness-orthogonal basis vectors (see further [6]).

The first order correction modes simply correspond to the static displacement of the external force patterns. As indicated by Eq. 2.33, the jth-order static modes can be interpreted as displacements due to inertia forces associated to the set of $(j-1)$th-order static modes (cf. Figure 2.4). Furthermore, note that the sequence of correction vectors form a so-called block-Krylov subspace, given by:

$$\mathcal{K}_r(\mathbf{K}^{-1}\mathbf{M}; \mathbf{K}^{-1}\mathbf{F}) = \text{span}\left(\mathbf{K}^{-1}\mathbf{F}, (\mathbf{K}^{-1}\mathbf{M})\mathbf{K}^{-1}\mathbf{F}, \dots, (\mathbf{K}^{-1}\mathbf{M})^{r-1}\mathbf{K}^{-1}\mathbf{F}\right). \tag{2.36}$$

Krylov subspace methods originating from system and control (see e.g. [10,11]) are thus closely related to the technique using higher-order static corrections, as introduced above.

2.2.4 Generalized mode acceleration method

As discussed in Section 2.2.2, the dynamic response can be approximated by means of a modal truncation, i.e.:

$$\mathbf{u}(t) \approx \sum_{j=1}^{k} \phi_j q_j(t). \tag{2.37}$$

Hence, using this approach, the responses of the discarded modes ϕ_j ($j = k+1, k+2, \ldots, n$) are neglected. If the eigenfrequencies of the discarded modes ω_j is much higher than the forcing frequency ω (which in general is the case), it is reasonable to assume that the responses of these modes are essentially static. Hence, if $\omega_j \gg \omega$ the response of mode j can be approximated by a static analysis (for comparison, consider an SDOF system subjected to a forcing frequency much lower than the natural frequency). This is the essence of the mode-acceleration (MA) method [9].

The equation of motion for an undamped system may be written as:

$$\mathbf{M}\boldsymbol{\Phi}\ddot{\mathbf{q}}(t) + \mathbf{K}\mathbf{u}(t) = \mathbf{f}(t) \tag{2.38}$$

where $\ddot{\mathbf{q}}$ are the modal accelerations. Further, if the eigenmodes are mass-normalized, the spectral expansion of the inverse stiffness matrix is given by:

$$\mathbf{K}^{-1} = \boldsymbol{\Phi}\tilde{\mathbf{K}}^{-1}\boldsymbol{\Phi}^{\top} = \sum_{j=1}^{n} \frac{\phi_j \phi_j^{\top}}{\omega_j^2}. \tag{2.39}$$

This is a very useful expression which will be used in several techniques investigated herein (see Sections 2.2.5 and 3.2.3). Furthermore, Eq. 2.38 may be rewritten as:

$$\mathbf{u}(t) = \mathbf{K}^{-1}\left(\mathbf{f} - \mathbf{M}\boldsymbol{\Phi}\ddot{\mathbf{q}}\right) \tag{2.40}$$

substituting Eq. 2.39 in Eq. 2.40 and rearranging the terms yields:

$$\mathbf{u}(t) = \mathbf{K}^{-1}\mathbf{f} - \boldsymbol{\Phi}\tilde{\mathbf{K}}^{-1}\boldsymbol{\Phi}^{\top}\mathbf{M}\boldsymbol{\Phi}\ddot{\mathbf{q}} = \mathbf{K}^{-1}\mathbf{f} - \boldsymbol{\Phi}\tilde{\mathbf{K}}^{-1}\ddot{\mathbf{q}} = \mathbf{K}^{-1}\mathbf{f} - \sum_{j=1}^{n} \frac{\ddot{q}_j(t)}{\omega_j^2}\phi_j. \tag{2.41}$$

Now, assume that the dynamic response is only computed for the first k modes, then

$$\mathbf{u}(t) \approx \mathbf{K}^{-1}\mathbf{f} - \sum_{j=1}^{k} \frac{\ddot{q}_j(t)}{\omega_j^2}\phi_j. \tag{2.42}$$

The above expression is thus employed in the MA method, where the first term in Eq. 2.42 can be interpreted as the pseudo-static response modified by the second term to obtain the dynamic response. Note that the above procedure indeed implies that the response due to static loading in general cannot be resolved by a truncated modal basis. In an approach using Krylov-subspace methods, however, the static solution is by definition included in the reduction basis.

The mode-acceleration method may be derived in a slightly different manner using an approach referred to as the *static correction method*. Even though both methods are referred to in the literature, the MD method and the static correction method are in fact equivalent, i.e. both methods provide the exact same results [9]. The only difference lies in how the expressions are derived (except for, possibly, differences due to round-off errors in a computational implementation). Here, however, the alternative formulation employed in the static correction method will be useful in Section 2.2.5, being the starting point in a derivation of the modal truncation augmentation method as well as certain dynamic substructuring methods discussed in Chapter 3.

In the static correction method, the displacement is expressed as:

$$\mathbf{u}(t) \approx \sum_{j=1}^{k} (\phi_j q_j) + \mathbf{u}_{\text{cor}} \tag{2.43}$$

where $\mathbf{u}_{\text{cor}}$ is a static correction term. Furthermore, by substituting the inverse stiffness matrix in Eq. 2.42 with its spectral expansion (see Eq. 2.39), and separating the summation, the following expression is obtained:

$$\mathbf{u}(t) \approx \left(\sum_{j=1}^{k} \frac{\phi_j \phi_j^\top}{\omega_j^2} + \sum_{j=k+1}^{n} \frac{\phi_j \phi_j^\top}{\omega_j^2} \right) \mathbf{f} - \sum_{j=1}^{k} \frac{\ddot{q}_j}{\omega_j^2} \phi_j \tag{2.44}$$

further, recall that $\ddot{q}_j + q_j \omega_j^2 = \phi_j^\top \mathbf{f}$, thus:

$$\sum_{j=1}^{k} \phi_j q_j = \sum_{j=1}^{k} \frac{\phi_j \phi_j^\top}{\omega_j^2} \mathbf{f} - \sum_{j=1}^{k} \frac{\ddot{q}_j(t)}{\omega_j^2} \phi_j. \tag{2.45}$$

By substituting Eq. 2.45 in Eq. 2.44 the following expression is obtained:

$$\mathbf{u}(t) \approx \sum_{j=1}^{k} \phi_j q_j + \sum_{j=k+1}^{n} \frac{\phi_j \phi_j^\top}{\omega_j^2} \mathbf{f} \tag{2.46}$$

thus, by comparing Eq. 2.46 and Eq. 2.43, it follows that the correction term is given by:

$$\mathbf{u}_{\text{cor}} = \sum_{j=k+1}^{n} \frac{\phi_j \phi_j^\top}{\omega_j^2} \mathbf{f}. \tag{2.47}$$

In general, however, the above expression cannot be used in practice, because a computation of all the n eigenmodes is not feasible. Therefore, using Eq. 2.39, the following alternative expression may be utilized:

$$\mathbf{u}_{\text{cor}} = \left(\mathbf{K}^{-1} - \sum_{j=1}^{k} \frac{\phi_j \phi_j^\top}{\omega_j^2} \right) \mathbf{f}. \tag{2.48}$$

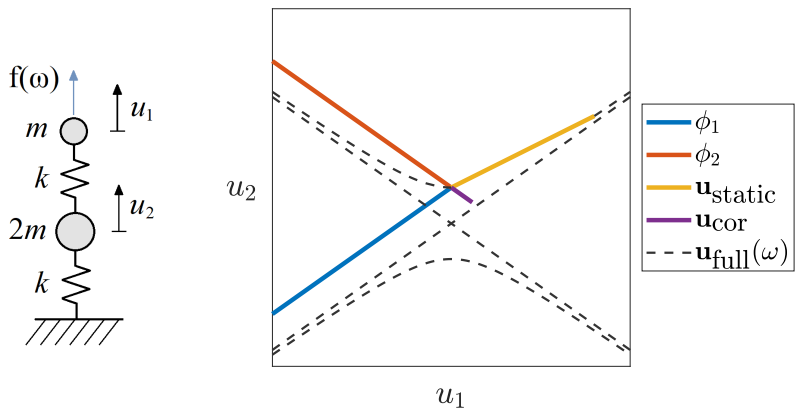

Figure 2.5: Example of static correction vector, $\mathbf{u}_{\text{cor}}$, for a 2DOF system.

The static correction vector $\mathbf{u}_{\text{cor}}$ is illustrated in Figure 2.5 for a 2DOF system. As shown in the figure, both eigenmodes are required to resolve the static displacement due to the external point load. Further, the dashed gray line correspond to the solution provided by the full model, i.e. where both eigenmodes are considered. Moreover, note that the response of the second mode is indeed essentially static for a forcing frequency close to the first resonance.

The MA method may be generalized to include higher order corrections, referred to as the *generalized MA* method [6]. In fact, the higher order corrections can be derived in a manner similar to the force-dependent modes discussed in Section 2.2.3. Notice that setting $k = 1$ in Eq. 2.31 correspond to the pseudo-static solution, which in turn is equal to the static correction provided by Eq. 2.48 if the modal responses are neglected. Furthermore, if including k modal responses, it follows that the higher order corrections can be computed as:

$$\mathbf{u}_{\text{cor},\,j} = \left(\mathbf{K}^{-1} - \sum_{j=1}^{k} \frac{\phi_j \phi_j^\top}{\omega_j^2} \right) \left(-\mathbf{M}\mathbf{K}^{-1} \right)^{j-1} \frac{\mathrm{d}^{2(j-1)}\mathbf{f}}{\mathrm{d}t^{2(j-1)}}. \tag{2.49}$$

Hence, the response is approximated as

$$\mathbf{u}(t) \approx \sum_{s}^{k} \boldsymbol{\phi}_s q_s(t) + \sum_{j}^{l} \mathbf{u}_{\text{cor},\,j} \tag{2.50}$$

where l is the static correction order. Note that setting $l = 1$ in Eq. 2.50 indeed provides and expression equivalent to the static correction method.

2.2.5 Generalized modal truncation augmentation

Using a procedure similar to the Krylov-subspace method discussed in Section 2.2.3, the truncated modal matrix can be augmented by higher order correction modes. Hence, the idea is to utilize higher order correction vectors as additional Ritz-vectors instead of computing the higher order derivatives in Eq. 2.49. This approach is often referred to as a generalized Modal Truncation Augmentation (generalized MTA) [6].

The set of jth-order correction modes are then given by:

$$\mathbf{x}_{\text{cor},j} = \left(\mathbf{K}^{-1} - \sum_{j=1}^{k} \left(\frac{\phi_j \phi_j^\top}{\omega_j^2} \right) \right) \left(\mathbf{M}\mathbf{K}^{-1} \right)^{j-1} \mathbf{F} \tag{2.51}$$

which are both mass- and stiffness orthogonalized with repsect to the retained eigenmodes. A reduction basis is then formed including the eigenmodes as well as the higher order correction modes, e.g. expressed as:

$$\mathbf{\Psi}_{\text{MTA}} = \begin{bmatrix} \boldsymbol{\phi}_1 & \boldsymbol{\phi}_2 & \dots & \boldsymbol{\phi}_k & \mathbf{x}_{\text{cor},1} & \mathbf{x}_{\text{cor},2} & \dots & \mathbf{x}_{\text{cor},l} \end{bmatrix} \tag{2.52}$$

where l is the number of higher order corrections. A reduced system may then be formed using Eq. 2.13. As discussed in Section 2.2.3, the basis vectors may be orthogonalized to avoid numerical round-off errors.

2.3 DAMPING MODELS FOR TIME DOMAIN ANALYSES

As discussed in Section 2.2.2, the orthogonality property of the eigenmodes result in a diagonal modal mass and stiffness matrix. Accordingly, a modal transformation can be utilized for diagonalizing the system matrices and, consequently, a solution can be obtain by a mode superposition, where each modal response is obtained by solving the corresponding uncoupled differential equation. So far, however, damping has been neglected.

For structures subjected to free vibration, a steadily diminishing displacement amplitude is observed. Hence, energy is dissipated due to various mechanisms, such as opening/closing of small cracks, friction between structural members etc, which is referred to as *damping* [9]. It turns out that a viscous damping model is convenient in linear analyses because it enables analytical solutions. However, it should be emphasized that, in most structural engineering applications, this model is unphysical. Thus, it is merely a mathematical model that can be calibrated to mimic the damping of the real structure. In particular, a viscous damping model is frequency dependent, as e.g. indicated by Eq. 2.10 where the damping force correspond to the damping coefficient c multiplied with the velocity. Nonetheless, the viscous damping model has several benefits regrading computational aspects that, in most engineering applications, far outweighs the gain of using a more realistic and complex damping model, requiring computational expensive solution methods.

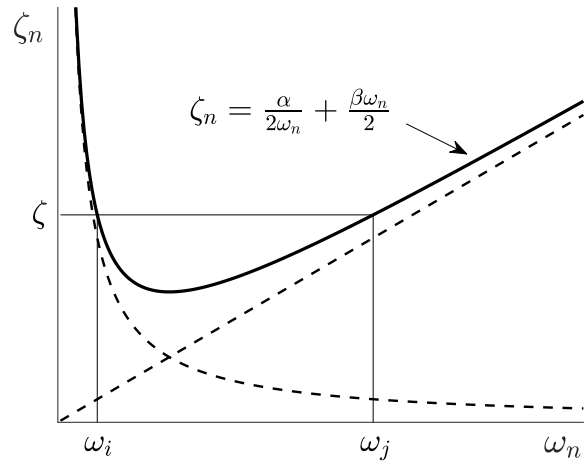

Figure 2.6: Rayleigh damping: variation of modal damping ratios ζ_n with natural frequency ω_n.

2.3.1 Rayleigh damping

Because both the modal mass and stiffness matrix are diagonal, one way to ensure that also the viscous damping matrix $\mathbf{C}$ is diagonalized is to construct the damping matrix as a weighted sum of the mass and stiffness matrix, thus

$$\mathbf{C} = \alpha\mathbf{M} + \beta\mathbf{K}. \tag{2.53}$$

This damping model is referred to as *Rayleigh damping* or *proportional* damping [9]. The damping coefficients α and β, thus, determine the contribution of mass- and stiffness-proportional damping, respectively.

If the eigenmodes are mass normalized, the set of uncoupled differential equations including viscous damping can be expressed as:

$$\ddot{q} + 2\zeta_j\omega_j\dot{q} + \omega_j^2 q = \boldsymbol{\phi}_j^\top \mathbf{f} \quad j = 1, 2, \ldots, n \tag{2.54}$$

then, it follows that the Rayleigh damping coefficients can be expressed as

$$2\zeta_j\omega_j = \alpha + \omega_j^2\beta \Rightarrow \zeta_j = \frac{1}{2}\left(\frac{\alpha}{\omega_j} + \omega_j\beta\right) \quad j = 1, 2, \ldots, n \tag{2.55}$$

where ζ_j is the *modal damping ratio* for mode j. As discussed further below, a useful property of the Rayleigh damping model is that the mass-proportional damping is inversely proportional to the eigenfrequency, whereas the stiffness-proportional damping is linearly proportional to the eigenfrequency.

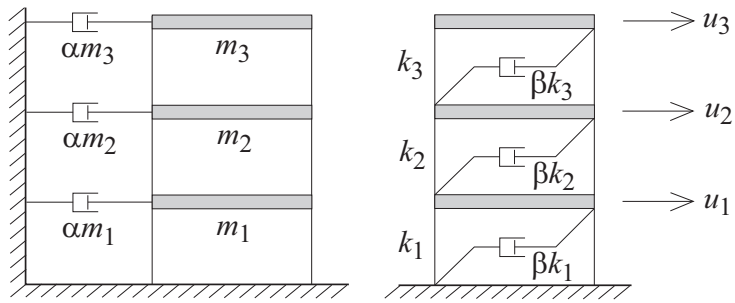

Figure 2.7: Mass-proportional (left) and stiffness-proportional damping (right).

For many materials, experimental data typically suggests that the damping ratio is frequency-independent [9]. Nonetheless, a viscous damping model where the amount of damping increases linearly with the forcing frequency (cf. Eq. 2.54) is often employed due to its utility in time domain analysis of linear systems. Using the Rayleigh damping model, however, the coefficients α and β can be adjusted such that the desired modal damping ratio is fulfilled for two eigenfrequencies [9]. Assuming that the desired damping ratio is equal for all modes, frequencies in-between the selected eigenfrequencies will then be slightly underdamped whereas frequencies below and above the selected eigenfrequencies will be overdamped, as shown in Figure 2.6.

To ensure that the damping is not overestimated for modes significantly contributing to the response, the set of eigenmodes used for calibrating the Rayleigh coefficients may be chosen such that the frequency of important eigenmodes lies in-between the eigenfrequencies of the selected modes. Furthermore, it should be noted that the Rayleigh damping model is applicable in mode superposition methods as well as in a direct time-integration of systems expressed in terms of physical displacements being one of the main advantages using this damping model.

The implication of prescribing a mass- and stiffness-proportional damping is shown in Figure 2.7 [9]. Clearly, the mass-proportional part, corresponding to dashpots connected to ground, is unphysical. For example, a mass-proportional damping associates damping to rigid body modes. Nonetheless, a pure stiffness-proportional viscous damping being linearly proportional to the forcing frequency is in general not appropriate. Thus, a mass-proportional part is useful in practical applications. For structures having a irregular mass distribution, however, a mass-proportional damping model might not be appropriate and should be used with care.

2.3.2 Modal damping

As discussed in Section 2.3.1, the frequency dependency of a viscous damping model can be somewhat controlled by combining a mass- and stiffness proportional damping. An alternative, however, is to explicitly prescribe modal damping in the modal domain [9]. Recall that a modal transformation decouples the modal responses, as shown in Eq. 2.54. Thus, the de-

sired *modal damping ratio* may be prescribed explicitly in Eq. 2.54. In a modal analysis, this approach is obviously advantageous compared to Rayleigh damping. The drawback, however, is that this damping model is in principle only applicable in modal domain analyses, whereas the Rayleigh damping model can also be employed for systems expressed in terms of physical DOFs. It should be mentioned, however, that it is actually possible to expand the modal damping matrix to obtain a corresponding damping matrix in the physical domain. Such an approach should be used with great care, however—in general the resulting damping matrix will be full and, moreover, may be physically impossible requiring external as well as negative damping elements. Thus, the Rayleigh damping model is in general the preferred choice in time domain analysis of systems formulated in the physical domain.

2.3.3 Modal strain energy method

An approach using modal damping requires proportional, also referred to as *classical*, damping. However, in several practical applications the damping is non-proportional, e.g. in models representing buildings having a lower part made of concrete and an upper part made of steel or rubber components interacting with steel or glass structures. A Rayleigh damping model can be employed for such systems. Then, the Rayleigh damping coefficients are derived for each subsystem, respectively, by means of the global undamped eigenfrequencies and the desired damping ratios [9].

However, because the damping matrix is not proportional, the corresponding generalized damping matrix may not be diagonal. For solving the response of such MDOF systems either a direct time-integration of the coupled equations of motion or a mode superposition using the complex modes of the damped system is required [12]. However, there is another approximate strategy for solving for the response of non-proportional MDOF systems, namely the modal strain energy (MSE) method [13,14]. As e.g. shown by the numerical studies presented in [14], this approach is sufficiently accurate for lightly damped structures having a damping below approximately 20%. In practical applications, damping ratios are often below this level, at least considering civil engineering structures. Using this approach a direct time-integration, which can be computationally expensive and requires an appropriate time discretization, can be avoided. Moreover, a solution strategy using the damped eigenmodes requires a state-space formulation, that doubles the number of system variables, which, in addition, are complex. Moreover, an evaluation of the undamped eigenmodes can be of great utility, to get further insight into the structural behavior. A corresponding physical interpretation of the damped eigenmodes, consisting of complex displacements as well as velocities, is less straightforward, however.

In the following, the MSE method is presented using the approach in [14]. The damping ratio of an SDOF system representing a modal coordinate can be expressed as:

$$\zeta = \frac{E_D}{4\pi E_S} \tag{2.56}$$

where E_D is is the one-cycle modal energy loss due to viscous damping and E_S is the modal strain energy amplitude, given by:

$$E_S = \frac{1}{2}\boldsymbol{\phi}_j^\top \mathbf{K}\boldsymbol{\phi}_j \tag{2.57}$$

where $\mathbf{K}$ is the global stiffness matrix for a structure with non-proportional damping, and $\boldsymbol{\phi}_j$ is the global eigenmode for mode j.

In accordance with the MSE method, the modal energy loss is computed as:

$$E_D = \pi\omega_j \boldsymbol{\phi}_j^\top \mathbf{C}\boldsymbol{\phi}_j \tag{2.58}$$

where ω_j is the eigenfrequency for mode j and $\mathbf{C}$ is the global damping matrix containing the damping submatrices related to the substructures having different levels of damping. Assuming that the modal basis is mass-normalized, it follows that the modal damping ratio for mode j can be estimated as:

$$\zeta_j = \frac{\boldsymbol{\phi}_j^\top \mathbf{C}\boldsymbol{\phi}_j}{2\omega_j} \tag{2.59}$$

Using the above procedure, a solution can be obtained by means of mode superposition of the undamped eigenmodes even though a non-proportional damping is considered. It should be emphasized, however, that the MSE method is indeed an approximation due to that possible off-diagonal terms in the modal damping matrix is not considered.

2.4 DYNAMIC ANALYSIS

In general, the following strategies may be employed for solving for the response of MDOF systems in the time domain:

- mode superposition using the undamped eigenmodes,
- mode superposition using the complex damped eigenmodes, or
- by direct time-integration of the coupled system equations.

Here, only the first and third methods are considered. The damping levels for the structures considered (see further Chapter 4) are fairly low, hence, an approximate mode-superposition approach using the undamped eigenmodes are sufficiently accurate. Moreover, it should be noted that, in addition to the time domain methods listed above, the response can be computed using a frequency domain approach, by establishing complex frequency response functions (FRF) (see further [9]). Frequency domain methods are, however, not within the scope of this dissertation.

2.4.1 Mode superposition methods

Each modal response can be represented by a corresponding SDOF system, i.e. Eq. 2.2. and Eq. 2.54 are equivalent. It follows that all the methods available for computing the dynamic response of SDOF systems can be utilized for computing the modal responses. In particular, a closed-form solution can be established for computing the damped free vibration response:

$$q_j(t) = e^{-\zeta_j \omega_j t}\left(q_j(0)\cos(\omega_{jD}t) + \frac{\dot{q_j}(0) + \zeta_j\omega_j q_j(0)}{\omega_{jD}}\sin(\omega_{jD}t)\right) \tag{2.60}$$

where $\omega_{jD} = \omega_j\sqrt{1-\zeta_j^2}$ is the jth natural frequency with damping [9].

A time discretization is clearly needed to consider a load varying arbitrary through time. Nonetheless, for such load cases, highly efficient numerical procedures are available that provides the "exact" response of a load varying linearly between a range of time increments, i.e. the accuracy merely depend on the time discretization of the problem. Moreover, a closed-form solution can be established for certain pulse loads, periodic loads and, in particular, harmonic loads, which in turn may be utilized for solving for arbitrary loading by means of frequency domain methods [9].

2.4.2 Direct time-integration methods

The computationally efficient analytical solution methods discussed in Section 2.4.1 require that the system equations are linear. For nonlinear problems, however, a direct time integration of the equations of motion is required. Several time-stepping methods can be found in the literature (see e.g. [15]), which can be divided into one-step and multi-step methods, where the former implies that only two time increments are involved in the computations at a given time, whereas the latter may include several time increments. In structural dynamics applications the most common time-integration methods are one-step methods.

Furthermore, a time-stepping scheme may be *implicit*, which implies knowledge of the accelerations in the computation of the velocity and displacements at a given time step, or *explicit*, if the displacements and velocities are computed without prior knowledge of the accelerations.

One of the most important time stepping methods is the Newmark method—a one-step method based on the following equations [15]:

$$\dot{\mathbf{u}}_{n+1} = \dot{\mathbf{u}}_n + (1-\gamma)\,h\ddot{\mathbf{u}}_n + \gamma h\ddot{\mathbf{u}}_{n+1} \tag{2.61a}$$

$$\mathbf{u}_{n+1} = \mathbf{u}_n + h\dot{\mathbf{u}}_n + h^2\left(\frac{1}{2}-\beta\right)\ddot{\mathbf{u}}_n + h^2\beta\ddot{\mathbf{u}}_{n+1} \tag{2.61b}$$

where h is the time increment (i.e. $t_{n+1} = t_n + h$), and γ and β are parameters that defines the variation of acceleration over a time step. In particular, setting $\gamma = \frac{1}{2}$ and $\beta = \frac{1}{4}$ correspond

to constant average acceleration, which result in an unconditionally stable scheme, meaning that the time increment size only have to be adjusted to obtain sufficient accuracy [15].

Another important time-stepping technique is the central difference method (CDM), where the velocity and accelerations are expressed as [9,15]:

$$\dot{\mathbf{u}}_n = \frac{\mathbf{u}_{n+1} - \mathbf{u}_{n-1}}{2h} \tag{2.62a}$$

$$\ddot{\mathbf{u}}_n = \frac{\mathbf{u}_{n+1} - 2\mathbf{u}_n + \mathbf{u}_{n-1}}{h^2}. \tag{2.62b}$$

In fact, the above expressions can be derived from Newmark's formula by setting $\gamma = \frac{1}{2}$ and $\beta = 0$. The CDM method is a second order accurate explicit scheme, i.e. it can be formulated such that the displacements and velocities can be computed without prior knowledge of the accelerations. In particular, a computationally efficient implementation of the CDM method can be achieved for undamped systems having a diagonal lumped mass matrix, an approach commonly employed in highly nonlinear and transient problems, such as crash simulations and impact loading. The CDM method is conditionally stable, however, requiring that $\omega_{cr} h \leq 2$, where ω_{cr} is the highest eigenfrequiency of the system [15].

Using an explicit time-stepping scheme, such as the CDM method, for solving nonlinear systems is straightforward, because the nonlinear forces may be computed explicitly (however, a stable time increment must be ensured). In an implicit time integration scheme, however, the nonlinear equilibrium equations typically requires an iterative solution method, such as the modified Newton–Raphson method (see e.g. [9]).

3 Dynamic substructuring

The dynamic response of linear systems can be efficiently computed by use of modal dynamics; the system matrices are diagonalized and reduced by projecting the system equations onto a truncated modal basis. However, for large systems it can be beneficial to divide the system into substructures and employ dynamic substructuring (DS) to perform a reduction on the substructure level, e.g. as a preconditioning in the process of computing the global eigenmodes. Solving several substructures can be computationally less expensive than solving one large system.

Moreover, DS can be employed for reducing linear structures interacting with nonlinear structures or having nonlinear boundary conditions. In particular, local nonlinearities can be considered, such as plastic hinges in concrete structures or local contact interactions, as illustrated by various applications in Chapter 4. The parts of the structure that remain linear elastic are then represented by a reduced set of generalized coordinates, whereas the nonlinear parts are expressed in terms of physical displacements.

Several DS methods have been developed since the late 1960s, extensive reviews of existing methods are e.g. presented in [1, 16]. In particular, DS may be applied in both time domain and frequency domain analyses. Here, however, focus is on DS for time domain analysis.

Section 3.1 presents assembly methods, which is an important aspect of DS. To this end, the fundamental equilibrium and compatibility conditions are introduced, as formulated in [16], which then provide a basis in a derivation of various assembly techniques. In particular, a global assembly may be formed such that a unique set of DOFs or, in contrast, dual DOFs are retained at interfaces.

In most DS methods a reduction is performed on the substructure level using some form of mode superposition approach. Hence, the substructure response is expressed in terms of generalized coordinates representing the amplitudes of a specific set of *component modes* (in the following, the terms *substructure* and *component* are used interchangeably). This class of DS approaches are often referred to as component-mode synthesis (CMS) and is further discussed in Section 3.2. In particular, CMS methods may be formulated using a so-called free- or fixed-interface approach. In the applications discussed in Chapter 4, it turns out that a fixed-interface approach is often advantageous. For the sake of completeness, however, both free-

and fixed-interface methods are considered here. Further, an investigation of the principal differences between the fixed- and free-interface methods provide a basis for determining the preferred modeling approach in specific applications.

3.1 ASSEMBLY METHODS

The equations of motion for a structure consisting of N substructures and the associated compatibility and equilibrium conditions may be written as [16]:

$$\begin{cases} \mathbf{M}\ddot{\mathbf{u}} + \mathbf{C}\dot{\mathbf{u}} + \mathbf{K}\mathbf{u} = \mathbf{f} + \mathbf{g} & \text{(3.1a)} \\ \mathbf{B}\mathbf{u} = \mathbf{0} & \text{(3.1b)} \\ \mathbf{L}^\top \mathbf{g} = \mathbf{0} & \text{(3.1c)} \end{cases}$$

where

$$\begin{aligned} \mathbf{M} &= \operatorname{diag}\left(\mathbf{M}^{(1)}, \mathbf{M}^{(2)}, \ldots, \mathbf{M}^{(N)}\right) \\ \mathbf{C} &= \operatorname{diag}\left(\mathbf{C}^{(1)}, \mathbf{C}^{(2)}, \ldots, \mathbf{C}^{(N)}\right) \\ \mathbf{K} &= \operatorname{diag}\left(\mathbf{K}^{(1)}, \mathbf{K}^{(2)}, \ldots, \mathbf{K}^{(N)}\right) \\ \mathbf{u} &= \begin{bmatrix} \mathbf{u}^{(1)\top} & \mathbf{u}^{(2)\top} & \ldots & \mathbf{u}^{(N)\top} \end{bmatrix}^\top \\ \mathbf{f} &= \begin{bmatrix} \mathbf{f}^{(1)\top} & \mathbf{f}^{(2)\top} & \ldots & \mathbf{f}^{(N)\top} \end{bmatrix}^\top \\ \mathbf{g} &= \begin{bmatrix} \mathbf{g}^{(1)\top} & \mathbf{g}^{(2)\top} & \ldots & \mathbf{g}^{(N)\top} \end{bmatrix}^\top . \end{aligned}$$

Here, $\mathbf{M}$, $\mathbf{C}$, and $\mathbf{K}$ are the global mass, damping and stiffness matrices, respectively, $\mathbf{u}$ is the global displacement vector and $\mathbf{f}$ and $\mathbf{g}$ are the external and interface force vectors, respectively. Furthermore, note that the global system equations (Eq. 3.1a) are written in block-diagonal form which implies that dual DOFs are present at interfaces between substructures.

Eq. 3.1b considers the compatibility condition. More specifically, it includes equations describing how DOFs are constrained. For example, consider the constraint equation $u_i - u_j = 0$, i.e. the displacement in DOF i is equal to the displacement in DOFj. This correspond to $\mathbf{B}$ being a row vector of the form:

$$\mathbf{B} = \begin{bmatrix} 0 \cdots\cdots 1 \cdots\cdots -1 \cdots\cdots 0 \\ \qquad\quad u_i \qquad\quad u_j \end{bmatrix} \tag{3.3}$$

Hence, if assuming conforming discretizations on interfaces, $\mathbf{B}$ will be a signed $n_c \times n$ Boolean matrix, where n_c is the number of constraints and n the number of DOFs in the dually assembled global system.

Eq. 3.1c considers the equilibrium condition where, in the case of a conforming interface discretization, $\mathbf{L}$ is a Boolean localization matrix. For example, consider again the constraint

equation $u_i - u_j = 0$ and the associated equilibrium condition $g_i + g_j = 0$. This correspond to $\mathbf{L}$ being a $n \times (n-1)$ matrix given by (with blank entries being zero):

$$\mathbf{L} = \begin{bmatrix} 1 & & & & & \\ & \ddots & & & & \\ & & 1 & & & \\ & & & 1 & & \\ & & & & \ddots & \\ & & & & & 1 \end{bmatrix} \begin{matrix} \\ \\ \\ u_i \\ \\ u_j \end{matrix} \tag{3.4}$$

The global displacement vector may be partitioned into a set of unique $\mathbf{u}_u$ and redundant $\mathbf{u}_r$ DOFs. Hence, the unique DOFs include one set of interface DOFs and, possibly, interior DOFs being substructure DOFs that are not part of the substructure boundary (a selection of interface DOFs is thus required). Then, the compatibility condition can be expressed as:

$$\begin{bmatrix} \mathbf{B}_{rr} & \mathbf{B}_{ru} \end{bmatrix} \begin{bmatrix} \mathbf{u}_r \\ \mathbf{u}_u \end{bmatrix} = \mathbf{0}. \tag{3.5}$$

Further, by rewriting Eq. 3.5, the redundant DOFs can be expressed in terms of the unique DOFs:

$$\mathbf{u}_r = -\mathbf{B}_{rr}^{-1}\mathbf{B}_{ru}\mathbf{u}_u. \tag{3.6}$$

Hence, the following transformation may be defined:

$$\mathbf{u} = \mathbf{L}\mathbf{u}_u = \begin{bmatrix} -\mathbf{B}_{rr}^{-1}\mathbf{B}_{ru} \\ \mathbf{I}_{uu} \end{bmatrix} \mathbf{u}_u. \tag{3.7}$$

Thus, the Boolean localization matrix $\mathbf{L}$, that transforms the unique set of DOFs to dual form, can readily be obtained if $\mathbf{B}$ is available.

Furthermore, substituting Eq. 3.7 into Eq. 3.1. and pre-multiplying with $\mathbf{L}^\top$ yields:

$$\mathbf{M}_P\ddot{\mathbf{u}}_u + \mathbf{C}_P\dot{\mathbf{u}}_u + \mathbf{K}_P\mathbf{u}_u = \mathbf{f}_P \tag{3.8}$$

where

$$\mathbf{M}_P = \mathbf{L}^\top\mathbf{M}\mathbf{L}, \quad \mathbf{C}_P = \mathbf{L}^\top\mathbf{C}\mathbf{L}, \quad \mathbf{K}_P = \mathbf{L}^\top\mathbf{K}\mathbf{L}, \quad \mathbf{f}_P = \mathbf{L}^\top\mathbf{f}.$$

Here, $\mathbf{M}_P$, $\mathbf{C}_P$ and $\mathbf{K}_P$ are $n_P \times n_P$ system matrices and $\mathbf{f}_P$ is a $n_P \times 1$ external force vector, where n_P is the number of unique DOFs in a so-called *primal* formulation. Notice that this primal approach correspond to the assembly procedure commonly employed in standard FE modeling, i.e. the original displacement vector is replaced by a set of unique DOFs. Moreover, substituting Eq. 3.7 into the compatibility condition yields $\mathbf{B}\mathbf{u} = \mathbf{B}\mathbf{L}\mathbf{u}_u = \mathbf{0}$. Hence, the

Boolean localization matrix $\mathbf{L}$ represents the null-space of $\mathbf{B}$, i.e. $\mathbf{BL} = \mathbf{0}$ [16]. Accordingly, a primal assembly is actually obtained by projecting the system equations onto the null-space of $\mathbf{B}$ (cf. Eqs. 2.13 and 3.8). Furthermore, it follows that $(\mathbf{BL})^\top = \mathbf{L}^\top\mathbf{B}^\top = \mathbf{0}$, i.e. $\mathbf{B}^\top$ is the null-space of $\mathbf{L}^\top$.

Instead of using a primal formulation, the compatibility and equilibrium conditions (Eqs. 3.1b and 3.1c) can be enforced such that dual DOFs are retained at interfaces, e.g. by means of Lagrange multipliers [16]. Then, the interface forces may be selected such that:

$$\mathbf{g} = -\mathbf{B}^\top\lambda \tag{3.9}$$

where λ is a $n_c \times 1$ vector containing Lagrange multipliers. Further, by substituting Eq. 3.9 into the equilibrium equation (Eq. 3.1b) one obtains:

$$\mathbf{L}^\top\mathbf{g} = -\mathbf{L}^\top\mathbf{B}^\top\lambda = \mathbf{0}. \tag{3.10}$$

Hence, because $\mathbf{B}^\top$ is the null-space of $\mathbf{L}^\top$ the equilibrium condition is always satisfied. It then remains to enforce the compatibility condition, i.e. $\mathbf{Bu} = \mathbf{0}$. In matrix form, the dually assembled system can thus be written as:

$$\begin{bmatrix} \mathbf{M} & \mathbf{0} \\ \mathbf{0} & \mathbf{0} \end{bmatrix} \begin{bmatrix} \ddot{\mathbf{u}} \\ \lambda \end{bmatrix} + \begin{bmatrix} \mathbf{C} & \mathbf{0} \\ \mathbf{0} & \mathbf{0} \end{bmatrix} \begin{bmatrix} \dot{\mathbf{u}} \\ \lambda \end{bmatrix} + \begin{bmatrix} \mathbf{K} & \mathbf{B}^\top \\ \mathbf{B} & \mathbf{0} \end{bmatrix} \begin{bmatrix} \mathbf{u} \\ \lambda \end{bmatrix} = \begin{bmatrix} \mathbf{f} \\ \mathbf{0} \end{bmatrix} \tag{3.11}$$

where both the equilibrium and compatibility conditions are satisfied.

Furthermore, a dually assembled system can be enforced in an approximate manner using a penalty formulation, e.g. expressed as:

$$\mathbf{M\ddot{u}} + \mathbf{C\dot{u}} + \left(\mathbf{K} + \alpha\mathbf{B}^\top\mathbf{B}\right)\mathbf{u} = \mathbf{f} \tag{3.12}$$

where α is a penalty stiffness being sufficiently large such that $\mathbf{Bu} \approx \mathbf{0}$ [4]. Again, consider the constraint equation $u_i - u_j = 0$ and the corresponding signed Boolean matrix $\mathbf{B}$ (cf. Eq. 3.3). It follows that:

$$\alpha\mathbf{B}^\top\mathbf{B} = \begin{bmatrix} & 0 & 0 & \\ & \vdots & \vdots & \\ 0 \cdots & \alpha & -\alpha & \cdots 0 \\ & \vdots & \vdots & \\ 0 \cdots & -\alpha & \alpha & \cdots 0 \\ & \vdots & \vdots & \\ & 0 & 0 & \end{bmatrix} \begin{matrix} \\ \\ u_i \\ \\ u_j \\ \\ \\ \end{matrix} \\ \begin{matrix} \\ u_i \end{matrix} \quad \begin{matrix} \\ u_j \end{matrix} \tag{3.13}$$

hence, using the penalty formulation, the constraint is indeed enforced by means of a spring element having stiffness α.

The preferred assembly method depend on the specific application. A primal formulation where the number of global DOFs are reduced can be cumbersome in some applications. On the contrary, it can be problematic to ensure stability in direct time-integration schemes for systems including Lagrange multipliers [17]. Even though methods to ensure stability exist, the available time-integration schemes are at least limited (for example, a standard Newmark time-integration, assuming constant average accelerations, is in this case unconditionally unstable). If using the penalty method, a suitable penalty stiffness must be determined—if it is too low, the constraint equations might not be enforced properly and if it is too large, the system equations can be ill-conditioned with respect to inversion. Moreover, if using a conditionally stable time-integration scheme, such as the central difference method, a large penalty stiffness might result in a very small critical time increment (see Section 2.4.2).

3.2 COMPONENT MODE SYNTHESIS

On the substructure level, the linear system equations are expressed in terms of the substructure displacements $\mathbf{u}^{(s)}$, which can be replaced by a reduced set of generalized coordinates $\mathbf{q}^{(s)}$. The transformation can be expressed as

$$\mathbf{u}^{(s)} = \mathbf{T}\mathbf{q}^{(s)} \tag{3.14}$$

where superscript s is the substructure label and $\mathbf{T}$ is a $n^{(s)} \times m^{(s)}$ transformation matrix representing a reduction basis. Here, $n^{(s)}$ and $m^{(s)}$ are the number of variables in the unreduced and reduced subsystem, respectively. Typically, $m^{(s)} \ll n^{(s)}$.

A FE formulation of a substructure leads to a linear equation of motion of the following form:

$$\mathbf{M}^{(s)}\ddot{\mathbf{u}}^{(s)} + \mathbf{C}^{(s)}\dot{\mathbf{u}}^{(s)} + \mathbf{K}^{(s)}\mathbf{u}^{(s)} = \mathbf{f}^{(s)} \tag{3.15}$$

where $\mathbf{M}^{(s)}$, $\mathbf{C}^{(s)}$ and $\mathbf{K}^{(s)}$ are the $n^{(s)} \times n^{(s)}$ substructure mass, damping and stiffness matrices, respectively, and $\mathbf{f}^{(s)}$ is a $n^{(s)} \times 1$ substructure load vector. By inserting Eq. 3.14 in Eq. 3.15 and pre-multiplying with $\mathbf{T}^\top$ a reduced subsystem is given by:

$$\tilde{\mathbf{M}}^{(s)}\ddot{\mathbf{q}}^{(s)} + \tilde{\mathbf{C}}^{(s)}\dot{\mathbf{q}}^{(s)} + \tilde{\mathbf{K}}^{(s)}\mathbf{q}^{(s)} = \tilde{\mathbf{f}}^{(s)} \tag{3.16}$$

where

$$\tilde{\mathbf{M}}^{(s)} = \mathbf{T}^\top\mathbf{M}^{(s)}\mathbf{T}, \quad \tilde{\mathbf{C}}^{(s)} = \mathbf{T}^\top\mathbf{C}^{(s)}\mathbf{T}, \quad \tilde{\mathbf{K}}^{(s)} = \mathbf{T}^\top\mathbf{K}^{(s)}\mathbf{T}, \quad \tilde{\mathbf{f}}^{(s)} = \mathbf{T}^\top\mathbf{f}^{(s)}.$$

Here, $\tilde{\mathbf{M}}^{(s)}$, $\tilde{\mathbf{C}}^{(s)}$ and $\tilde{\mathbf{K}}^{(z)}$ are the $m^{(s)} \times m^{(s)}$ reduced system matrices and $\tilde{\mathbf{f}}^{(s)}$ is a $m^{(s)} \times 1$ reduced load vector (henceforth, the superscript s will be left out to simplify the notation).

In most CMS methods, a reduction basis is constructed using some form of pseudo-static and vibrational modes [7]. In particular, a set of pseudo-static modes may be constructed such that the generalized coordinates correspond to the physical displacements in the substructure boundary DOFs. This is convenient when enforcing intercomponent compatibility, i.e. the

components can be assembled in a standard fashion as superelements. Accordingly, the reduced coordinate vector $\mathbf{q}^{(s)}$ may include both physical DOFs, referred to as master or boundary DOFs, and generalized coordinates representing the amplitudes of component modes.

3.2.1 Condensation methods

Neglecting damping, the equation of motion in partitioned form for a substructure can be written as:

$$\begin{bmatrix} \mathbf{M}_{ii} & \mathbf{M}_{ib} \\ \mathbf{M}_{bi} & \mathbf{M}_{bb} \end{bmatrix} \begin{bmatrix} \ddot{\mathbf{u}}_i \\ \ddot{\mathbf{u}}_b \end{bmatrix} + \begin{bmatrix} \mathbf{K}_{ii} & \mathbf{K}_{ib} \\ \mathbf{K}_{bi} & \mathbf{K}_{bb} \end{bmatrix} \begin{bmatrix} \mathbf{u}_i \\ \mathbf{u}_b \end{bmatrix} = \begin{bmatrix} \mathbf{f}_i \\ \mathbf{f}_b \end{bmatrix} \tag{3.17}$$

where the subscripts i and b denotes the interior and interface boundary DOFs, respectively. If assumed force-free, the interior DOFs can be expressed as:

$$\mathbf{u}_i = -\mathbf{K}_{ii}^{-1} \left(\mathbf{M}_{ii}\ddot{\mathbf{u}}_i + \mathbf{M}_{ib}\ddot{\mathbf{u}}_b + \mathbf{K}_{ib}\mathbf{u}_b \right). \tag{3.18}$$

Using a CMS approach, the inertia effects related to the interior DOFs are considered by a component mode superposition according to Eq. 3.14. In particular, CMS methods where $\mathbf{q}$ only contains physical master DOFs are often referred to as *condensation methods*, which are arguably the most straightforward techniques.

The most common condensation method is Guyan reduction [18], where the inertia terms in Eq. 2.7 are ignored. This leads to the following transformation matrix:

$$\begin{bmatrix} \mathbf{u}_i \\ \mathbf{u}_b \end{bmatrix} = \begin{bmatrix} \mathbf{\Psi}_{ib} \\ \mathbf{I}_{bb} \end{bmatrix} \mathbf{u}_b = \mathbf{T}_G \mathbf{q} \tag{3.19}$$

where $\mathbf{I}_{bb}$ is a $m \times m$ identity matrix, $\mathbf{\Psi}_{ib} = -\mathbf{K}_{ii}^{-1}\mathbf{K}_{ib}$ is the interior part of the component modes, and $\mathbf{T}_G$ is the $n \times m$ Guyan transformation matrix. The columns of the transformation matrix are the so-called constraint modes, obtained by prescribing a unit displacement for a boundary DOF, while the interior DOFs are force-free and the other boundary DOFs are held fixed. Thus, for a beam element, the constraint modes correspond to the mode shapes shown in Figure 2.3. Further, note that if retaining only one boundary DOF, the reduced system is in fact a *generalized* SDOF system, as discussed in Section 2.1.1.

Using condensation methods, the displacement of the boundary nodes is related to a set of component modes. In the Guyan reduction technique, these modes are based on the static displacement of the boundary, and accordingly "exact" results are achieved for static loading on the substructure boundary. For dynamic loading, however, the accuracy is highly dependent on the forcing frequency and the selected master DOFs.

Other condensation methods have been developed where the component modes are chosen differently. For example, the stiffness matrix can be replaced by the dynamic stiffness matrix, often referred to as dynamic reduction. Using this approach "exact" results can be obtained in

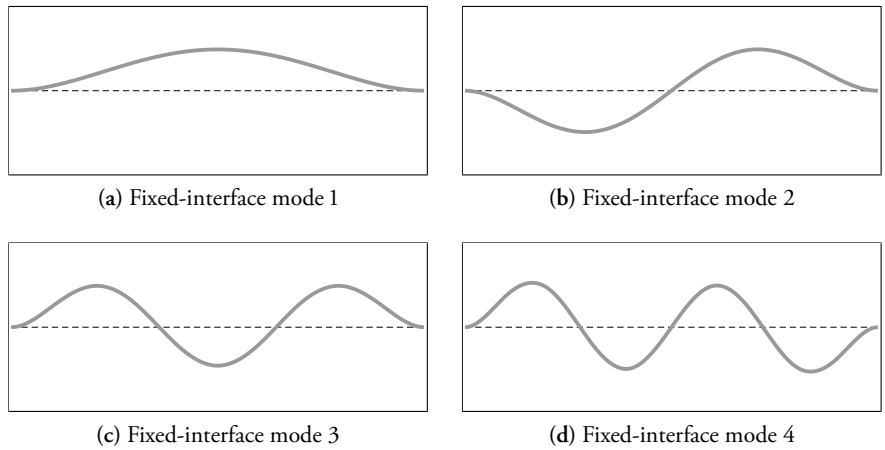

(**a**) Fixed-interface mode 1 (**b**) Fixed-interface mode 2

(**c**) Fixed-interface mode 3 (**d**) Fixed-interface mode 4

Figure 3.1: First four fixed-interface normal modes for beam element, with rotational and transversal DOFs at beam ends being boundary DOFs.

a steady state analysis for a certain forcing frequency. However, such a system is not "statically complete", i.e. the set of component modes does not span the possible displacements of the interior DOFs due to static loading on the boundary (note that the Guyan reduction can be interpreted as a dynamic reduction being evaluated at zero frequency). Other more sophisticated condensation methods have been developed, such as Improved Reduction System (IRS) and System Equivalent Reduction Expansion Process (SEREP) [11]. However, the number of exact resonances is always less or equal to the number of boundary nodes.

3.2.2 Fixed-interface methods

The component modes associated to the boundary DOFs, employed in the condensation methods, can be complemented by additional modes which enables reduced models that are both statically complete and that compensates for the neglected inertia terms related to the interior DOFs (cf. Eq. 3.18). These reduction methods, where the reduced coordinate vector includes both physical and/or generalized coordinates, may be divided into fixed- and free-interface methods [1]. The most common method is a fixed-interface method, namely the Craig–Bampton (C-B) method developed in the late 1960s [19], where the constraint modes are augmented by a set of fixed-interface normal modes (see Figure 3.1).

By setting the boundary displacements to zero in Eq. 3.17, the fixed-interface normal modes are obtained by the generalized eigenvalue problem:

$$\left(\mathbf{K}_{ii} - \omega_j^2 \mathbf{M}_{ii}\right) \{\phi_i\}_j = 0 \tag{3.20}$$

where $\mathbf{K}_{ii}$ and $\mathbf{M}_{ii}$ are the interior stiffness and mass matrices, respectively. The transforma-

tion matrix is then given by:

$$\begin{bmatrix} \mathbf{u}_i \\ \mathbf{u}_b \end{bmatrix} = \begin{bmatrix} \mathbf{\Phi}_{ik} & \mathbf{\Psi}_{ib} \\ \mathbf{0}_{bk} & \mathbf{I}_{bb} \end{bmatrix} \begin{bmatrix} \mathbf{q}_k \\ \mathbf{u}_b \end{bmatrix} = \mathbf{T}_{\mathrm{C-B}}\mathbf{q} \tag{3.21}$$

where the subscript k denotes the retained fixed-interface normal modes, $\mathbf{T}_{\mathrm{C-B}}$ is the Craig-Bampton transformation matrix, and $\mathbf{\Phi}_{ik}$ and $\mathbf{\Psi}_{ib}$ are the interior part of the set of fixed-interface normal modes and constraint modes, respectively. By setting $k \ll n_i$, a reduction is achieved in terms of a truncated fixed-interface modal basis. In contrast, if all fixed-interface modes are included in the basis, one obtain a pure transformation, without reducing the number of variables. Moreover, an important property of the C-B method is that the portion of the reduced system matrices related to the fixed-interface normal modes will by diagonal, thus, the reduced system matrices will in general be sparse (see further [1]).

A transformation according to Eq. 3.21 is employed in the standard C-B approach. In the early 2000s, an extension of the C-B method was proposed where the set of fixed-interface normal modes is augmented by higher order static correction modes [6]. The approach is similar to the generalized MTA method, discussed in Section 2.2.5. In particular, loading on the substructure boundary is considered in the derivation and, moreover, the static modes can be generated in a computationally efficient manner by means of matrix–vector multiplications.

If assuming that the external forces only act on boundary DOFs, the top row of Eq. 3.17 can be rewritten as:

$$\mathbf{M}_{ii}\ddot{\mathbf{u}}_i + \mathbf{K}_{ii}\mathbf{u}_i = -\mathbf{M}_{ib}\ddot{\mathbf{u}}_b - \mathbf{K}_{ib}\mathbf{u}_b. \tag{3.22}$$

Hence, the substructure interior DOFs can be considered excited by imposed displacement on its boundary. Similarly to the derivation in Section 2.2.3, a recursive procedure can be derived such that the displacement of the interior DOFs can be approximated as:

$$\mathbf{u}_i \approx -\mathbf{K}_{ii}^{-1}\mathbf{K}_{ib}\mathbf{u}_b + \sum_{j=1}^{k} \left(-\mathbf{K}_{ii}^{-1}\mathbf{M}_{ii}\right)^{j-1} \mathbf{K}_{ii}^{-1}\mathbf{Y}\frac{\mathrm{d}^{2j}\mathbf{u}_b}{\mathrm{d}t^{2j}} \tag{3.23}$$

where $\mathbf{Y} = \mathbf{M}_{ii}\mathbf{K}_{ii}^{-1}\mathbf{K}_{ib} - \mathbf{M}_{ib}$. As in the generalized MTA method, the higher order derivatives may be replaced by generalized coordinates in a dynamic response analysis. Moreover, the static corrections may be computed using the residual flexibility, as discussed in Section 2.2.5 (recall that the inverse of the stiffness matrix can be expressed in terms of a spectral expansion, cf. Eq. 2.39). Then, a set of jth-order corrections modes are given by:

$$\psi_{i,\mathrm{cor}.j} = \left(\mathbf{K}_{ii}^{-1} - \sum_{r=1}^{k} \frac{\phi_r\phi_r^\top}{\omega_r^2}\right) \left(\mathbf{M}_{ii}\mathbf{K}_{ii}^{-1}\right)^{j-1}\mathbf{Y}. \tag{3.24}$$

The resulting set of correction modes are mass- and stiffness-orthogonal to the fixed-interface normal modes. Similarly to the generalized MTA method, the correction modes can be made mutually orthogonal by solving a small eigenvalue problem. Then, a transformation matrix of

the following form can be obtained:

$$\begin{bmatrix} \mathbf{u}_i \\ \mathbf{u}_b \end{bmatrix} = \begin{bmatrix} \mathbf{\Phi}_{ik} & \widetilde{\mathbf{\Psi}}_{il,\text{cor.}} & \mathbf{\Psi}_{ib} \\ \mathbf{0}_{bk} & \mathbf{0}_{bl} & \mathbf{I}_{bb} \end{bmatrix} \begin{bmatrix} \mathbf{q}_k \\ \mathbf{q}_l \\ \mathbf{u}_b \end{bmatrix} = \mathbf{T}_{\text{C-B,cor.}}\mathbf{q} \tag{3.25}$$

where the columns of the matrix $\widetilde{\mathbf{\Psi}}_{il,\text{cor.}}$ are the total set of l pseudostatic modes and $\mathbf{T}_{\text{C-B,cor.}}$ is the transformation matrix where the fixed-interface modal basis is augmented by higher order static modes.

The higher order static modes, as introduced above, are force-dependent in the sense that loading on the substructure boundary DOFs is considered. However, it should be noted that the above procedure implies that the number of pseudo-static modes generated in each iteration correspond to the number of boundary DOFs. Hence, if the number of boundary DOFs is large, this methodology is best used in combination with a interface reduction technique, as further discussed in Section 3.2.4.

In both the standard C-B method and in an approach where the fixed-interface modal basis is augmented by higher order static modes, the physical boundary DOFs are retained in the reduction process. Hence, a global assembly can be formed in a straightforward manner using any of the assembly methods discussed in Section 3.1.

3.2.3 Free-interface methods

In the 1970s, so-called free-interface methods where developed by MacNeal, Rubin, and Craig and Chang [20–22]. Instead of fixed-interface component modes, these methods uses a reduction basis including free-interface normal modes and, possibly, rigid body modes.

The free-interface normal modes ϕ_j (cf. Figure 3.2) are obtained by the generalized eigenvalue problem:

$$\left(\mathbf{K} - \omega_j^2\mathbf{M}\right)\{\phi\}_j = 0 \tag{3.26}$$

where $\mathbf{K}$ and $\mathbf{M}$ are the component stiffness and mass matrices, respectively. Note that these matrices, in contrast to the system matrices in Eq. 3.20, include partitions related to both the interior and boundary DOFs (cf. Eq. 3.17).

Further, using a free-interface approach, the constraint modes employed in the fixed interface methods are replaced by attachment modes, corresponding to unit loading on the boundary DOFs. More specifically, an attachment mode correspond to a unit load applied on a boundary DOF while the other DOFs are force-free.

Moreover, the attachment modes can be computed based on the component residual flexibility, i.e. similar to what is done in the generalized MTA method as well as the fixed-interface CMS approach including higher-order static modes (see Sections 2.2.5 and 3.2.2, respectively).

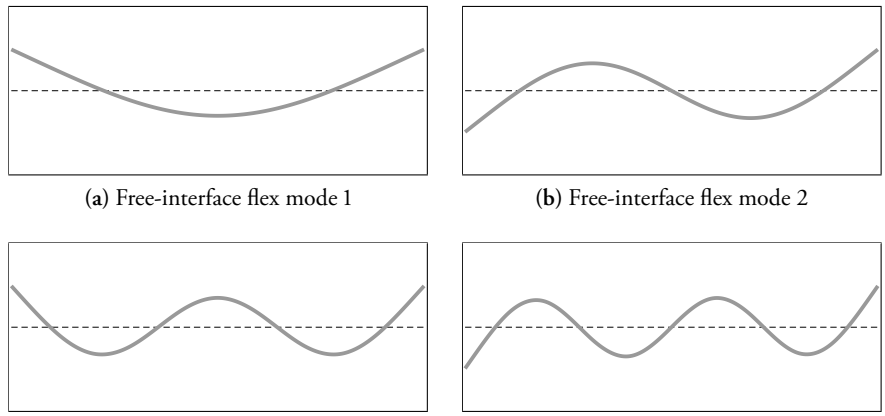

(a) Free-interface flex mode 1 (b) Free-interface flex mode 2

(c) Free-interface flex mode 3 (d) Free-interface flex mode 4

Figure 3.2: First four free-interface flex modes for beam element with free-free boundary conditions.

Then, the *residual* attachment modes can be expressed as:

$$\mathbf{\Psi}_{nb} = \begin{bmatrix} \mathbf{\Psi}_{ib} \\ \mathbf{\Psi}_{bb} \end{bmatrix} = \mathbf{G}_{\text{res}} \begin{bmatrix} \mathbf{0}_{ib} \\ \mathbf{I}_{bb} \end{bmatrix} \tag{3.27}$$

where $\mathbf{G}_{\text{res}}$ is the components residual flexibility matrix. Hence, in accordance with Eq. 3.27, the residual attachment modes correspond to columns of the residual flexibility matrix.

Furthermore, the residual flexibility matrix can be expressed in terms of the spectral expansion of the inverse stiffness matrix (cf. Section 2.2.5):

$$\mathbf{G}_{\text{res}} = \sum_{j=k+1}^{n} \frac{\phi_j \phi_j^\top}{\omega_j^2} = \left(\mathbf{K}^+ - \sum_{j=1}^{k} \frac{\phi_j \phi_j^\top}{\omega_j^2} \right) \tag{3.28}$$

where, k is the number of retained free-interface eigenmodes ϕ_j (excluding rigid body modes), with the corresponding eigenfrequency ω_j. Further, $\mathbf{K}^+$ is a pseudo-inverse of the component stiffness matrix. Here, it should be noted that a computation of $\mathbf{G}_{\text{res}}$ based on the discarded modes, i.e. using the summation from $k+1$ to n in Eq. 3.28, is in general not feasible, because it necessitates a computation of all free-interface eigenmodes. Therefore, the second expression in Eq. 3.28 is used in practice.

For components constrained such that there are no rigid body modes, the component stiffness matrix is invertible and the residual attachment modes can be computed in a straightforward manner (i.e. $\mathbf{K}^+ = \mathbf{K}^{-1}$). However, if rigid body modes are present, which in general is the case, the stiffness matrix will be singular and a pseudo-inverse of the stiffness matrix is required.

Recall that the attachment modes correspond to unit loading on the boundary DOFs (cf. Eq 3.27). It follows that the problem of finding a pseudo-inverse can in principle be replaced by

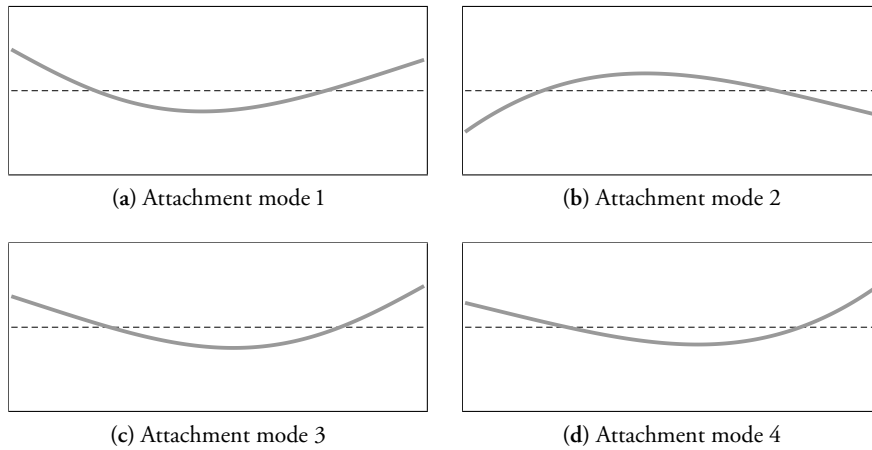

(**a**) Attachment mode 1 (**b**) Attachment mode 2

(**c**) Attachment mode 3 (**d**) Attachment mode 4

Figure 3.3: Inertia-relief attachment modes corresponding to loading at transversal (1 and 3) and rotational (2 and 4) DOFs at beam ends.

the problem of finding self-equilibrated force systems replacing the unit forces on the boundary DOFs (cf. Figure 3.3). A detailed description of how to compute a pseudo-inverse using this approach can e.g. be found in [1]. In summary, a pseudo-inverse, referred to as the *constrained flexibillity matrix*, is first computed by constraining suitable DOFs. Then, a projection matrix termed *inertia-relief projection matrix* is constructed which converts a given force vector to a self-equilibrated force system. Further, by post-mutiplying the constrained flexibillity matrix with the inertia-relief projection matrix one obtain a matrix whose columns correspond to modes of self-equilibrated force systems. Finally, by pre-multiplying with the transpose of the inertia-relief projection matrix the corresponding modes are made orthogonal to the rigid body modes. The pseudo-inverse obtained using this procedure actually correspond to the elastic flexibility matrix, i.e. a spectral expansion of the inverse of the stiffness matrix where the rigid body modes are excluded (indeed, including rigid body modes in Eq. 3.28 would imply division by zero).

Now, a transformation matrix can be defined based on the rigid body modes, free-interface eigenmodes, and the residual-flexibility attachment modes, i.e.

$$\begin{bmatrix} \mathbf{u}_i \\ \mathbf{u}_b \end{bmatrix} = \begin{bmatrix} \boldsymbol{\Phi}_{ir} & \boldsymbol{\Phi}_{ik} & \boldsymbol{\Psi}_{ib} \\ \boldsymbol{\Phi}_{br} & \boldsymbol{\Phi}_{bk} & \boldsymbol{\Psi}_{bb} \end{bmatrix} \begin{bmatrix} \mathbf{q}_r \\ \mathbf{q}_k \\ \mathbf{g}_b \end{bmatrix} = \mathbf{T}_{\mathrm{RFA}} \mathbf{q}. \tag{3.29}$$

Here, r denotes the rigid body modes, $\mathbf{g}_b$ contain the generalized coordinates representing the amplitude of the residual attachment modes, and $\mathbf{T}_{\mathrm{RFA}}$ is the so-called *augmented free-interface transformation matrix* [1].

In a CMS technique where the boundary DOFs are kept as physical DOFs, an assembly can be formed in a straightforward manner using any of the assembly methods discussed in Section 3.1. Using a transformation according to Eq. 3.29, where the constraint modes are re-

placed by attachment modes, this approach is not feasible. Instead, a global assembly has to be formed using alternative procedures, as further discussed below.

Using Eq. 3.1b, it follows that the compatibility condition can be expressed as:

$$\mathbf{B}\mathbf{u} = \mathbf{B}\hat{\mathbf{T}}\hat{\mathbf{q}} = \mathbf{B}_q\hat{\mathbf{q}} = \mathbf{0} \tag{3.30}$$

where

$$\hat{\mathbf{T}} = \operatorname{diag}\left(\mathbf{T}^{(1)}, \mathbf{T}^{(2)}, \ldots, \mathbf{T}^{(N)}\right) \quad \hat{\mathbf{q}} = \operatorname{diag}\left(\mathbf{q}^{(1)}, \mathbf{q}^{(2)}, \ldots, \mathbf{q}^{(N)}\right).$$

Furthermore, a matrix $\mathbf{L}_\mathbf{q} = \operatorname{null}(\mathbf{B}_q)$ may be formed. It follows that a global assembly may be enforced using e.g. a primal formulation according to Eq. 3.8 (recall that a primal assembly is enforced by projection onto the null-space of $\mathbf{B}$). Here, $\mathbf{B}_q$ and $\mathbf{L}_q$ are in general non-Boolean.

However, to further simplify the assembly process, it is convenient to formulate the reduced components such that the boundary DOFs are available on the substructure level, i.e. so that each component can be treated as a superelement. This can be achieved using MacNeal's and Rubin's methods, being free-interface methods that keeps the physical boundary DOFs.

By rearranging the terms in the bottom row of Eq. 3.29, the generalized coordinates $\mathbf{g}_b$ can be expressed as:

$$\mathbf{g}_b = \boldsymbol{\Psi}_{bb}^{-1}\left(\mathbf{u}_b - \boldsymbol{\Phi}_{br}\mathbf{q}_r - \boldsymbol{\Phi}_{bk}\mathbf{q}_k\right). \tag{3.31}$$

Then it follows that an additional transformation may be defined, i.e.:

$$\begin{bmatrix} \mathbf{q}_r \\ \mathbf{q}_k \\ \mathbf{g}_b \end{bmatrix} = \begin{bmatrix} \mathbf{I}_{rr} & \mathbf{0} & \mathbf{0} \\ \mathbf{0} & \mathbf{I}_{kk} & \mathbf{0} \\ -\boldsymbol{\Psi}_{bb}^{-1}\boldsymbol{\Phi}_{br} & -\boldsymbol{\Psi}_{bb}^{-1}\boldsymbol{\Phi}_{bk} & \boldsymbol{\Psi}_{bb}^{-1} \end{bmatrix} \begin{bmatrix} \mathbf{q}_r \\ \mathbf{q}_k \\ \mathbf{u}_b \end{bmatrix}. \tag{3.32}$$

Finally, by using both transformations, given by Eq. 3.29 and Eq. 3.32, a reduced substructure can be constructed such that the physical boundary DOFs are kept in the coordinate vector. Accordingly, a global assembly can be formed in a straightforward manner in terms of physical coordinates using any of the assembly methods in Section 3.1. This procedure is employed in the Rubin method. The MacNeal approach is very similar—an alternative approach is used for constructing a diagonal mass matrix, whereas the reduced stiffness matrix is identical in both methods (see e.g. [7] for further details).

In the Craig–Chang (C-C) method, the compatibility and equilibrium conditions are enforced in a slightly different manner. In particular, two assumptions regarding the generalized coordinate $\mathbf{g}_b$ are made, namely (1) that the inertia terms related to the corresponding residual attachment modes can be neglected and (2) that the interface forces alone drive the residual attachment modes [1]. To illustrate the assembly approach, consider two substructures, labeled 1 and 2, which are to be connected. Then, using the C-C approach, the compatibility and

equilibrium condition, respectively, are expressed as:

$$\begin{cases} \mathbf{u}_b^{(1)} - \mathbf{u}_b^{(2)} = \mathbf{0} & \text{(3.33a)} \\ \mathbf{g}_b^{(1)} + \mathbf{g}_b^{(2)} = \mathbf{0}. & \text{(3.33b)} \end{cases}$$

Further, Eq. 3.33 can be written in matrix form

$$\mathbf{B}_{\mathrm{C-C}}\mathbf{q} = \begin{bmatrix} \boldsymbol{\Phi}_{br}^{(1)} & \boldsymbol{\Phi}_{bk}^{(1)} & \boldsymbol{\Psi}_{bb}^{(1)} & -\boldsymbol{\Phi}_{br}^{(2)} & -\boldsymbol{\Phi}_{bk}^{(2)} & -\boldsymbol{\Psi}_{bb}^{(2)} \\ \mathbf{0} & \mathbf{0} & \mathbf{I} & \mathbf{0} & \mathbf{0} & \mathbf{I} \end{bmatrix} \begin{bmatrix} \mathbf{q}_r^{(1)} \\ \mathbf{q}_k^{(1)} \\ \mathbf{g}_b^{(1)} \\ \mathbf{q}_r^{(2)} \\ \mathbf{q}_k^{(2)} \\ \mathbf{g}_b^{(2)} \end{bmatrix} = \begin{bmatrix} \mathbf{0} \\ \mathbf{0} \end{bmatrix}. \tag{3.34}$$

Now, a transformation matrix $\mathbf{L}_{\mathrm{C-C}}$ may be formed using Eq. 3.7, by setting $\mathbf{B} = \mathbf{B}_{\mathrm{C-C}}$. It follows that a primal assembled system can be obtained using Eq. 3.8. Here, the matrix $\mathbf{B}_{\mathrm{C-C}}$ is in general non-boolean.

Using the C-C method, the generalized coordinates $\mathbf{g}_b$ corresponding to the residual attachment modes can be reduced out such that only the free-interface normal modes of the substructures are retained in the global coordinate vector. This may be advantageous in some applications, i.e. to keep the number of system variables to a minimum. A drawback, however, is that the physical boundary DOFs are not available in the assembled coordinate vector and, consequently, the reduced substructures cannot be coupled to e.g. nonlinear substructures being modeled in terms of physical displacements. Moreover, it should be noted that the interface forces are not required to be equal to the generalized coordinates $\mathbf{g}_b$ if using a C-C approach [1] (Eq. 3.33b actually states that the residual attachment mode coordinates should be equal, not the interface forces).

In contrast to the fixed-interface methods, the sparsity of the system matrices are in general lost when using the free-interface approaches discussed above. However, another free-interface method was developed in the early 2000s, referred to as the dual C-B method [23] which, unlike the other free-interface methods, preserves the sparsity of the system matrices. It does not employ a true Rayleigh–Ritz transformation, however, and the compatibility condition is enforced in a weakened sense. In particular, it requires special techniques to ensure stability in direct time-integration schemes [24].

Finally, it should be mentioned that also the free-interface reduction bases discussed above can be augmented by higher order quasi-static modes, see e.g. [25]. This is, however, not further investigated herein.

3.2.4 Interface reduction

In practical applications, the number of physical interface DOFs can often be very large and, therefore, much can be gained if an interface reduction is performed. In both the free- and fixed-interface CMS approaches the sparsity is lost in the parts of the system matrices related to interface DOFs. Hence, models including a large number of boundary DOFs can become computationally expensive.

Various approaches can be used for reducing the number of interface DOFs (see e.g. [26, 27]). In general, the preferred interface reduction approach depend on the specific application. In particular, a reduction may be performed on the substructure level, before the substructures are assembled or, in contrast, on the global assembled structure.

The simplest interface reduction approach is obtained by assuming rigid interfaces, i.e. by constraining the interface DOFs to the motion of a virtual master node, having three translational and three rotational DOFs (in a three-dimensional domain). Using a similar approach, the displacement of a virtual node may be defined as the weighted mean value of the interface DOFs, a constraint referred to as a *distributed coupling* (see e.g. [28, 29]). In particular, it turns out that the interface-forces on the interface DOFs are related to the weights. Accordingly, the sum of the weights is related to the interface force acting on the virtual node (also referred to as condensation node or master node). Hence, a distributed coupling can be employed for establishing a coupling with an arbitrary interface-force distribution (see further Paper C).

Furthermore, a reduction may be performed using a secondary eigenvalue analysis on the *bb*-partitions of the assembled system [1]. Thus, the interface DOFs are replaced by a truncated set of interface eigenvectors. Using this approach, however, the physical interface DOFs are lost in the reduction process.

4 Applications: structures with local nonlinearities

This chapter presents examples of structural engineering applications in which computationally efficient models can be of great utility in the design process, allowing for an interactive workflow where different design concepts may be tested. In particular, the structural dynamics problems involve transient loading and various forms of local nonlinear behavior, e.g. due to a nonlinear material behavior or local contact interactions. Consequently, a reduced order model cannot be established in a standard fashion using modal expansion techniques. However, since the nonlinear behavior is limited to certain spatial locations, reduced order models may be formulated using DS. Hence, the parts of the structures that remain linear-elastic may be represented by a reduced set of generalized coordinates, whereas the nonlinear parts are expressed in terms of physical displacements.

Strategies for establishing computationally efficient models are investigated in the appended papers using the methods discussed in Chapters 2 and 3. In particular, the developed models are suitable for implementation in user-friendly design tools, being streamlined for specific applications. For example, a parametric modeling process may be adopted, allowing for a time-efficient evaluation of modified parameters, such as dimensions and material properties.

Structural engineering applications within two relatively different areas are investigated, namely the design of concrete structures subjected to blast loading (Papers A and B) and glass panels subjected to impact loading (Paper C). Interestingly, however, some of the challenges with regard to the structural dynamics problems are similar. In particular, the response of higher order modes can be of considerable importance to achieve an accurate prediction of important output quantities. Furthermore, an accurate response prediction often necessitates a structural model that considers local nonlinearities, such as plastic hinges or local contact interactions.

(a) Flexural failure

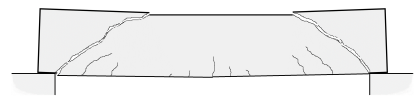

(b) Diagonal shear failure

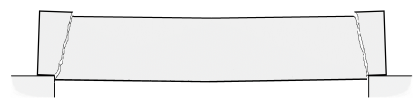

(c) Direct shear failure

Figure 4.1: Example of failure modes for reinforced concrete beam subjected to uniform impulse pressure.

4.1 CONCRETE STRUCTURES SUBJECTED TO BLAST LOADING

Several aspects in the structural design of concrete structures subjected to blast loading are fundamentally different compared to a verification of static loads. Not only the load-bearing capacity, but also the ductility of the structure is of considerable importance. To ensure that the structure can withstand the external pulse, it must be designed such that the induced kinetic energy can be absorbed. For example, the kinetic energy may be converted into elastic and plastic strain energy. Thus, the ductility of the structure, i.e. the capability to deform plastically without failure, is of importance. In particular, concrete members, such as beams and plates, must be designed to resist brittle failure modes.

With regard to the semi-global response (i.e. the global response of an individual member, such as beams and slabs) at least three failure modes must be considered to ensure an adequate design—flexural failure, diagonal shear failure, and direct shear failure, as shown in Figure 4.1 [3]. If designed using a bending reinforcement with sufficient ductility and an appropriate reinforcement arrangement, a flexural failure mode is typically desirable, while brittle failure modes, such as shear failure, should be avoided. Further, if a flexural failure mode can be ensured, the elastic strain energy upon failure is often significantly smaller than the plastic dissipation. Consequently, a model that considers the nonlinear structural behavior is required to avoid a too conservative design.

Generalized SDOF systems (cf. Section 2.1.1) are frequently used for evaluating concrete members, such as beams and slabs, subjected to blast loading. More specifically, a so-called equivalent SDOF system is formulated by means of an assumed shape function and a physical reference point, e.g. located at midspan. Then, equivalent stiffness, mass, and load are com-

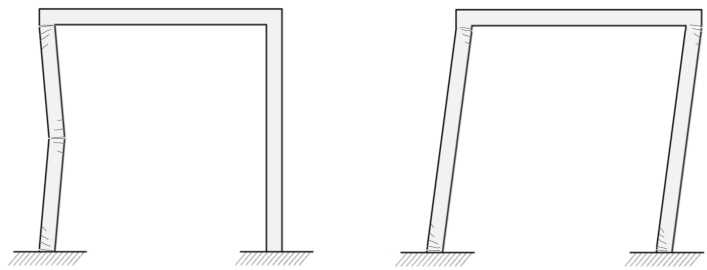

(**a**) Progressive collapse (**b**) Lateral stability

Figure 4.2: Example of failure modes for concrete frame structure subjected to blast loading.

puted such that the internal energy, kinetic energy, and external work is equivalent for the SDOF system and the continuous structure (see e.g. [30]). In particular, this approach allows for estimating the nonlinear elasto-plastic response of beams or slabs where plastic hinges/yield lines may develop, at least in an approximate manner. However, the locations of the plastic hinges are then predefined, e.g. at midspan for a simply supported beam. Further, the assumed mode shape is no longer continuous. Instead, a shape function is often obtained by neglecting the elastic deformation and only consider the plastic rotation at the plastic joints. Hence, the shape function correspond to a rigid body mode of the system, assuming free-rotation at the predefined joints (however, a combined elastic and plastic shape function can be considered in an approximate manner using weight factors). This methodology, proposed already in the mid 1960s [31], can be very useful, particularly in the conceptual design phase. In fact, if assuming that the pulse time is negligible, which is reasonable in many practical applications, a peak response can be estimated without conducting a response analysis, simply by considering the kinetic energy induced in the system due to the external impulse pressure.

Despite its utility, the approach using an equivalent SDOF system have several limitations. In particular, the response of higher order modes is neglected. For a concrete member subjected to blast loading, resulting in a very large pressure with short duration, the influence of higher order modes can, however, have a significant influence on the response. For example, the shear force close to supports might not be accurately represented by an SDOF model (see e.g. [32]). Particularly for concrete members without shear reinforcement, brittle failure modes such as shear failure can be of considerable importance.

In Paper A, the influence of higher order modes on the shear force close to supports is further investigated. More specifically, reduced models of beams with predefined plastic joints were developed by use of DS. The rotational DOFs at the plastic joints were selected as boundary DOFs, while the remaining structure being linear elastic was represented by a few fixed-interface eigenmodes. It should be emphasized, however, that a model having predefined plastic hinges only considers the ductility of flexural failure modes. Thus, any ductile behavior related to the shear failure modes is not considered. In practical applications, however, this is in general a reasonably conservative assumption.

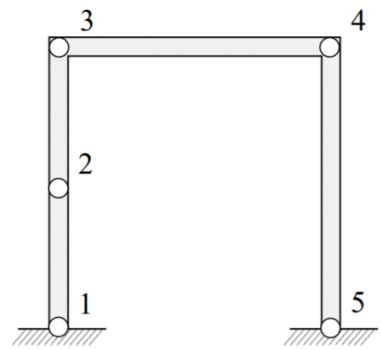

Figure 4.3: Example of predefined plastic hinges in an approximate model.

Moreover, using an SDOF model, a proper representation of the interaction between structural members and/or the global load-bearing structure is in general not attainable. Instead, the global structure is often considered rigid in the response analysis of an individual member. In many applications, this simplified approach can be sufficiently accurate, because the mass of the adjacent structure is often large compared to the effective mass of the individual member. However, in some applications a more refined representation of the interaction can be of importance. For example, consider the concrete frame in Figure 4.2, subjected to a uniformly distributed horizontal impulse pressure on the left column. Indeed, a verification of the failure modes shown in the figure, related to the lateral stability and progressive collapse, generally requires an integrated analysis, where the response of the frame columns and the horizontal beam are computed simultaneously (i.e. to consider mixed failure modes).

In Paper B, strategies are presented for modeling concrete-frame structures with an arbitrary number of predefined plastic joints. Furthermore, to enable computationally efficient models parts remaining linear elastic were reduced by means of DS. Considering the frame in Figure 4.2, an approximate model, being suitable at least in a conceptual design phase, can be established by allowing plastic hinges to be developed at five positions, as marked in Figure 4.3. Furthermore, a more accurate model can be obtained by including additional joints, e.g. by adding multiple joints at the frame corners, such that the mass of the frame corners are considered.

4.2 SOFT-BODY IMPACT ON GLASS PANELS

Building regulations in most countries prescribes that glass barriers, such as full-height façades and parapets for balconies or interior level changes, must be designed to withstand accidental impact of humans, if it constitutes a safety risk for building occupants. Accordingly, a verification of the load-bearing capacity with regards to soft-body impact may be required. To this end, a structural verification is often conducted by means of experimental tests using a stand-

ardized impactor described in EN 12600 [33]. Alternatively, the structural dynamic response is evaluated using dynamic calculations methods. In general, a simplified approach is employed where the response of higher order modes is neglected. Similarly to the methodology used for design of concrete members, a generalized SDOF system is established. Here, however, an integrated analysis of the glass panel and the soft impact body is in general necessary, thus, the glass panel is represented by a SDOF model which interacts with the soft impact body being modeled by a (linear or nonlinear) SDOF system. Hence, the structural dynamics problem at hand consist of a 2DOF system subjected to an initial velocity (see e.g. [34]).

The simplified modeling approach for verifying glass panels is similar to the approximate approach commonly used for concrete members in two ways—firstly, higher order modes of the glass panel/concrete member is neglected and, secondly, the adjacent structure is considered rigid. However, glass is a very brittle material, being essentially linear elastic before failure [35], while the steel reinforcement in a concrete structure can be arranged to obtain a ductile behavior. Hence, a nonlinear material description is often necessary in an analysis of concrete members while a glass panel can be considered linear elastic before failure. However, the load–displacement response of the standardized impactor, consisting of two pneumatic tires and steel weights, is nonlinear. Moreover, the contact interaction between the glass panel and the impactor gives rise to a nonlinear response. Thus, local nonlinearities are involved in both structural dynamics problems; local plastic hinges and local contact interactions, respectively. In addition, the response of glass panels, having a small thickness compared to the span width, can be nonlinear due to second order effects (i.e. membrane action). In many practical applications, however, the influence of geometric nonlinearity, being especially pronounced for

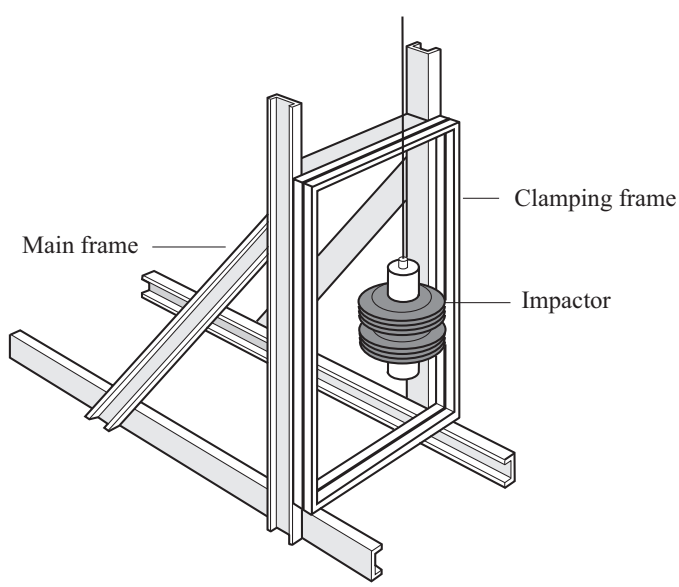

Figure 4.4: Standardized soft-body pendulum for glass classification according to the European Standard EN 12600 [33].

large glass panels with certain support conditions, can be neglected to obtain a reasonably conservative estimation of the glass strain.

In Paper C, experimental as well as numerical studies of simply-supported monolithic glass panels subjected to soft-body impacts are presented. In particular, the pre-failure elastic glass strain was measured on simply supported monolithic glass panels subjected to impact loading. The glass panels were mounted in a steel frame and impact loads were generated by releasing the standardized EN 12600 impactor from various drop heights. Furthermore, a detailed investigation was conducted to characterize the dynamic behavior of the standardized EN 12600 impactor. Moreover, a nonlinear viscous SDOF model representing the impactor was developed. The linear elastic response of the glass panel was represented by a reduced basis including a set of force-dependent Krylov-vectors (see Sections 2.2.3 and 3.2.2). A coupled system, including the impactor SDOF model as well as the reduced model representing the glass panel, was established by means of DS. For the load cases studied, it was shown that a 2DOF model can be fairly accurate. However, the problem of identifying an appropriate shape function for the glass panel is conveniently solved using a small reduction basis using a Krylov-subspace approach. Moreover, the influence of higher order modes can be expected to be more pronounced for larger glass panels or glass panels with other fixing methods.

5 Summary of appended papers

PAPER A

Reduced order modeling for the dynamic analysis of structures with nonlinear interfaces.

Linus Andersson, Peter Persson, Per-Erik Austrell, Kent Persson

In proceedings of COMPDYN 2019, 7:th International Conference on Computational Methods in Structural Dynamics and Earthquake Engineering, pp. 2395–2406, Crete, Greece, 2019.

Abstract

In the present paper, linear substructures with nonlinearities localized at their interfaces, such as the joints in a beam structure, are studied. By subdivision of the total structure into substructures, reduced subsystems are obtained by component mode synthesis. Nonlinear elements are introduced at supports or between substructures. A numerical example is presented where a beam subjected to blast loading is studied. The influence of the nonlinear behavior as well as the number of retained fixed-interface normal modes in the reduced subsystems are evaluated. The response is also compared to the response of equivalent single-degree-of-freedom systems, which are frequently employed in blast load design calculations. For the load cases studied, the displacement computed from an equivalent single-degree-of-freedom system correspond fairly well to the displacement given by a refined two-dimensional beam model, reduced by substructuring. In contrast, the shear force differs significantly due to that higher order modes are neglected in the single-degree-of-freedom system.

Contributions by Linus Andersson

Main author of the paper and wrote the manuscript. He formulated research aims, developed the modeling strategies, implemented the models and performed the simulations as well as synthesized the results and drew conclusions.

PAPER B

Model reduction for structures subjected to blast loading by use of dynamic substructuring.

Linus Andersson, Peter Persson, Kent Persson

In proceedings of EURODYN 2020, XI International Conference on Structural dynamics, pp. 2544–2564, Streamed from Athens, Greece, 2020.

Abstract

In the present study, strategies are developed to enable time-efficient models for structures subjected to blast loading, appropriate for use in a structural design process. Dynamic substructuring is employed to obtain reduced models with localized nonlinearities, such as predefined plastic hinges in a beam–column structure. The parts of the substructures that remains linear elastic are modeled by Ritz-vectors whereas parts with a nonlinear response are retained as physical degrees-of-freedom. Furthermore, a time-stepping method is presented that is shown to be suitable for reduced models including local and predefined rigid–plastic behavior. The proposed methodology is applied and demonstrated in a numerical example of a concrete frame structure. Both the well-established Craig-Bampton method and reduction bases enriched by so-called correction modes are evaluated. For the load case studied, it is shown that the standard Craig-Bampton technique is suitable for reducing the substructures. Furthermore, it is shown that only a few Ritz-vectors are needed to sufficiently describe the deformation of the structure. However, additional modes are needed to ensure an accurate representation of the interface forces between the substructures.

Contributions by Linus Andersson

Main author of the paper and wrote the manuscript. He formulated research aims, developed the modeling strategies, implemented the numerical models and performed the simulations. He synthesized the results and contributed to the conclusions drawn.

PAPER C

Reduced order modeling of soft-body impact on glass panels.

Linus Andersson, Marcin Kozłowski, Peter Persson, Per-Erik Austrell, Kent Persson

Submitted for publication in international journal.

Abstract

In the paper, strategies for reduced order modeling of glass panels subjected to soft-body impact are developed by means of dynamic substructuring. The aim is to obtain accurate and computationally efficient models for prediction of the pre-failure elastic response. More specifically, a reduction basis for the subsystem representing the glass panel is established using correction modes, being fixed-interface component modes that considers loading on the substructure boundary. The soft-body impactor is effectively modeled by a nonlinear single-degree-of-freedom system, calibrated by experimental data. Furthermore, a simplified and computationally efficient modeling approach is proposed for the contact interaction between the glass panel and the impact body. An experimental campaign was carried out to validate the developed models. In particular, the glass strain was measured on simply supported monolithic glass panels subjected to soft-body impact. Additional impact tests were performed to determine the dynamic characteristics of the impactor. Moreover, a detailed numerical reference model was developed to evaluate the discrepancy between the experimental tests and the results provided by the reduced order models. The developed models show good agreement with the experimental results. For the studied load cases, it is shown that an accurate prediction of the pre-failure glass strain can be obtained by systems including only a few generalized degrees-of-freedom.

Contributions by Linus Andersson

Main author of the paper and wrote the manuscript. He contributed to the conceptualization of ideas and experimental methodologies. He developed the numerical modeling strategies, implemented the numerical models and performed the simulations. He synthesized the results and contributed to the conclusions drawn.

6 Concluding remarks

6.1 CONCLUSIONS

Reduced order models were developed for use in structural engineering applications within two different areas, namely concrete structures subjected to blast loading and glass structures subjected to soft-body impact. In particular, modeling strategies were developed that are sufficiently accurate, computationally efficient and suitable for use in a structural design process. Moreover, the models consider the response of higher order modes as well as local nonlinearities. The main contributions to the research field are:

- Time-efficient and accurate modeling strategies for estimating the shear force in concrete structures subjected to blast loading (see Papers A and B).
- A time-stepping scheme for systems with local rigid–plastic behavior was proposed (see Paper B).
- Modeling strategies considering the response of higher order modes of glass panels subjected to soft-body impact (see Paper C).
- An experimental methodology for estimating the damping of the standardized EN 12600 impactor (see Paper C).
- A novel nonlinear viscous SDOF model was proposed for reduced modeling of the standardized EN 12600 impactor. In particular, a methodology for calibrating the model based on detailed FE models was presented (see Paper C).

Furthermore, a review of various reduced order modeling techniques is presented which, in a broader perspective, provide a basis for developing reduced order models in various structural engineering applications.

6.2 FURTHER RESEARCH

As mentioned in Chapter 4, the pre-failure elastic response of glass panels, having a small thickness compared to the span width, can be nonlinear due to second order effects (i.e. membrane action). Even though the influence of geometric nonlinearity is often negligible, it can be of importance in certain applications, e.g. for large four-sided, continuously supported glass panels. In fact, an SDOF model where the influence of second order effects is considered can be established in a straightforward manner. Because the model only include one generalized DOF, clearly, an arbitrary load-dependency may be defined. However, if the response is represented using a mode-superposition approach, this is no longer possible, at least not in a straightforward manner. Hence, a mode-superposition method requires a set of linearly independent mode shapes such that the total response can be obtained by summation of the modal contributions.

However, in the case of geometric nonlinearity, the polynomial structure of the nonlinear forces can be utilized to obtain a nonlinear reduced model. In particular, so-called nonintrusive methods have been developed during the last decades [36, 37]. The name nonintrusive refers to that the method can be employed without detailed knowledge of the source code of an FE-solver. More specifically, the nonlinear stiffness coefficients are determined using several static test cases. Using this methodology, reduced models that considers geometric nonlinearity may be developed, applied for analyzing glass panels as well as concrete structures.

References

[1] Craig, R.J., Kurdila, A. (2006), *Fundamentals of Structural Dynamics, 2nd Edition*, John Wiley & Sons, New Jersey.

[2] Pilkey, W. (2005), *Formulas for Stress, Strain and Structural Matrices, Second Edition*, Wiley, New York.

[3] Unified Facilities Criteria (UFC) (2008), *Structures to Resist the Effects of Accidental Explosions*, UFC 3-340-02, U. S. Army Corps of Engineers, Naval Facilities Engineering Command, Air Force Civil Engineer Support Agency.

[4] Bathe, K. (2006), *Finite element procedures*, Prentice Hall.

[5] Ottosen, N., Petersson, H. (1992), *Introduction to the finite element method*, Prentice Hall.

[6] Rixen, D. (2002), *High Order Static Correction Modes for Component Mode Synthesis*, in: *Proceedings of the fifth World Congress on Computational Mechanics, Vienna, Austria*.

[7] Voormeeren, S. (2012), *Dynamic Substructuring Methodologies for Integrated Dynamic Analysis of Wind Turbines*, PhD thesis, TU Delft.

[8] Trefethen, L., Bau III, D. (1997), *Numerical Linear Algebra*, SIAM, Philadelphia.

[9] Chopra, A. (2016), *Dynamics of structures. Theory and Applications to Earthquake Engineering, 5th Edition.*, Prentice Hall, New Jersey.

[10] Besselink, B., Tabak, U., Lutowska, A., van de Wouw, N., Nijmeijer, H., Rixen, D., Hochstenbach, M., Schilders, W. (2013), *A comparison of model reduction techniques from structural dynamics, numerical mathematics and systems and control*, Journal of Sound and Vibration **332**, 4403–4422.

[11] Flodén, O., Persson, K., Sandberg, G. (2014), *Reduction methods for the dynamic analysis of substructure models of lightweight building structures*, Computers and Structures **138**, 49–61.

[12] Hoen, C. (2005), *An Engineering Interpretation of the Complex Eigensolution of Linear Dynamic Systems*, in: *IMAC XXIII, Orlando, USA*.

[13] Jiang, Q., Zhou, Z., Huang, W. (2015), *Investigation on the Modal Strain Energy for Dynamic Analysis of Steel-Concrete Vertically Mixed Structures*, Journal of Asian Architecture and Building Engineering **14**(3), 671–678.

[14] Tsai, M., Chang, K. (2001), *A study of the modal strain energy method for viscoelastically damped structures*, Journal of the Chinese Institute of Engineers **24**(3), 311–320.

[15] Geradin, M., Rixen, D. (2014), *Mechanical Vibrations: Theory and Applications to Structural Dynamics, Third Edition*, Wiley, New York.

[16] de Klerk, D., Rixen, D., Voormeeren, S. (2008), *General Framework for Dynamic Substructuring: History, Review, and Classification of Techniques*, AIAA Journal **46**(5), 1169–1181.

[17] Farhat, C., Crivelli, L., Géradin, M. (1995), *Implicit time integration of a class of constrained hybrid formulations—Part I: Spectral stability theory*, Computer Methods in Applied Mechanics and Engineering **125**(1–4), 71–107.

[18] Guyan, R. (1965), *Reduction of Stiffness and Mass Matrices*, AIAA Journal **3**(2), 380.

[19] Craig, R., Bampton, M. (1968), *Coupling of Substructures for Dynamic Analysis*, AIAA Journal **6**(7), 1313–1319.

[20] MacNeal, R. (1971), *A Hybrid Method of Component Mode Synthesis*, Computers and Structures **1**(4), 581–601.

[21] Rubin, S. (1975), *Improved Component-Mode Representation for Structural Dynamic Analysis*, AIAA Journal **13**(8), 995–1006.

[22] Craig, R., Chang, C. (1977), *On the Use of Attachment Modes in Substructure Coupling for Dynamic Analysis*, in: *Proceedings of the 18th Structures, Structural Dynamics and Material Conference, San Diego, California*.

[23] Rixen, D. (2004), *A dual Craig–Bampton method for dynamic substructuring*, Journal of Computational and Applied Mathematics **168**(1–2), 383–391.

[24] Gruber, F., Gille, M., Rixen, D. (2017), *Time integration of dual Craig-Bampton reduced systems*, in: *Proceedings of the 6th ECCOMAS Thematic Conference on Computational Methods in Structural Dynamics and Earthquake Engineering (COMPDYN 2017), Rhodes Island, Greece*.

[25] Rixen, D. (2009), *Dual Craig-Bampton with enrichment to avoid spurious modes*, in: *Proceedings of the IMAC-XXVII, Orlando, USA*.

[26] Krattiger, D., Wu, L., Zacharczuk, M., Buck, M., Kuether, R., Allen, M., Tiso, P., Brake, M. (2019), *Interface reduction for Hurty/Craig-Bampton substructured models: Review and improvements*, Mechanical Systems and Signal Processing **114**, 579–603.

[27] Gibanica, M., Abrahamsson, T., Rixen, D. (2019), *Multifidelity component interface reduction and modal truncation augmentation*, International Journal for Numerical Methods in Engineering **120**(1), 105–124.

[28] Persson, P., Persson, K., Sandberg, G. (2016), *Reduced order modelling of liquid-filled pipe systems*, Journal of Fluids and Structures **61**, 205–217.

[29] Floden, O., Sandberg, G., Persson, K. (2018), *Reduced order modelling of elastomeric vibration isolators in dynamic substructuring*, Engineering Structures **155**, 102–114.

[30] Johansson, M., Laine, L. (2012), *Bebyggelsens motståndsförmåga mot extrem dynamisk belastning (in Swedish)*, Tech. Rep. MSB142, Swedish Civil Contingencies Agency (MSB).

[31] Biggs, J. (1964), *Introduction to Structural Dynamics*, McGraw-Hill, New York.

[32] Johansson, M. (2015), *Beräkningsstöd, Moment och tvärkraft (in Swedish)*, Tech. Rep. B06-201, Swedish Civil Contingencies Agency (MSB).

[33] SS-EN-12600 (2003), *Glass in building-pendulum test-impact test method and classification for flat glass*, Swedish Standards Institute.

[34] Schneider, J., Schula, S. (2016), *Simulating soft body impact on glass structures*, Proceedings of the Institution of Civil Engineers: Structures and Buildings **169**(6), 416–31.

[35] M., F., Kaspar, R., Abeln, B., Gessler, A., Langosch, K., Beyer, J.e.a. (2014), *Guidance for European structural design of glass components*, Publications Office of the European Union.

[36] Muravyov, A., Rizzi, S. (2003), *Determination of nonlinear stiffness with application to random vibration of geometrically nonlinear structures*, Computers and Structures **81**, 1513–1523.

[37] Mignolet, M., Przekop, A., Rizzi, S., Spottswood, S. (2013), *A review of indirect/non-intrusive reduced order modeling of nonlinear geometric structures*, Journal of Sound and Vibration **332**, 2437–2460.

Part II

Appended Publications

Paper A

Available online at www.eccomasproceedia.org
Eccomas Proceedia COMPDYN (2019) 2395-2406

ECCOMAS
Proceedia

COMPDYN 2019
7th ECCOMAS Thematic Conference on
Computational Methods in Structural Dynamics and Earthquake Engineering
M. Papadrakakis, M. Fragiadakis (eds.)
Crete, Greece, 24–26 June 2019

REDUCED ORDER MODELING FOR THE DYNAMIC ANALYSIS OF STRUCTURES WITH NONLINEAR INTERFACES

Linus Andersson [1], **Peter Persson** [1], **Per-Erik Austrell** [1], **Kent Persson** [1]

[1] Department of Construction Sciences, Lund University
P.O. Box 118, SE-221 00 Lund, Sweden
e-mail: {linus.andersson,peter.persson,per_erik.austrell,kent.persson}@construction.lth.se

Abstract

In the present paper, linear substructures with nonlinearities localized at their interfaces, such as the joints in a beam structure, are studied. By subdivision of the total structure into substructures, reduced subsystems are obtained by component mode synthesis. Nonlinear elements are introduced at supports or between substructures. A numerical example is presented where a beam subjected to blast loading is studied. The influence of the nonlinear behavior as well as the number of retained fixed-interface normal modes in the reduced subsystems are evaluated. The response is also compared to the response of equivalent single-degree-of-freedom systems, which are frequently employed in blast load design calculations. For the load cases studied, the displacement computed from an equivalent single-degree-of-freedom system correspond fairly well to the displacement given by a refined two-dimensional beam model, reduced by substructuring. In contrast, the shear force differs significantly due to that higher order modes are neglected in the single-degree-of-freedom system.

Keywords: Substructuring, Component Mode Synthesis, Blast Loading, Structural Dynamics

ISSN:2623-3347
Peer-review under responsibility of the organizing committee of COMPDYN 2019.
doi: 10.7712/120119.7082.19746

1 INTRODUCTION

Design of structures subjected to accidental loading, such as impact and blast loading, can be challenging compared to the design of static loading. As for dynamic loading in general, the structure mass, stiffness and strength affect the response and must be considered to determine whether a certain design fulfill the design code requirements. Consequently, it is often necessary to consider accidental loads in both the conceptual and detailed design phase and, therefore, it is important to employ simplified, conservative and computationally efficient models to estimate the structure response in a time-efficient manner. Moreover, the response computed from a large complex nonlinear model can be difficult to interpret and verify, hence, a smaller and less complex model simplifies the result evaluation.

In the present paper, linear substructures with nonlinearities localized at their interfaces, such as the joints in a beam structure, are studied. By subdivision of the total structure into substructures, reduced subsystems are obtained by dynamic substructuring [1]. Nonlinear elements are introduced at supports or between substructures [3]. The concept is presented in a numerical example in which a simply supported beam subjected to blast loading is studied. The influence of the nonlinear behavior as well as the number of retained fixed-interface normal modes in the reduced subsystem are evaluated. The response is also compared to the response of equivalent single-degree-of-freedom (SDOF) systems which are frequently employed in blast load design calculations.

2 REDUCED ORDER MODELING OF BEAMS SUBJECTED TO BLAST LOADING

The response of a linear structural dynamic system can be analyzed in a computationally efficient manner by considering an approximate reduced order model. For example, the response of a few important eigenmodes can form a reduced model. However, in analyses related to blast loading it is important to include the nonlinear behavior to ensure a model that predicts a realistic structural response. The material nonlinearities are often localized to certain areas such as plastic hinges in heavily loaded beams and plates. Hence, the structure can be subdivided into substructures with a linear response, connecting the nonlinear elements introduced at the supports or between substructures. Since each subsystem is linear, dynamic substructuring can be employed to form a reduced model.

2.1 Impulse pressure due to unconfined explosion

An unconfined explosion results in a shock wave that moves radially away from the center of the explosion [6]. Upon impact, the initial wave is reinforced and reflected. The reflected impulse acting on the structure is characterized by a very large pressure and short duration. For design purposes, the reflected impulse can, in general, be replaced by an equivalent triangular pulse where the actual duration is replaced by a fictitious duration, calculated based on the peak reflected pressure and reflected impulse. Moreover, if the explosion is unconfined and the explosion center is reasonable far from the structure considered, the pressure acting on a structure member can, in general, be approximated by a uniform pressure.

2.2 Single-degree-of-freedom systems

Equivalent SDOF systems are frequently employed for the design of the semi-global response of structural members subjected to blast loading, e.g. as proposed in [4]. This is a well-established approach compatible with the requirements in several design codes, e.g. UFC [6].

Equivalent SDOF systems can be derived for structures idealized as either beams or plates. In the study presented here only beams are considered.

The main assumption when developing an equivalent SDOF system is that the member deforms according to an assumed shape, $\varphi(x)$, which is constant through time. Hence, the member deflection $u(x,t)$ can be expressed as $\varphi(x)u_s(t)$, where u_s is the displacement of a reference point, e.g. the point of maximum displacement, see Figure 1. The shape function $\varphi(x)$ is often chosen as a Ritz vector corresponding to the static deflection of the external pressure. Note that, as for the deformed shape, the load distribution is assumed constant through time. The beam model is then transformed into a SDOF system by calculating an equivalent mass, stiffness and load in terms of the reference point displacement.

The equation of motion for an equivalent SDOF system can be expressed as:

$$\kappa_m m\ddot{u} + \kappa_k R(u) = \kappa_F p(t) \tag{1}$$

where κ_m, κ_k and κ_F are dimensionless transformation factors for the mass (m), resistance (R) and load (p), respectively. The mass factor, by which the total distributed mass of an element is multiplied to obtain an equivalent lumped mass, is derived by assuming conservation of kinetic energy [4]. If the mass is uniformly distributed, the mass factor for a beam with length L is given by:

$$\kappa_m = \frac{1}{L}\int_0^L \frac{\varphi(x)^2}{u_s{}^2}\,\mathrm{d}x \tag{2}$$

The load factor, by which the total pressure on the element is multiplied to obtain an equivalent concentrated force, is derived by assuming conservation of external work [4]. If the external pressure is uniformly distributed, the load factor for a beam with length L is given by:

$$\kappa_F = \frac{1}{L}\int_0^L \frac{\varphi(x)}{u_s}\,\mathrm{d}x \tag{3}$$

The resistance factor, by which the resistance of the structural element is multiplied to obtain the equivalent resistance of the SDOF system, is derived by assuming conservation of strain energy for the structural member, computed based on the assumed deformed shape. According to [4], it can be shown that the resistance-factor must always be equal to the load-factor, i.e.:

$$\kappa_k = \kappa_F \tag{4}$$

Hence, the equation of motion (1) for the SDOF system can be rewritten as

$$\frac{\kappa_m}{\kappa_F} m\ddot{u} + R(u) = p(t) \tag{5}$$

Consequently, the beam can be transformed into an equivalent SDOF system by scaling the mass only and, therefore, it is convenient to define a load-mass factor $\kappa_{mF} = \kappa_m/\kappa_F$.

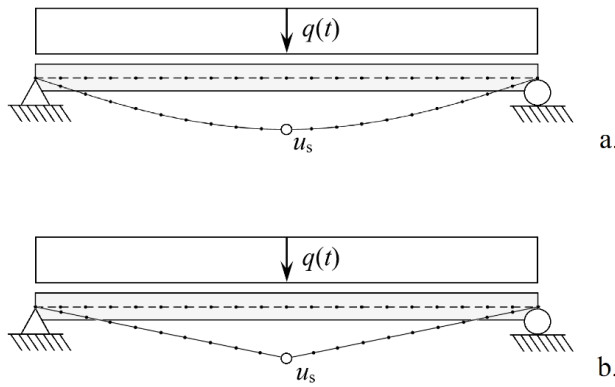

Figure 1: Assumed shape for elastic (a) and plastic (b) response.

When the ultimate moment capacity of a beam member is reached, in general, a plastic hinge is developed, which indeed affect the shape of the deflection. Hence, the assumed deflection shape considered for an elastic response, reasonable in the initial stage, differ significantly from the assumed plastic deflection shape which is reasonable in the second stage where a plastic hinge has been developed, cf. Figure 1. Moreover, the transformation factors given by Eqs. (2) and (3), which are constant through time, depend on the assumed shape $\varphi(x)$. Consequently, the equivalent SDOF system must be derived based on either an elastic or plastic deflection shape. For example, the κ_{mF} factors corresponding to a simply supported beam subjected to a uniform pressure are 0.787 and 0.667 for an elastic and plastic deflection shape respectively.

For a simply supported beam subjected to a uniform pressure the ultimate resistance can be calculated as:

$$R_{\mathrm{u}} = \frac{8M_{\mathrm{u}}}{L} \tag{6}$$

where M_{u} is the ultimate moment capacity, which implies that the maximum shear force at the supports can be calculated as $V = R_{\mathrm{u}}/2$. Hence, the ultimate moment capacity has, in general, a large impact on the shear force magnitude and clearly a larger moment capacity is not beneficial (however, the moment capacity must be sufficiently large to ensure that the plastic rotation is smaller than the rotation capacity). For example, if the amount of bending reinforcement in a concrete member is increased the amount of shear reinforcement due to blast loading must be increased accordingly. Since both the mass, stiffness and ultimate capacity affect the response, the design often requires iterative design calculations where simplified models, as the equivalent SDOF system, are important.

However, it should be noted that the shear force given by an equivalent SDOF system is computed with the assumption that the beam deflection shape is constant through time and, consequently, higher order modes are neglected. Furthermore, the shear forces are in general large at the initial stage, due to that higher order modes are excited. As e.g. observed in [7], the neglection of higher order modes indeed affect the precision of the shear force computed from an equivalent SDOF analysis.

For concrete members, a shear failure at the initial stage is referred to as a *direct shear* failure and is characterized by a rapid propagation of a vertical crack, located at the supports. Unlike *diagonal shear* failure, shear reinforcement perpendicular to the beam axis does not prevent this type of failure, instead inclined bars may be needed to ensure an adequate design. However,

it is in general not possible to determine the actual magnitude of the maximum shear force based on the response computed from an equivalent SDOF system.

2.3 Substructuring of beam model with plastic hinges

The response of a beam subjected to blast loading is, in general, elastic in a first stage and a mixture of both elastic and plastic in a second stage. Furthermore, in contrast to the response computed from an equivalent SDOF system, the fundamental mode as well as higher order modes are excited. To fully capture the structural behavior, it is therefore necessary to employ a nonlinear multi-degree-of-freedom (MDOF) model. Nonlinear analyses of large systems are, however, time consuming and might not be suitable in a design calculation. Nevertheless, a more refined model, compared to an equivalent SDOF system, might be necessary to enable accurate predictions of both the maximum displacement and shear force.

If the material nonlinearities are localized to certain areas, such as plastic hinges in heavily loaded beams, the total structure can be subdivided into substructures. Each substructure then consists of a subsystem with a linear response, connecting the nonlinear elements introduced at interfaces, i.e. at the supports or between substructures. Since each subsystem is linear, it is straight-forward to employ component mode synthesis (CMS) to form a reduced model [3]. Hence, a reduced model that captures a combined elastic and plastic response as well as including higher order modes can be derived. This procedure can be extended further to include both material and geometrically nonlinearities, i.e. to allow for large translations and rotations of the substructures. However, in the study presented here only material nonlinearities are considered.

The substructures can for example be reduced by condensation methods, such as Guyan reduction [2], where only physical DOFs are involved or by hybrid methods, such as component mode synthesis by Craig-Bampton or Krylov subspace component mode synthesis, where both physical and generalized DOFs are considered [8].

A finite element formulation of a subsystem leads to a linear equation of motion of the following form:

$$\mathbf{M}\ddot{\mathbf{u}} + \mathbf{C}\dot{\mathbf{u}} + \mathbf{K}\mathbf{u} = \mathbf{p} \tag{7}$$

Neglecting damping the partitioned mass and stiffness matrices can be written as:

$$\begin{bmatrix} \mathbf{M}_{ii} & \mathbf{M}_{ib} \\ \mathbf{M}_{bi} & \mathbf{M}_{bb} \end{bmatrix} \begin{bmatrix} \ddot{\mathbf{u}}_i \\ \ddot{\mathbf{u}}_b \end{bmatrix} + \begin{bmatrix} \mathbf{K}_{ii} & \mathbf{K}_{ib} \\ \mathbf{K}_{bi} & \mathbf{K}_{bb} \end{bmatrix} \begin{bmatrix} \mathbf{u}_i \\ \mathbf{u}_b \end{bmatrix} = \begin{bmatrix} \mathbf{p}_i \\ \mathbf{p}_b \end{bmatrix} \tag{8}$$

where the subscripts *i* and *b* denotes the *interior* and interface *boundary* DOFs, respectively. If assumed force-free, the interior DOFs can be expressed as:

$$\mathbf{u}_i = -\mathbf{K}_{ii}^{-1}(\mathbf{M}_{ii}\ddot{\mathbf{u}}_i + \mathbf{M}_{ib}\ddot{\mathbf{u}}_b + \mathbf{K}_{ib}\mathbf{u}_b) \tag{9}$$

By neglecting the inertia terms this leads to the following transformation matrix:

$$\begin{bmatrix} \mathbf{u}_i \\ \mathbf{u}_b \end{bmatrix} = \begin{bmatrix} -\mathbf{K}_{ii}^{-1}\mathbf{K}_{ib} \\ \mathbf{I}_{bb} \end{bmatrix} \mathbf{u}_b = \begin{bmatrix} \mathbf{\Psi}_{ib} \\ \mathbf{I}_{bb} \end{bmatrix} \mathbf{u}_b = \mathbf{T}_G \mathbf{u}_b \tag{10}$$

where $\mathbf{T}_G$ is the Guyan transformation matrix. By applying the transformation matrix to Eq. (7) a reduced system is given by:

$$\mathbf{M}_G\ddot{\mathbf{u}}_b + \mathbf{C}_G\dot{\mathbf{u}}_b + \mathbf{K}_G\mathbf{u}_b = \mathbf{p}_G \tag{11}$$

where,

$$\begin{aligned} \mathbf{M}_{\mathrm{G}} &= \mathbf{T}_{\mathrm{G}}{}^{\mathrm{T}}\mathbf{M}\mathbf{T}_{\mathrm{G}} \\ \mathbf{C}_{\mathrm{G}} &= \mathbf{T}_{\mathrm{G}}{}^{\mathrm{T}}\mathbf{C}\mathbf{T}_{\mathrm{G}} \\ \mathbf{K}_{\mathrm{G}} &= \mathbf{T}_{\mathrm{G}}{}^{\mathrm{T}}\mathbf{K}\mathbf{T}_{\mathrm{G}} \\ \mathbf{p}_{\mathrm{G}} &= \mathbf{T}_{\mathrm{G}}{}^{\mathrm{T}}\mathbf{p} \end{aligned} \tag{12}$$

The Craig-Bampton method combines the retained physical DOFs with fixed-interface normal modes, obtained by the generalized eigenvalue problem:

$$\left(\mathbf{K}_{ii} - \omega_j^2 \mathbf{M}_{ii}\right)\left\{\boldsymbol{\phi}_i\right\}_j = 0 \tag{13}$$

The eigenvectors are then normalized in order that

$$\boldsymbol{\Phi}_{ii}{}^{\mathrm{T}}\mathbf{M}_{ii}\boldsymbol{\Phi}_{ii} = \mathbf{I}_{ii} \tag{14}$$

where $\boldsymbol{\Phi}_{ii}$ is the complete set of fixed-interface normal modes. The physical coordinates can be represented as:

$$\begin{bmatrix}\mathbf{u}_i \\ \mathbf{u}_b\end{bmatrix} = \begin{bmatrix}\boldsymbol{\Phi}_{ik} & \boldsymbol{\Psi}_{ib} \\ \mathbf{0}_{bi} & \mathbf{I}_{bb}\end{bmatrix}\begin{bmatrix}\mathbf{q}_k \\ \mathbf{u}_b\end{bmatrix} = \mathbf{T}_{\mathrm{C\text{-}B}}\begin{bmatrix}\mathbf{q}_k \\ \mathbf{u}_b\end{bmatrix} \tag{15}$$

where the subscript k denotes the retained (*kept*) fixed-interface normal modes, $\mathbf{T}_{\mathrm{C\text{-}B}}$ is the Craig-Bampton transformation matrix, $\mathbf{q}_k$ is the generalized DOFs and $[\boldsymbol{\Psi}_{ib} \quad \mathbf{I}_{bb}]^{\mathrm{T}}$ is the interface constraint mode matrix, equal to the Guyan transformation matrix. Hence, the Craig-Bampton method can be interpreted as an extension of the Guyan reduction where the neglected inertia terms are compensated by including a set of fixed-interface normal modes.

By applying the transformation matrix to Eq. (7) a reduced system is given by:

$$\mathbf{M}_{\mathrm{C\text{-}B}}\begin{bmatrix}\ddot{\mathbf{q}}_k \\ \ddot{\mathbf{u}}_b\end{bmatrix} + \mathbf{C}_{\mathrm{C\text{-}B}}\begin{bmatrix}\dot{\mathbf{q}}_k \\ \dot{\mathbf{u}}_b\end{bmatrix} + \mathbf{K}_{\mathrm{C\text{-}B}}\begin{bmatrix}\mathbf{q}_k \\ \mathbf{u}_b\end{bmatrix} = \mathbf{p}_{\mathrm{C\text{-}B}} \tag{16}$$

where,

$$\begin{aligned} \mathbf{M}_{\mathrm{C\text{-}B}} &= \mathbf{T}_{\mathrm{C\text{-}B}}{}^{\mathrm{T}}\mathbf{M}\mathbf{T}_{\mathrm{C\text{-}B}} \\ \mathbf{C}_{\mathrm{C\text{-}B}} &= \mathbf{T}_{\mathrm{C\text{-}B}}{}^{\mathrm{T}}\mathbf{C}\mathbf{T}_{\mathrm{C\text{-}B}} \\ \mathbf{K}_{\mathrm{C\text{-}B}} &= \mathbf{T}_{\mathrm{C\text{-}B}}{}^{\mathrm{T}}\mathbf{K}\mathbf{T}_{\mathrm{C\text{-}B}} \\ \mathbf{p}_{\mathrm{C\text{-}B}} &= \mathbf{T}_{\mathrm{C\text{-}B}}{}^{\mathrm{T}}\mathbf{p} \end{aligned} \tag{17}$$

Note that each constraint mode is the deflection shape due to a unit displacement of a boundary DOF, while the interior DOFs are force-free and the other boundary DOFs are held fixed, i.e.

$$\begin{bmatrix}\mathbf{K}_{ii} & \mathbf{K}_{ib} \\ \mathbf{K}_{bi} & \mathbf{K}_{bb}\end{bmatrix}\begin{bmatrix}\boldsymbol{\Psi}_{ib} \\ \mathbf{I}_{bb}\end{bmatrix} = \begin{bmatrix}\mathbf{0}_{ib} \\ \mathbf{R}_{bb}\end{bmatrix} \tag{18}$$

where $\mathbf{R}_{bb}$ is the reaction forces acting on the substructure.

By using a similar procedure as presented above, the fixed-interface normal modes employed in the Craig-Bampton method can be replaced by other Ritz vectors, e.g. Krylov subspace vectors derived from a suitable load distribution, see for example [5].

3 NUMERICAL EXAMPLE: SIMPLY SUPPORTED CONCRETE BEAM SUBJECTED TO BLAST LOADING

3.1 Reduced two-dimensional beam model

The effect of higher order modes on the displacement and shear force is studied by evaluating the response for a simply supported concrete beam subjected to a uniform distributed impulse pressure. The beam length is L = 3 m and the cross-section width and height is 1000 mm and 200 mm respectively. The load consists of a uniform reflected impulse pressure of 1500 Pa·s. Two load cases are studied with a peak reflected pressure of 1000 kPa in Load Case 1 and 300 kPa in Load Case 2, respectively. The pulse is approximated by an equivalent triangular pulse, hence, a fictitious duration can be calculated to 3 ms and 10 ms for Load Cases 1 and 2 respectively.

The beam is assumed to consist of concrete C30/37 with reinforcement Ø16s200 K500C-T. The modulus of elasticity for concrete and reinforcement steel is 32 GPa and 200 GPa respectively and the density for reinforced concrete is set to 2500 kg/m^3. The ultimate moment capacity is set to M_p = 80 kNm. The response is calculated with a two-dimensional beam model with a total of 20 Euler-Bernoulli two-node beam elements, as shown in Figure 2. Due to symmetry, only half of the beam is included in the FE model. Furthermore, small deformations are considered and the axial DOFs of the beam elements are neglected. It is assumed that a plastic hinge can appear at the beam midspan only. The plastic hinge is modelled by adding a rigid-perfectly plastic rotational spring to the rotational DOF at the symmetry line, as shown in Figure 2. Several effects are neglected in the model, e.g. catenary effects, reduced stiffness due to concrete cracking, concrete spalling etc. Nevertheless, the beam model is appropriate for evaluating the influence of higher order modes on the shear force and midspan displacement.

The beam model consists of a linear elastic subsystem, namely the beam element assemblage, which is connected to a nonlinear element. As discussed in Section 2, a reduced model can therefore be obtained by substructuring, e.g. by Guyan reduction or CMS by Craig-Bampton. Only one boundary DOF is kept, i.e. the rotational DOF at the beam symmetry line, denoted with superscript *b* in Figure 2. All other DOFs are internal DOFs and denoted with superscript *i* in Figure 2. Accordingly, the fixed-interface normal modes are calculated with fixed boundaries, i.e. with fixed rotation at the symmetry line. Hence, the substructure normal modes correspond to the symmetric eigenmodes for a simply supported beam, which are also the only modes that are excited by a uniform load. Thus, for an elastic response the system response is equivalent to the response of a linear elastic simply supported beam analyzed with modal truncation.

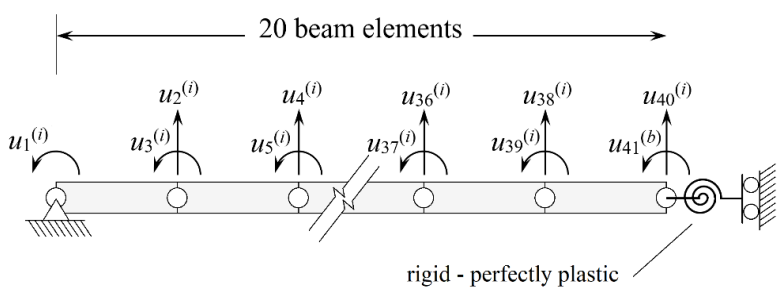

Figure 2: Two-dimensional beam model with nonlinear rotational spring at the symmetry line.

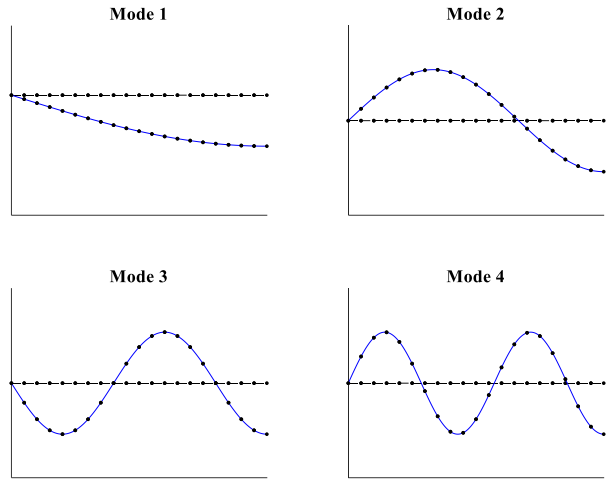

Figure 3: First four fixed-interface normal modes.

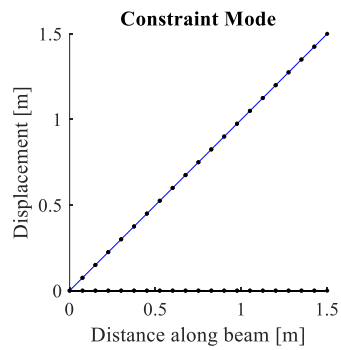

Figure 4: Constraint mode.

3.2 Structural analysis and results

In Figure 3 the first four fixed-interface normal modes are shown, which correspond to the first, third, fifth and seventh eigenmodes for a simply supported beam. Hence, by employing a symmetry model instead of a full model both the number of physical DOFs and modal coordinates are halved.

The constraint mode is shown in Figure 4 and correspond to a unit rotation of the boundary DOF, i.e. a unit rotation of the rotational DOF at the symmetry line. Hence, the constraint mode corresponds to a rigid body mode of the beam element assemblage which in turn correspond to the plastic deflection shape considered for an equivalent SDOF system, cf. Figure 1b.

The nonlinear dynamic response is calculated using the Newmark β-method with $\gamma = ½$ and $\beta = ¼$ (constant average acceleration) combined with the modified Newton-Raphson method. The total analysis time is 50 ms and the time-stepping is performed with very fine time increment < 0.01 ms to ensure sufficient resolution of the shear force.

The midspan displacement and shear force at the supports are evaluated for the beam model reduced by both Guyan reduction and the Craig-Bampton method for Load Cases 1 and 2 respectively. The response is compared to the response computed from an equivalent SDOF system. The stiffness of the SDOF system is calculated based on an uncracked cross section and the ultimate resistance is computed from the ultimate moment capacity, according to Eq. (6). A plastic deflection shape in accordance with Figure 1b is considered when determining the load-mass factor.

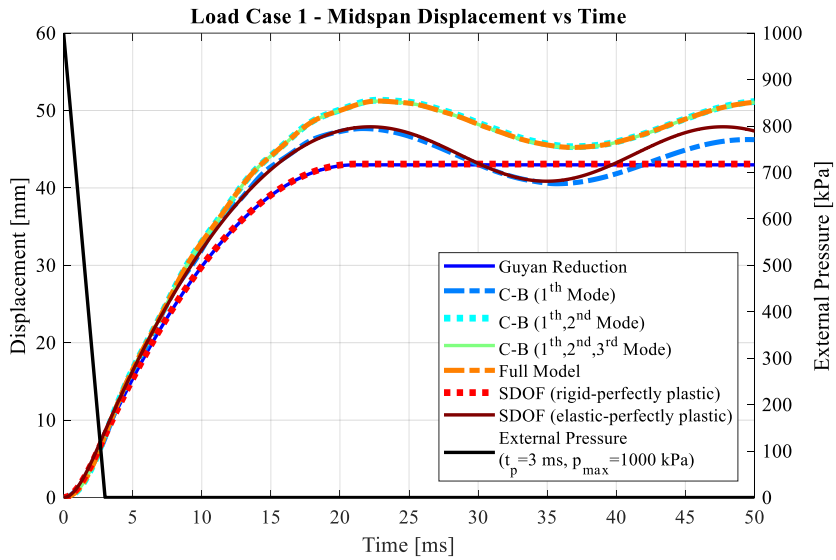

Figure 5: Midspan displacement vs. time for Load Case 1.

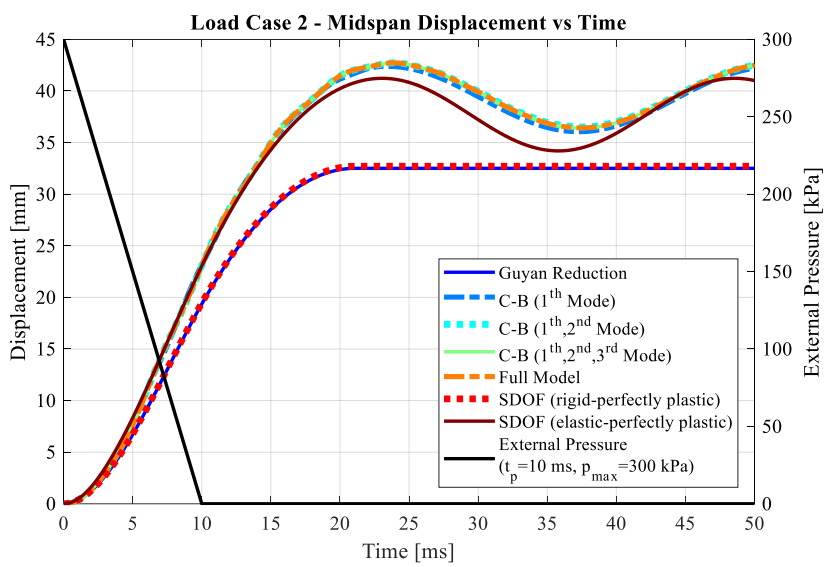

Figure 6: Midspan displacement vs. time for Load Case 2.

As shown in Figure 6, the midspan displacement for Load Case 2 calculated by the two-dimensional beam model is close to the displacement computed from an equivalent SDOF system. However, for Load Case 1 the response somewhat differs due to a larger influence of higher order modes, see Figure 5. Furthermore, as shown in Figures 5 and 6, only two fixed-interface normal modes need to be retained to obtain a response very close to the response for the full unreduced model.

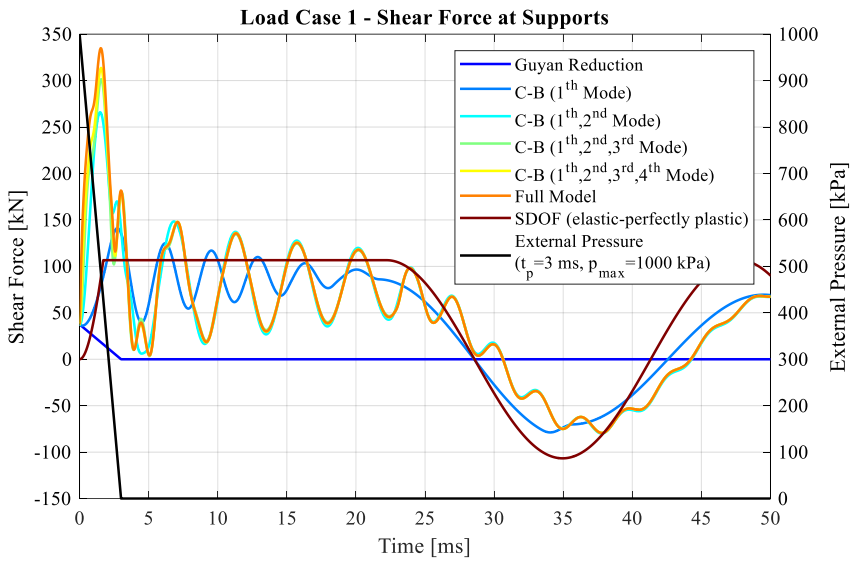

Figure 7: Shear force at supports for Load Case 1.

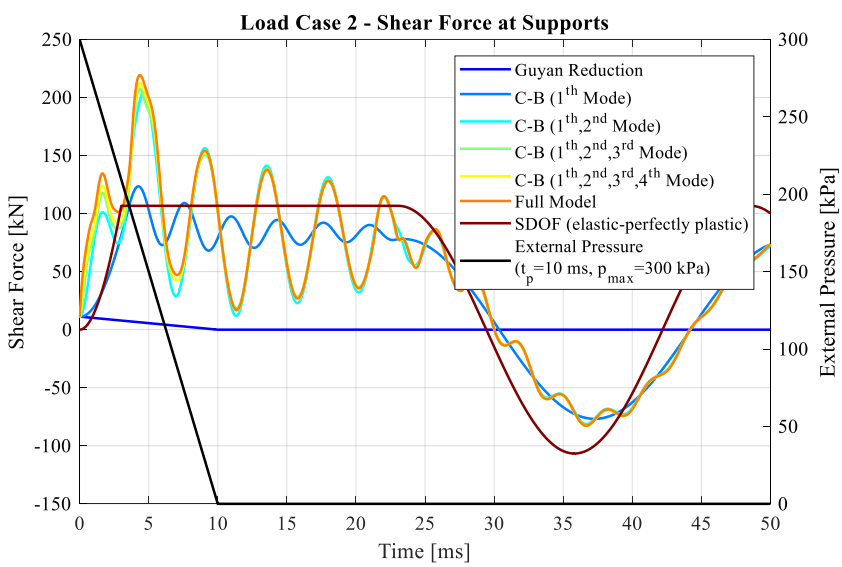

Figure 8: Shear force at the supports for Load Case 2.

The response obtained with Guyan reduction is included for comparison only. Additional boundary (or master) DOFs must be added to increase the precision of the Guyan reduction. As shown in Figures 5 and 6, a Guyan reduction where only the rotational DOF at the symmetry line is kept correspond to an equivalent rigid-plastic SDOF system, i.e. only the rigid mode of the beam assemblage is activated and the external work is dissipated by plastic deformation of the rigid-perfectly plastic rotational spring alone.

The shear force at the supports for Load Cases 1 and 2, computed from both an equivalent SDOF system and the two-dimensional beam model, are shown in Figures 7 and 8, respectively. As shown in the figures, the shear force computed from the two-dimensional model is, as expected, much larger due to that higher order modes are considered. The difference is greater for Load Case 1, where the impulse duration is shorter. As shown in Figure 7, at least four fixed-interface normal modes need to be included to capture the peak shear force. For Load Case 2, however, the shear force computed from a reduced model with two to three fixed-interface normal modes is fairly close to the peak shear force given by the full model.

Note that the shear force is $V \neq 0$ at $t = 0$. This is due to the discretization of the beam substructure. Half of the pressure on the beam element connected to the vertical support is instantaneously transferred to the support. Hence, the shear force/reaction force at $t = 0$ due to discretization can be calculated as $V(0) = p(0) \cdot L/(2 \cdot 2 \cdot \mathrm{n})$, where n is the number of beam elements in the symmetry model. Since a Guyan reduction only includes a rigid body mode of the beam elements the shear force should clearly be equal to zero, thus, the shear force shown in the diagrams is only due to the discretization of the beam assemblage. For Load Cases 1 and 2 the shear force due to discretization is calculated to 38 kN and 11 kN, respectively, i.e. in accordance with the response shown in Figures 7 and 8.

4 CONCLUSIONS

In the present paper, linear substructures with nonlinearities localized at their interfaces, such as plastic hinges in a beam member, are studied. By subdivision of the structure into substructures, reduced subsystems are obtained by use of the Craig-Bampton method. A numerical example is presented where a simply supported beam subjected to blast loading is studied.

For the Load Cases studied, the midspan displacement computed from an equivalent SDOF system, which are frequently employed in blast load design calculations, correspond fairly well to the displacement computed from a refined two-dimensional beam model, reduced by substructuring. In contrast, the shear force computed from an equivalent SDOF systems differ significantly from the peak shear force given by a refined two-dimensional beam model. This is due to that higher order modes are neglected in the equivalent SDOF system. As expected, the difference is greater for Load Case 1, where the beam is subjected to a pulse with higher peak pressure and shorter duration. To capture the peak shear force at least the first three to four fixed-interface normal modes need to be included in the reduced model. However, one boundary DOF and three to four generalized DOFs result in a MDOF system with five DOFs, which is still a very small system appropriate for time efficient iterative design calculations in both the conceptual and detailed design phase.

For a simply supported beam with a plastic hinge at the midspan the boundary DOFs in the Craig-Bampton method can be selected so that the linear response is equivalent to a linear elastic beam analyzed by modal truncation. Furthermore, the fixed-interface normal modes employed in the Craig-Bampton method can be replaced by other Ritz vectors, such as Krylov subspace vectors, which are derived from the current load configuration. Krylov subspace component mode synthesis can be expected to be efficient if the load configuration does not match the first normal modes.

ACKNOWLEDGMENTS

The research was carried out in the framework of the project "Urban Tranquility" under the Interreg V program funded by the European Regional Development Fund, as well as within the research project titled "Wooden Buildings in Silent Sustainable Cities", funded by the Swedish Governmental Agency for Innovation Systems (Vinnova), grant ref. no. 2018-04159.

REFERENCES

[1] D. de Klerk, D.J. Rixen, S.N. Voormeeren, General Framework for Dynamic Substructuring: History, Review, and Classification of Techniques, *AIAA Journal*, **46 (5)**, 1169-1181, 2008.

[2] R.J. Guyan, Reduction of Stiffness and Mass Matrices, *AIAA Journal*, **3 (2)**, 380, 1965.

[3] Bathe K.-J., Gracewski S., On nonlinear dynamic analysis using substructuring and mode superposition, *Computers and Structures*, **13**, 699-707, 1981.

[4] Biggs J.M., *Introduction to Structural Dynamics*, McGraw-Hill, New York, 1964.

[5] O. Flodén, K. Persson, G. Sandberg, Reduction methods for the dynamic analysis of substructure models of lightweight building structures, *Computers and Structures*, **138**, 49-61, 2014.

[6] Unified Facilities Criteria (UFC), *Structures to Resist the Effects of Accidental Explosions*, U. S. Army Corps of Engineers, Naval Facilities Engineering Command, Air Force Civil Engineer Support Agency, UFC 3-340-02, 5 December 2008.

[7] M. Johansson, B06-201, *Beräkningsstöd, Moment och tvärkraft* (in Swedish), Swedish Civil Contingencies Agency (MSB), 2015.

[8] R.R. Jr. Craig, A.J. Kurdila, *Fundamentals of Structural Dynamics, 2nd Edition*, John Wiley & Sons, New Jersey, 2006.

Paper B

Available online at www.easdprocedia.org
EASD Procedia EURODYN (2020) 2544-2564

EASD Procedia

EURODYN 2020
XI International Conference on Structural Dynamics
M. Papadrakakis, M. Fragiadakis, C. Papadimitriou (eds.)
Athens, Greece, 23–26 November 2020

MODEL REDUCTION FOR STRUCTURES SUBJECTED TO BLAST LOADING BY USE OF DYNAMIC SUBSTRUCTURING

Linus Andersson, Peter Persson, Kent Persson

Department of Construction Sciences, Lund University
P.O. Box 118, SE-221 00 Lund, Sweden
e-mail: {linus.andersson, peter.persson, kent.persson}@construction.lth.se

Keywords: Dynamic substructuring, Blast loading, Direct time-integration, Beam frame structure

Abstract. *In the present study, strategies are developed to enable time-efficient models for structures subjected to blast loading, appropriate for use in a structural design process. Dynamic substructuring is employed to obtain reduced models with localized nonlinearities, such as predefined plastic hinges in a beam–column structure. The parts of the substructures that remains linear elastic are modeled by Ritz-vectors whereas parts with a nonlinear response are retained as physical degrees-of-freedom. Furthermore, a time-stepping method is presented that is shown to be suitable for reduced models including local and predefined rigid–plastic behavior. The proposed methodology is applied and demonstrated in a numerical example of a concrete frame structure. Both the well-established Craig-Bampton method and reduction bases enriched by so-called correction modes are evaluated. For the load case studied, it is shown that the standard Craig-Bampton technique is suitable for reducing the substructures. Furthermore, it is shown that only a few Ritz-vectors are needed to sufficiently describe the deformation of the structure. However, additional modes are needed to ensure an accurate representation of the interface forces between the substructures.*

ISSN:2311-9020
Peer-review under responsibility of the Organizing Committee of EURODYN 2020.
doi: 10.47964/1120.9207.19160

1 INTRODUCTION

Simplified models, such as equivalent single-degree-of-freedom (SDOF) systems, are often used for design of concrete members subjected to blast loading, an approach proposed already in the mid-1960s [1]. When this simplified approach is used for studying individual structural members, the supporting global structure is often considered as rigid and thus represented by prescribed displacement boundary conditions in the local response analyses. Hence, if a global response analysis is required it is in general performed in a subsequent stage, where the reaction forces computed in the local analyses are applied on the global structure. Such a procedure can be suitable if the stiffness and/or mass of the global structure are relatively large. However, in cases where the structural member is stiff and heavy, or even integrated as a part of the global lateral load-bearing structure, it can be necessary to employ a model of the coupled system. Furthermore, it can be necessary to include higher order modes to accurately capture the force transmitted between individual members and the global structure, in particular if the structure is subjected to a pulse with short duration and large peak pressure, as e.g. discussed in [2].

The dynamic response of a structure can e.g. be computed by use of a nonlinear finite element (FE) model, including the members subjected to external loading and the supporting global structure. However, the design of concrete structures subjected to blast loading is often an iterative process, where the cross-section dimensions and the amount and arrangement of bending reinforcement affect the dynamic response. Therefore, simplified and computationally efficient models are key in the conceptual design phase.

In the present study, strategies are developed to enable time-efficient models for structures subjected to blast loading, appropriate for use in a structural design process. More specifically, reduced models with localized nonlinearities, such as predefined plastic hinges in a beam–column structure, are obtained by use of dynamic substructuring (DS) (for an overview of DS techniques see e.g. [3,4]). Hence, parts that remains linear elastic are reduced and modeled by Ritz-vectors whereas the degrees-of-freedom (DOFs) included in parts with a nonlinear response are retained as physical DOFs. Furthermore, a time-stepping scheme is presented that is shown to be suitable for reduced models including local and predefined rigid–plastic behavior, such as frame structures with plastic hinges.

2 SIMPLIFIED MODELING OF CONCRETE STRUCTURES SUBJECTED TO BLAST LOADING

As for dynamic loading in general, the design of concrete structures subjected to blast loading can be challenging due to that the response is affected by the structure's mass, stiffness and strength. Hence, a modification of the dimensions, the amount and/or arrangement of reinforcement must, in general, be verified by an updated dynamic response analyses. Furthermore, a nonlinear response analysis is often required. The kinetic energy induced by the external pressure is converted into elastic and plastic strain energy, and if the plastic dissipation is omitted in the analysis the response can be inaccurate, e.g. resulting in a very conservative design. Therefore, simplified nonlinear SDOF models are often employed to evaluate the response of individual structural members.

In addition to the design of individual members, the global structure must be designed to resist progressive collapse and to ensure lateral stability. If a nonlinear response analysis is required for studying the global response, it is in general not straight-forward to construct a simplified model. Hence, a more refined nonlinear FE model of the whole structure can be necessary.

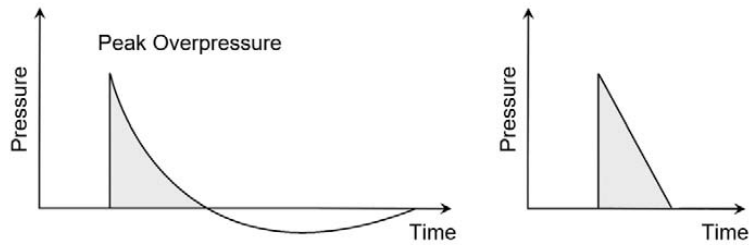

Figure 1: Typical (left) and idealized (right) blast pressure–time history.

2.1 Impulse pressure due to unconfined explosion

An unconfined explosion located on the ground surface results in a ground reflected shock wave that moves radially away from the center of the explosion [5]. If the explosion center is reasonable far from a structure, the pressure acting on the structure can be approximated by a uniform pressure. Upon impact, the initial wave is reinforced and reflected. The reflected impulse pressure acting on the structure is characterized by a very short duration and large peak pressure. For design purposes, the reflected impulse can, in general, be replaced by an equivalent triangular pulse, as shown in Figure 1. The actual duration is then replaced by a fictitious duration, computed from the peak reflected pressure and the reflected impulse.

2.2 Reduced models for design of concrete members

To ensure an adequate design of concrete members, such as beams and plates, subjected to blast loading, both the local response and the semi-global response (i.e. the global response of an individual member) must be considered. Hence, concrete members must be designed to resist local failure modes, such as punching shear failure, scabbing, spalling and penetration. Further, the shear force capacity and rotation capacity must be sufficiently large. Thus, it is crucial to ensure sufficient ductility and to avoid brittle failure modes.

A common procedure when evaluating the semi-global response of beams and plates is to set up an equivalent elasto-plastic SDOF system, where the yield force is derived from the ultimate moment capacity [1]. In fact, the yield force corresponds to the ultimate load, which implies that the maximum shear force in the dynamic response analysis is equal to the shear force given by a static yield line analysis. As e.g. shown in [2], the shear force computed using this simplified approach might be underestimated due to the neglection of higher order modes. Nonetheless, the approach can be reasonably accurate and in accordance with several design codes, such as UFC [5].

Using a simplified equivalent SDOF system implies that the position of the yield lines and/or plastic hinges can by assumed in accordance with a static yield line analysis, where the spatial load distribution correspond to the spatial distribution of the impulse pressure. This assumption is also the basis in the modeling strategies developed in Sections 3 and 4. However, it should be noted that this approach is primarily intended to be used in a conceptual design phase, i.e. a full nonlinear analysis can be necessary to verify the final design.

3 DYNAMIC SUBSTRUCTURING OF STRUCTURES WITH PLASTIC HINGES

By use of dynamic substructuring (DS) the aim is to efficiently compute the dynamic response of a structure by subdivision of the structure into substructures. Solving several substructures can be computationally less expensive than solving one large system. Moreover, DS can be employed to reduce systems with localized nonlinearities, such as predefined plastic

hinges in a beam–column structure. The parts of the structure that remains linear elastic is then reduced and modeled by Ritz-vectors whereas the DOFs included in parts with a nonlinear response are retained as physical DOFs.

In most DS techniques reduction is performed on the substructure level. Hence, the substructure displacements $\mathbf{u}^{(s)}$ are represented by a reduced set of coordinates $\mathbf{q}^{(s)}$, given by

$$\mathbf{u}^{(s)} = \mathbf{T}\mathbf{q}^{(s)} \tag{1}$$

where superscript s is the substructure label and $\mathbf{T}$ is a $n^{(s)} \times m^{(s)}$ transformation matrix, whose columns are Ritz-vectors, or so-called component modes. Depending on the DS technique, the reduced vector $\mathbf{q}^{(s)}$ can include physical master (or boundary) DOFs and/or generalized coordinates. Typically, $m^{(s)} << n^{(s)}$.

A FE formulation of a substructure leads to a linear equation of motion of the following form:

$$\mathbf{M}^{(s)}\ddot{\mathbf{u}}^{(s)} + \mathbf{C}^{(s)}\dot{\mathbf{u}}^{(s)} + \mathbf{K}^{(s)}\mathbf{u}^{(s)} = \mathbf{p}^{(s)} \tag{2}$$

where $\mathbf{p}^{(s)}$ is a $n^{(s)} \times 1$ substructure load vector and $\mathbf{M}^{(s)}$, $\mathbf{C}^{(s)}$ and $\mathbf{K}^{(s)}$ are the $n^{(s)} \times n^{(s)}$ substructure mass, damping and stiffness matrices, respectively. By inserting Equation (1) in (2) and pre-multiplying with $\mathbf{T}^{\mathrm{T}}$ the reduced subsystem is given by:

$$\widetilde{\mathbf{M}}^{(s)}\ddot{\mathbf{q}}^{(s)} + \widetilde{\mathbf{C}}^{(s)}\dot{\mathbf{q}}^{(s)} + \widetilde{\mathbf{K}}^{(s)}\mathbf{q}^{(s)} = \tilde{\mathbf{p}}^{(s)} \tag{3}$$

where

$$\widetilde{\mathbf{M}}^{(s)} = \mathbf{T}^{\mathrm{T}}\mathbf{M}^{(s)}\mathbf{T}, \qquad \widetilde{\mathbf{C}}^{(s)} = \mathbf{T}^{\mathrm{T}}\mathbf{C}^{(s)}\mathbf{T}, \qquad \widetilde{\mathbf{K}}^{(s)} = \mathbf{T}^{\mathrm{T}}\mathbf{K}^{(s)}\mathbf{T}, \qquad \tilde{\mathbf{p}}^{(s)} = \mathbf{T}^{\mathrm{T}}\mathbf{p}^{(s)} \tag{4}$$

The size of the reduced system matrices $\widetilde{\mathbf{M}}^{(s)}$, $\widetilde{\mathbf{C}}^{(s)}$ and $\widetilde{\mathbf{K}}^{(s)}$ is thus $m^{(s)} \times m^{(s)}$ and the reduced load vector $\tilde{\mathbf{p}}^{(s)}$ is $m^{(s)} \times 1$ (to simplify the notation the superscript s will be left out until Section 3.3, on substructure coupling procedures). The substructures are then reassembled to form a reduced model of the full coupled system, why DS is sometimes referred to as Component Mode Synthesis (CMS).

Arguably the most straight-forward methods within DS are the so-called condensation methods, where only physical master DOFs are included in $\mathbf{q}$. The most common condensation method is Guyan reduction, also referred to as static condensation due to that inertia effects are ignored [6]. The Guyan transformation matrix is given by

$$\begin{bmatrix}\mathbf{u}_i \\ \mathbf{u}_b\end{bmatrix} = \begin{bmatrix}-\mathbf{K}_{ii}^{-1}\mathbf{K}_{ib} \\ \mathbf{I}_{bb}\end{bmatrix}\mathbf{u}_b = \begin{bmatrix}\boldsymbol{\Psi}_{ib} \\ \mathbf{I}_{bb}\end{bmatrix}\mathbf{u}_b = \mathbf{T}_{\mathrm{G}}\mathbf{q} \tag{5}$$

where the subscripts i and b denotes the *interior* and interface *boundary* DOFs, $\mathbf{T}_{\mathrm{G}}$ is the Guyan transformation matrix and $\mathbf{q}$ contains the physical boundary DOFs. The columns of the transformation matrix are the so-called constraint modes, obtained by prescribing a unit displacement for a boundary DOF, while the interior DOFs are force-free and the other boundary DOFs are held fixed. Using this approach, "exact" results are achieved for static loading. However, due to neglected inertia effects the accuracy can be expected to decrease with an increasing forcing frequency.

Using a similar procedure but replacing the stiffness matrix with the dynamic stiffness matrix, exact result can instead be achieved for a certain forcing frequency, often referred to as dynamic reduction. There are also other more sophisticated condensation methods, such as Improved Reduction System (IRS) and System Equivalent Reduction Expansion Process (SEREP),

where the number of exact resonances is less or equal to the number of boundary DOFs [7]. However, using condensation methods, it is not possible to both obtain a reduced model that is "statically complete" (i.e. a basis for all possible deformations that result from loading at the substructure boundary nodes) and at the same time keeping exact resonances. To achieve this, a CMS approach is required that uses generalized coordinates representing the amplitudes of additional Ritz-vectors.

Several CMS techniques have been developed since the 1960s, which can be divided into *fixed-interface* and *free-interface* methods. The most popular approach, a fixed-interface method, is CMS by Craig-Bampton (C-B), developed in the late 1960s [8]. The C-B method combines fixed-interface normal modes with so-called constraint modes, see further Section 3.1. Free-interface methods, using so-called free-interface component modes, were developed by MacNeal, Rubin and Craig and Chang in the 1970s [9,10,11]. In addition, another free-interface method, the dual Craig-Bampton method, was proposed in the early 2000s which, in contrast to the other free-interface methods, preserves the sparsity of the system matrices [12].

Reducing a structure with plastic hinges, it is important to employ a DS technique where the physical boundary DOFs, namely the rotational DOFs at the plastic hinges, are retained. Therefore, the CMS method proposed by Craig and Chang is excluded due to an assembling procedure that removes the physical boundary DOFs. The dual C-B method is an interesting approach since the interface forces are kept as DOFs in the assembled system. However, this method produces negative eigenvalues which make a stable time integration impossible [13] (an approach to overcome this issue is e.g. proposed in [13], unfortunately this approach includes removing all physical DOFs).

Apart from retaining the physical boundary DOFs at the plastic hinges, the plastic deformations of the assembled system must be resolved. Hence, the reduced subsystems should be "statically complete" and rigid body modes of the subsystems should be included in the reduction basis. Using the C-B method, the rigid body modes are not explicitly included in the reduction basis. However, the rigid body modes are spanned by the constraint modes. In fact, the set of constraint modes is a basis for all possible deformations that result from loading at the substructure boundary nodes [14]. In addition to the C-B method, the free-interface methods by MacNeal and Rubin retains the physical boundary DOFs in the assembled system and explicitly includes the rigid body modes in the reduction basis.

In summary, either the fixed-interface C-B method or the free-interface methods by MacNeal and Rubin are judged to be the most suitable methods for reducing a beam–column structure including predefined plastic joints. A free-interface approach can be expected to be more accurate upon yielding, i.e. when the joint stiffness is zero, whereas a fixed-interface approach can be expected to be more accurate when the joints are fixed, i.e. when yielding does not occur. Based on this observation it is assumed that the classic C-B approach, which preserves the sparsity of the system matrices, is the preferred choice.

3.1 Craig-Bampton method

The Craig-Bampton method combines the retained physical DOFs with generalized coordinates corresponding to the amplitudes of so-called fixed-interface normal modes. Neglecting damping the partitioned mass and stiffness matrices can be written as:

$$\begin{bmatrix} \mathbf{M}_{ii} & \mathbf{M}_{ib} \\ \mathbf{M}_{bi} & \mathbf{M}_{bb} \end{bmatrix} \begin{bmatrix} \ddot{\mathbf{u}}_i \\ \ddot{\mathbf{u}}_b \end{bmatrix} + \begin{bmatrix} \mathbf{K}_{ii} & \mathbf{K}_{ib} \\ \mathbf{K}_{bi} & \mathbf{K}_{bb} \end{bmatrix} \begin{bmatrix} \mathbf{u}_i \\ \mathbf{u}_b \end{bmatrix} = \begin{bmatrix} \mathbf{p}_i \\ \mathbf{p}_b \end{bmatrix} \tag{6}$$

By setting the boundary displacements to zero in Equation (6), the fixed-interface normal modes are obtained by the generalized eigenvalue problem:

$$\left(\mathbf{K}_{ii} - \omega_j^2 \mathbf{M}_{ii}\right)\left\{\boldsymbol{\phi}_i\right\}_j = 0 \tag{7}$$

where $\mathbf{K}_{ii}$ and $\mathbf{M}_{ii}$ are the interior stiffness and mass matrices. The eigenvectors are normalized so that $\boldsymbol{\Phi}_{ii}{}^{\mathrm{T}}\mathbf{M}_{ii}\boldsymbol{\Phi}_{ii} = \mathbf{I}_{ii}$, where $\boldsymbol{\Phi}_{ii}$ is the complete set of fixed-interface normal modes. The physical coordinates can then be represented as:

$$\begin{bmatrix}\mathbf{u}_i \\ \mathbf{u}_b\end{bmatrix} = \begin{bmatrix}\boldsymbol{\Phi}_{ik} & \boldsymbol{\Psi}_{ib} \\ \mathbf{0}_{bk} & \mathbf{I}_{bb}\end{bmatrix}\begin{bmatrix}\mathbf{q}_k \\ \mathbf{u}_b\end{bmatrix} = \mathbf{T}_{\text{C-B}}\mathbf{q} \tag{8}$$

where the subscript k denotes the kept fixed-interface normal modes, $\mathbf{T}_{\text{C-B}}$ is the Craig-Bampton transformation matrix, $\mathbf{q}_k$ is the generalized coordinates and $[\boldsymbol{\Psi}_{ib} \quad \mathbf{I}_{bb}]^{\mathrm{T}}$is the constraint mode matrix, equivalent to the Guyan reduction basis. Hence, the Craig-Bampton method can be interpreted as an extension of the Guyan reduction where the neglected inertia terms are compensated by including a set of fixed-interface normal modes.

3.2 Craig-Bampton with Modal Truncation Augmentation

The fixed-interface normal modes included in the C-B reduction basis can be augmented by so-called high order static correction modes, which can be interpreted as a form of generalization of the Guyan static modes. The C-B method with so-called Modal Truncation Augmentation (MTA) is presented in [15].

If the internal forces are zero, the top row of Equation (6) can be rewritten as:

$$\mathbf{M}_{ii}\ddot{\mathbf{u}}_i + \mathbf{K}_{ii}\mathbf{u}_i = -\mathbf{M}_{ib}\ddot{\mathbf{u}}_b - \mathbf{K}_{ib}\mathbf{u}_b \tag{9}$$

Hence, the substructure can be considered excited by imposed displacements on its boundary. Further, the internal displacements can be approximated as

$$\mathbf{u}_i = \mathbf{u}_{i,\text{stat}} + \mathbf{y} \tag{10}$$

where $\mathbf{u}_{i,\text{stat}} = -\mathbf{K}_{ii}{}^{-1}\mathbf{K}_{ib}\mathbf{u}_b$ is the quasi-static solution modified by the second term $\mathbf{y}$ to obtain the dynamic response, i.e. similarly to the well-established mode acceleration method, e.g. described in [16]. By inserting Equation (10) into Equation (9) the dynamic response of the relative solution is given by

$$\mathbf{M}_{ii}\ddot{\mathbf{y}} + \mathbf{K}_{ii}\mathbf{y} = -\mathbf{M}_{ii}\ddot{\mathbf{u}}_{i,\text{stat}} - \mathbf{M}_{ib}\ddot{\mathbf{u}}_b = \mathbf{Y}\ddot{\mathbf{u}}_b \tag{11}$$

where $\mathbf{Y} = \mathbf{M}_{ii}\mathbf{K}_{ii}{}^{-1}\mathbf{K}_{ib} - \mathbf{M}_{ib}$, which can be interpreted as inertia forces associated to static modes [15]. This procedure can be continued by replacing $\mathbf{y}$ with a quasi-static solution and a dynamic correction. Hence, a recursive procedure is obtained, indicating that the dynamic response can be approximated as

$$\mathbf{u}_i \approx -\mathbf{K}_{ii}{}^{-1}\mathbf{K}_{ib}\mathbf{u}_b + \sum_{j=1}^{n}\left(-\mathbf{K}_{ii}{}^{-1}\mathbf{M}_{ii}\right)^{j-1}\mathbf{K}_{ii}{}^{-1}\mathbf{Y}\frac{\mathrm{d}^{2j}\mathbf{u}_b}{\mathrm{d}t^{2j}} \tag{12}$$

where n is the number of static corrections.

According to Equation (12) a dynamic response analysis is not included in the approximation. However, if a dynamic analysis including k eigenmodes has been performed, part of the corrections is already considered. The expression for the higher order corrections can then be rewritten as:

$$\mathbf{u}_{i,cor.j} \approx \left(\mathbf{K}_{ii}^{-1} - \sum_{r=1}^{k} \frac{\boldsymbol{\phi}_r \boldsymbol{\phi}_r^{\mathrm{T}}}{\omega_r^2} \right) \left(-\mathbf{M}_{ii} \mathbf{K}_{ii}^{-1} \right)^{j-1} \mathbf{Y} \frac{\mathrm{d}^{2j} \mathbf{u}_b}{\mathrm{d}t^{2j}} \tag{13}$$

where we use that the inverse of the stiffness matrix can be expressed as

$$\mathbf{K}_{ii}^{-1} = \sum_{r=1}^{N} \frac{\boldsymbol{\phi}_r \boldsymbol{\phi}_r^{\mathrm{T}}}{\omega_r^2} = \sum_{r=1}^{k} \frac{\boldsymbol{\phi}_r \boldsymbol{\phi}_r^{\mathrm{T}}}{\omega_r^2} + \sum_{r=k+1}^{N} \frac{\boldsymbol{\phi}_r \boldsymbol{\phi}_r^{\mathrm{T}}}{\omega_r^2} \tag{14}$$

where N is the total number of eigenmodes, and $\boldsymbol{\phi}_r$ and ω_r is the eigenmode and eigenfrequency for mode r. Hence, the space already spanned by the fixed-interface normal modes is removed from the corrections. The total response is then given by

$$\mathbf{u}_i \approx \sum_{r=1}^{k} \boldsymbol{\phi}_r q_r + \sum_{j=0}^{n} \mathbf{u}_{i,cor.j} \tag{15}$$

where $\mathbf{u}_{i,cor.0} = -\mathbf{K}_{ii}^{-1} \mathbf{K}_{ib} \mathbf{u}_b$. Furthermore, the amplitudes $\frac{\mathrm{d}^{2j} \mathbf{u}_b}{\mathrm{d}t^{2j}}$ can be treated as separate DOFs, i.e. instead of high order corrections the modal basis is augmented by high order correction *modes*, also referred to as force-dependent Ritz-vectors or Krylov vectors. Hence, the j-th order correction modes is given by:

$$\mathbf{x}_{i,cor.j} = \left(\mathbf{K}_{ii}^{-1} - \sum_{r=1}^{k} \frac{\boldsymbol{\phi}_r \boldsymbol{\phi}_r^{\mathrm{T}}}{\omega_r^2} \right) \left(\mathbf{M}_{ii} \mathbf{K}_{ii}^{-1} \right)^{j-1} \mathbf{Y} \tag{16}$$

Note that the number of vectors generated in each iteration equals the number of boundary DOFs, why the subspace spanned by the generated vectors is sometimes referred to as a block-Krylov subspace [14]. The static correction modes are both mass- and stiffness-orthogonal to the fixed-interface normal modes. However, they are not mutually orthogonal. This can e.g. be achieved by solving a small eigenvalue problem:

$$(\mathbf{X}_{cor}^{\mathrm{T}} \mathbf{K} \mathbf{X}_{cor}) \mathbf{Z} = (\mathbf{X}_{cor}^{\mathrm{T}} \mathbf{M} \mathbf{X}_{cor}) \mathbf{Z} \boldsymbol{\Lambda} \tag{17}$$

where $\mathbf{X}_{\mathrm{cor}}$ is the correction mode matrix. The eigenvectors are normalized so that $\mathbf{Z}^{\mathrm{T}} \left(\mathbf{X}_{\mathrm{cor}}^{\mathrm{T}} \mathbf{M} \mathbf{X}_{\mathrm{cor}} \right) \mathbf{Z} = \mathbf{I}$ and the orthonormal basis of the correction vectors is then given by $\widetilde{\mathbf{X}}_{\mathrm{cor}} = \mathbf{X}_{\mathrm{cor}} \mathbf{Z}$. The relation between the substructure physical DOFs and the reduced coordinate is then given by

$$\begin{bmatrix} \mathbf{u}_i \\ \mathbf{u}_b \end{bmatrix} = \begin{bmatrix} \boldsymbol{\Phi}_{ik} & \widetilde{\mathbf{X}}_{cor} & \boldsymbol{\Psi}_{ib} \\ \mathbf{0}_{bk} & \mathbf{0}_{bn} & \mathbf{I}_{bb} \end{bmatrix} \begin{bmatrix} \mathbf{q}_k \\ \mathbf{q}_n \\ \mathbf{u}_b \end{bmatrix} = \mathbf{T}_{\mathrm{C\text{-}B,cor}} \mathbf{q} \tag{18}$$

where $\mathbf{q}_n$ is the amplitudes of the correction modes and $\mathbf{T}_{\mathrm{C\text{-}B,cor}}$ is the C-B transformation matrix augmented by correction modes.

Using the above procedure, correction modes are generated based on interface excitation. Using a similar procedure, the correction modes, or so-called force dependent Ritz-vectors, can also be generated based on external loads applied to the substructure interior DOFs.

3.3 Substructure coupling procedures

Since the physical boundary DOFs are preserved in the C-B reduction process the assembly method is straight-forward, hence each substructure can be treated as a super-element. However, the substructures can either be assembled by eliminating one set of interface DOFs, a so-called *primal* assembled system, or so that all interface DOFs are preserved, a so-called *dual* assembled system.

The block diagonal system matrices for a structure consisting of N_s substructures are given by

$$\mathbf{M} = \mathrm{diag}(\mathbf{M}^{(s)}), \qquad \mathbf{C} = \mathrm{diag}(\mathbf{C}^{(s)}), \qquad \mathbf{K} = \mathrm{diag}(\mathbf{K}^{(s)}) \tag{19}$$

where **M**, **C** and **K** have size $n \times n$ and the superscript s is the substructure label. The equation of motion can then be written as

$$\mathbf{M}\ddot{\mathbf{u}} + \mathbf{C}\dot{\mathbf{u}} + \mathbf{K}\mathbf{u} = \mathbf{p} \tag{20}$$

where **u** is the $n \times 1$ global displacement vector, including all DOFs at the interfaces between substructures. Assuming compatible meshes, constraints enforced between substructures for individual DOF pairs, e.g. $u_i^{(s_1)} = u_j^{(s_2)}$, can be written in matrix form:

$$\mathbf{B}\mathbf{u} = \mathbf{0} \tag{21}$$

where the constraint matrix **B** is a signed Boolean matrix with size $m \times n$, where m is the number of constraints and n is the total number of DOFs.

As e.g. shown in [3], a primal assembly can be enforced by using the so-called Boolean localization matrix **L**, found by computing the null-space for **B**, i.e.

$$\mathbf{L} = \mathrm{Null}(\mathbf{B}) \tag{22}$$

The relation between the global displacement vector and a displacement vector with a unique set of interface DOFs, $\mathbf{u}_P$, is then given by

$$\mathbf{u} = \mathbf{L}\,\mathbf{u}_P \tag{23}$$

By inserting Equation (23) in Equation (20) and pre-multiplying with $\mathbf{L}^T$ the equation of motion for the primal assembled system is given by

$$\mathbf{M}_P\ddot{\mathbf{u}}_P + \mathbf{C}_P\dot{\mathbf{u}}_P + \mathbf{K}_P\mathbf{u}_P = \mathbf{p}_P \tag{24}$$

where

$$\mathbf{M}_P = \mathbf{L}^T\mathbf{M}\mathbf{L}, \qquad \mathbf{C}_P = \mathbf{L}^T\mathbf{C}\mathbf{L}, \qquad \mathbf{K}_P = \mathbf{L}^T\mathbf{K}\mathbf{L}, \qquad \mathbf{p}_P(t) = \mathbf{L}^T\mathbf{p} \tag{25}$$

The number of DOFs in the primal assembled system is thus $n_P = n - m$ and, accordingly, the size of $\mathbf{M}_P$, $\mathbf{C}_P$, $\mathbf{K}_P$ is $[n_P \times n_P]$ and $\mathbf{p}_P$ is $[n_P \times 1]$.

Instead of eliminating one set of DOFs, a dual assembled system can be achieved by enforcing the interface constraints using Lagrange multipliers $\boldsymbol{\lambda}$. The system of equations can then be written as

$$\begin{bmatrix} \mathbf{M} & \mathbf{0} \\ \mathbf{0} & \mathbf{0} \end{bmatrix} \begin{bmatrix} \ddot{\mathbf{u}} \\ \boldsymbol{\lambda} \end{bmatrix} + \begin{bmatrix} \mathbf{C} & \mathbf{0} \\ \mathbf{0} & \mathbf{0} \end{bmatrix} \begin{bmatrix} \dot{\mathbf{u}} \\ \boldsymbol{\lambda} \end{bmatrix} + \begin{bmatrix} \mathbf{K} & \mathbf{B}^{\mathrm{T}} \\ \mathbf{B} & \mathbf{0} \end{bmatrix} \begin{bmatrix} \mathbf{u} \\ \boldsymbol{\lambda} \end{bmatrix} = \begin{bmatrix} \mathbf{p} \\ \mathbf{0} \end{bmatrix} \tag{26}$$

thus, preserving all interface DOFs [17]. Note that $\boldsymbol{\lambda}$ can be interpreted as an interface force vector, i.e. the forces required to enforce equal displacements for interface DOF pairs.

A dual assembled system can also be enforced using the penalty method, e.g. expressed as

$$\mathbf{M}\ddot{\mathbf{u}} + \mathbf{C}\dot{\mathbf{u}} + (\mathbf{K} + \alpha \mathbf{B}^{\mathrm{T}}\mathbf{B})\mathbf{u} = \mathbf{p} \tag{27}$$

where α is the penalty stiffness, chosen sufficiently large so that $\mathbf{Bu} \approx \mathbf{0}$ [17]. Note that this approach corresponds to adding stiff springs between the constrained DOFs.

The preferred assembly method, or constraint enforcement method, depend on several factors such as the analysis type, the output data of interested, etc.

4 TIME-STEPPING METHOD FOR STRUCTURES WITH RIGID–PERFECTLY PLASTIC JOINTS

Simplified models are often used for design of concrete structures where linear elastic beam elements are combined with predefined discrete plastic hinges, approximated as rigid–perfectly plastic. To enforce a rigid–perfectly plastic coupling between two DOFs, namely the rotational DOFs at the plastic hinges, one alternative is to utilize the penalty method, i.e. by introducing a stiff elastic–perfectly plastic rotational spring. However, one obvious problem when using the penalty method is to choose a suitable penalty stiffness—if it is too low, the results will be inaccurate and if it is too large, the system equations will be ill-conditioned with respect to inversion. Furthermore, the highest eigenfrequency of the system can be expected to increase significantly, which can result in a very small critical time increment size in conditionally stable time integration schemes.

Another alternative is to set up a dual assembled system according to Equation (26) and setting a maximum value, corresponding to the plastic moment, for the Lagrange multipliers. The Lagrange multipliers will then be either known, i.e. treated as external forces equal to the plastic moments, or unknown. However, ensuring stability for a system including Lagrange multipliers, for so-called Differential-Algebraic Equations (DAEs), is often found to be problematic in direct time integration of dual assembled systems. For example, a standard Newmark time integration scheme, assuming constant average accelerations, is in this case unconditionally unstable. However, methods to ensure stability exist, see e.g. [18]. Nonetheless the available time integration schemes are somewhat limited.

Instead of using a pure dual or primal formulation, a methodology is proposed where the system is reassembled when yielding of the rigid–perfectly plastic hinges starts or stops. Such a procedure implies that the nonlinear analysis is performed as a series of linear analyses. Hence, the plastic hinges are either modeled as fixed by eliminating one of the rotational DOFs or as external moments applied on both rotational DOFs at the plastic hinges. This approach can be expected to be particularly suitable for systems consisting of reduced substructures, with a limited number of plastic hinges. The critical time increment is then related to the highest eigenfrequency of the assembled substructures, which in turn have already been reduced by a modal truncation on the substructure level, removing the high frequency content. Furthermore, high frequency noise induced by penalty elements is avoided.

4.1 Time-stepping algorithm

Starting with the system in Equation (20), a $m \times n$ signed Boolean matrix $\mathbf{B}$ can be constructed to define all the interface couplings between the substructures. The couplings can either be fixed constraints or rigid–perfectly plastic couplings. The matrix is then partitioned as:

$$\mathbf{B} = \begin{bmatrix} \mathbf{B}_r \\ \mathbf{B}_c \\ \mathbf{B}_y \end{bmatrix} \tag{28}$$

where $\mathbf{B}_r$ defines m_r constraints (or boundary conditions) that are not limited by a yield force, e.g. the translational DOFs at a plastic hinge, $\mathbf{B}_c$ defines the m_c rigid–plastic couplings not yielding and $\mathbf{B}_y$ defines the m_y rigid–plastic couplings currently yielding. Hence, the Boolean matrices $\mathbf{B}_c$ and $\mathbf{B}_y$ must be updated in a time-stepping scheme. The constraints defined by $\mathbf{B}_r$ are enforced using a primal formulation before the time-stepping is initialized, hence by eliminating m_r interface DOFs. The equation of motion for the assembled system can then be written as

$$\widehat{\mathbf{M}}\ddot{\mathbf{u}}_r + \widehat{\mathbf{C}}\dot{\mathbf{u}}_r + \widehat{\mathbf{K}}\mathbf{u}_r = \hat{\mathbf{p}} \tag{29}$$

where

$$\widehat{\mathbf{M}} = \mathbf{L}_r^{\mathrm{T}}\mathbf{M}\mathbf{L}_r, \qquad \widehat{\mathbf{C}} = \mathbf{L}_r^{\mathrm{T}}\mathbf{C}\mathbf{L}_r, \qquad \widehat{\mathbf{K}} = \mathbf{L}_r^{\mathrm{T}}\mathbf{K}\mathbf{L}_r, \qquad \hat{\mathbf{p}} = \mathbf{L}_r^{\mathrm{T}}\mathbf{p} \tag{30}$$

and where the Boolean localization matrix $\mathbf{L}_r = \mathrm{Null}(\mathbf{B}_r)$. To simplify the implementation the eliminated DOFs are then removed from the matrices $\mathbf{B}_c$ and $\mathbf{B}_y$, i.e. by removing the corresponding m_r columns containing zeros. The size of the updated matrices $\widehat{\mathbf{B}}_c$ and $\widehat{\mathbf{B}}_y$ is then $m_c \times (n - m_r)$ and $m_y \times (n - m_r)$, respectively. At the initial stage, the couplings defined by $\widehat{\mathbf{B}}_c$ is enforced in the same manner by computing $\mathbf{L}_c = \mathrm{Null}(\widehat{\mathbf{B}}_c)$. At each time increment $t^{(i)}$, the interface forces $\boldsymbol{\lambda}^{(i)}$ is computed from the expression

$$\widehat{\mathbf{B}}_c^{\mathrm{T}}\boldsymbol{\lambda}^{(i)} = \hat{\mathbf{p}}^{(i)} - \widehat{\mathbf{M}}\mathbf{L}_c\ddot{\mathbf{u}}_c{}^{(i)} - \widehat{\mathbf{C}}\mathbf{L}_c\dot{\mathbf{u}}_c{}^{(i)} - \widehat{\mathbf{K}}\mathbf{L}_c\mathbf{u}_c{}^{(i)} \tag{31}$$

where the relation $\mathbf{u}_r = \mathbf{L}_c\mathbf{u}_c$ has been applied. If the interface force for a coupling is larger than the specified yield force, the Boolean matrices $\widehat{\mathbf{B}}_c$ and $\widehat{\mathbf{B}}_y$ are updated, i.e. the row in $\widehat{\mathbf{B}}_c$ defining the coupling is moved to $\widehat{\mathbf{B}}_y$. Thereafter, the system is reassembled by computing the localization matrix $\mathbf{L}_c = \mathrm{Null}(\widehat{\mathbf{B}}_c)$ and applying it to Equation (29). The couplings currently yielding are then considered by adding the yield forces as external loads, hence

$$\mathbf{L}_c^{\mathrm{T}}\widehat{\mathbf{M}}\mathbf{L}_c\ddot{\mathbf{u}}_c{}^{(i)} + \mathbf{L}_c^{\mathrm{T}}\widehat{\mathbf{C}}\mathbf{L}_c\dot{\mathbf{u}}_c{}^{(i)} + \mathbf{L}_c^{\mathrm{T}}\widehat{\mathbf{K}}\mathbf{L}_c\mathbf{u}_c{}^{(i)} = \mathbf{L}_c^{\mathrm{T}}\left(\hat{\mathbf{p}}^{(i)} - \widehat{\mathbf{B}}_y^{\mathrm{T}}\mathbf{f}_y\right) \tag{32}$$

where $\mathbf{f}_y$ is a $m_y \times 1$ vector containing the specified yield forces. Unloading of the m_y couplings currently yielding is detected by checking the relative velocity sign, i.e. if

$$\mathrm{sign}\left(\left\{\widehat{\mathbf{B}}_y\dot{\mathbf{u}}_r{}^{(i)}\right\}_j\right) \neq \mathrm{sign}\left(\left\{\widehat{\mathbf{B}}_y\dot{\mathbf{u}}_r{}^{(i+1)}\right\}_j\right) \tag{33}$$

where subscript j denotes an element of the column vector $\widehat{\mathbf{B}}_y\dot{\mathbf{u}}_r$. If unloading occurs, the system is updated by moving rows from $\widehat{\mathbf{B}}_y$ to $\widehat{\mathbf{B}}_c$, computing the localization matrix $\mathbf{L}_c = \mathrm{Null}(\widehat{\mathbf{B}}_c)$ and applying it to Equation (29).

The time integration between the system updates can be performed in a standard manner by the Newmark-β method, as e.g. described in [19]. However, for a nonlinear system including both elastic and plastic deformations it is convenient to use incremental quantities,

$$\Delta\mathbf{u}^{(i)} = \mathbf{u}^{(i+1)} - \mathbf{u}^{(i)}, \quad \Delta\mathbf{u}^{(i)} = \mathbf{u}^{(i+1)} - \mathbf{u}^{(i)}, \quad \Delta\ddot{\mathbf{u}}^{(i)} = \ddot{\mathbf{u}}^{(i+1)} - \ddot{\mathbf{u}}^{(i)}, \quad \Delta\mathbf{p}^{(i)} = \mathbf{p}^{(i+1)} - \mathbf{p}^{(i)} \tag{34}$$

In fact, the time-stepping algorithm is constructed so that the computed incremental displacements are always transformed and appended to $\mathbf{u}_r$, thus

$$\mathbf{u}_r{}^{(i+1)} = \mathbf{u}_r{}^{(i)} + \mathbf{L}_c \Delta\mathbf{u}_c{}^{(i)} \tag{35}$$

Consequently, the displacement vector need not to be transformed at the system updates. Merging DOF pairs in couplings where yielding is stopped would certainly be an ambiguous operation, since the displacement in each DOF in general will differ.

Upon yielding, the system is updated so that couplings where yielding is initiated are released. The interpretation of this update is straight-forward since the initial state of the physical quantities (i.e. displacements, velocities, accelerations) in the new configuration is well defined by the previous state. If yielding is stopped, rigid couplings are enforced by eliminating one set of interface DOFs. The velocities for the constrained DOFs are by definition equal when unloading is detected and it is thus straight-forward to eliminate one set of DOFs. The initial acceleration in the updated system is computed as

$$\ddot{\mathbf{u}}_c{}^{(i)} = \left(\mathbf{L}_c^{\mathrm{T}}\widehat{\mathbf{M}}\mathbf{L}_c\right)^{-1}\mathbf{L}_c^{\mathrm{T}}\left(\hat{\mathbf{p}}^{(i)} - \widehat{\mathbf{B}}_y^{\mathrm{T}}\mathbf{f}_y - \widehat{\mathbf{C}}\dot{\mathbf{u}}_r{}^{(i)} - \widehat{\mathbf{K}}\mathbf{u}_r{}^{(i)}\right) \tag{36}$$

Note that the time increment between system updates, $\Delta t^{(i)} = t^{(i)} - t^{(i-1)}$, is zero. Hence, the velocities and deformations are equal in increment i and $i - 1$. However, the accelerations are changed at the system updates in accordance with Equation (36). Even though an instantaneous change of the accelerations might seem unreasonable, this is a consequence of the unphysical assumption of a perfectly rigid connection, which however can be a very useful approximation; in particular when modeling plastic hinges in beam–column structures. Furthermore, it should be noted that both the strain and kinetic energy is preserved.

4.2 Remarks on performance and accuracy

In contrast to a conventional implicit direct time integration, the proposed time-stepping scheme, as presented above, is a non-iterative procedure. However, in general an adjustment of the last increment size before a system update is needed to ensure that the system is updated just before yielding start or stop. This adjustment can be set up in an iterative fashion.

If the system consists of reduced substructures the critical time increment, in a conditionally stable time integration scheme, can be expected to be reasonably large since the high frequency content has been removed in the reduction process on the substructure level. The time increment size prescribed in the analysis is then instead governed by the precision of the requested time-histories. Consequently, the Newmark parameters can be optimized to increase the analysis accuracy (or performance) rather than to ensure stability. For example, setting the parameters to $\beta = 1/12$ and $\gamma = 1/2$ ensures forth-order accuracy and $\beta = 0$ and $\gamma = 1/2$ enables the explicit central difference scheme [19]. Furthermore, if the system at hand is relatively small and if the number of system updates can be assumed rather limited, the critical time increment can be updated based on an eigenvalue analysis of the updated system. However, an alternative is to prescribe a conservative time increment and thereby skip this check.

5 NUMERICAL EXAMPLE: CONCRETE FRAME SUBJECTED TO BLAST LOADING

A concrete frame structure subjected to blast loading is studied to demonstrate the discussed substructuring and time-stepping method. The dynamic response is computed using a simplified two-dimensional model, suitable in a conceptual design phase. Various strategies to reduce the model by use of DS are investigated, both in terms of accuracy and computationally efficiency (i.e. number of DOFs). Focus is primarily on evaluating DS techniques applied to the lateral load-bearing structure that is not subjected to external loading, i.e. the supporting structure consisting of the horizontal beam and the right column, as shown in Figure 2a. The dynamic response is computed using the time-stepping scheme proposed in Section 4. Furthermore, the highest eigenfrequency, which is related to the critical increment size in conditionally stable time-integration schemes, is evaluated for the reduced models.

The concrete frame is subjected to a uniformly distributed reflected impulse pressure of 1500 Pa·s, as shown in Figure 2a. The pulse is approximated by an equivalent triangular pulse with a fictitious duration of 10 ms and a peak reflected pressure of 300 kPa at $t = 0$ s. The length of the frame members is 3 m and the cross-section width and height, for the columns as well as the horizontal beam, are 1000 mm and 200 mm, respectively. Young's modulus for concrete is set to 32 GPa and the density for reinforced concrete is set to 2500 kg/m^3. The ultimate moment capacity for the columns and the horizontal beam is set to 60 kNm.

5.1 Frame structure model reduced by dynamic substructuring

The frame structure is analyzed with a two-dimensional beam model. The positions of possible plastic hinges are predefined and approximated as five discrete rigid–perfectly plastic joints, as shown in Figure 2b. Yielding of the frame corners are approximated by one distinct plastic hinge, i.e. Joints 3 and 4, respectively. However, it should be noted that a more accurate approximation can be achieved by modeling the corners as separate substructures. Moreover, several effects are neglected in the analysis, e.g. catenary effects, reduced stiffness due to concrete cracking etc. Nevertheless, the model is suitable for studying different DS techniques and to evaluate the efficiency of the proposed time-stepping method.

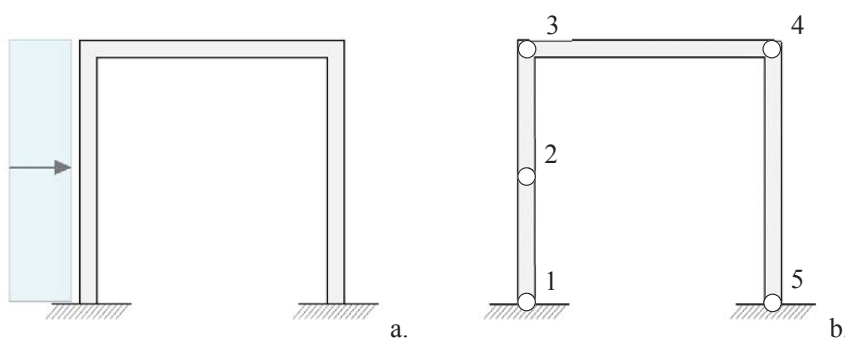

Figure 2: Concrete frame structure subjected to blast loading (a) and locations and labeling of plastic hinges (b).

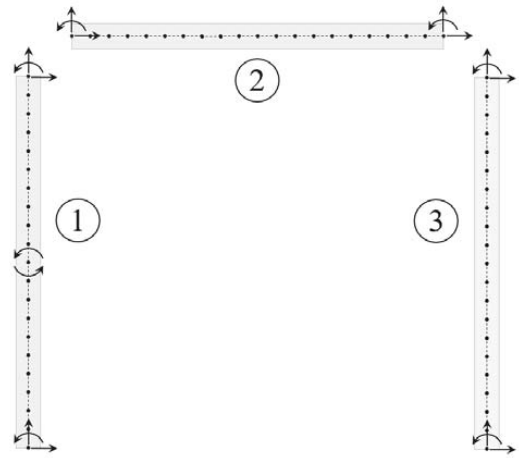

Figure 3: Boundary DOFs and numbering of substructures.

The structure is divided into three substructures, as shown in Figure 3. Each substructure is modeled by 20 Euler–Bernoulli two-node beam elements. Six interface DOFs are retained for Substructures 2 and 3, namely the translational and rotational DOFs at the beam ends. By selecting these boundary DOFs, the fixed-interface normal modes will be the exact mode-shapes of a fixed–fixed beam. Further, eight boundary DOFs are retained for Substructure 1, namely the translational and rotational DOFs at the top and bottom and the rotational DOFs at the joint positioned at midspan. By selecting these boundary DOFs the fixed-interface normal modes will include the exact symmetric modes for a fixed–fixed beam, whereas the antisymmetric modes will be affected by the constrained rotational DOFs at midspan. The fixed-interface normal modes and the constraint modes included in the reduction basis for Substructure 1 is shown in Figures 4 and 5. Note that the antisymmetric modes for a fixed–fixed beam are not excited by a uniformly distributed load. However, since Substructure 1 is not fully supported at the top, some antisymmetric normal modes (modes 2, 5 and 8) are included in the reduction basis.

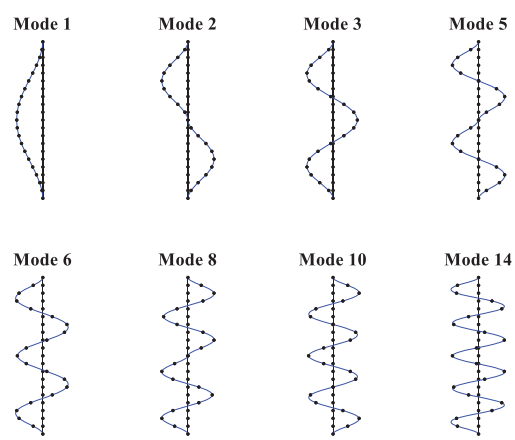

Figure 4: Substructure 1 – fixed-interface normal modes.

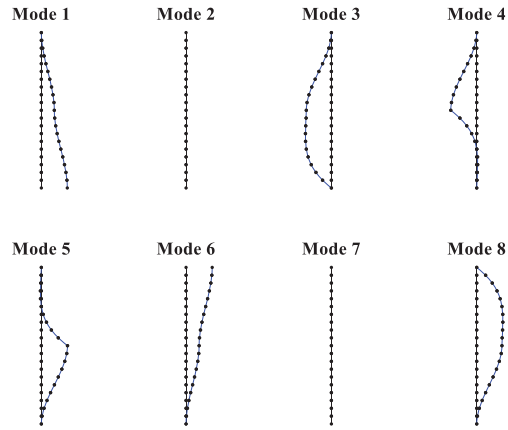

Figure 5: Substructure 1 – constraint modes.

During a dynamic response analysis, the predefined plastic hinges can be either fixed or free, i.e. non-yielding or yielding. A total of five predefined plastic hinges are included in the model, which implies that a response analysis can include up to ten different system configurations. However, to get a rough estimate of the reduced model accuracy two configurations are evaluated—where all joints are either fixed or free, respectively.

The eigenfrequencies for the assembled reduced systems are evaluated by computing the so-called normalized relative frequency difference (NRFD), given by $\text{NRFD} = \left|f_i^{red} - f_i^{full}\right| / f_i^{full}$, that relate the eigenfrequencies of the reduced system to those of the full system. As previously described, the reduction basis for Substructure 1 includes the fixed-interface normal modes and constraint modes shown in Figures 4 and 5, respectively. Five different reduction bases for Substructures 2 and 3 are evaluated. Using a standard C-B approach, reduction is performed including two or four fixed-interface normal modes. Furthermore, reduction bases including two or four correction modes, as described in Section 3.2, are evaluated. The correction modes are generated based on the constraint modes associated to the rotational boundary DOFs at the beam ends. Hence, two modes are generated by computing a set of first-order correction modes and two additional modes are generated by computing a set of second-order correction modes. In addition, the accuracy of a reduction basis including both four fixed-interface normal modes and two first-order correction modes is evaluated. The analyzed models are summarized in Table 1.

Model name	Normal modes	Correction modes[1]	No of DOFs[2]
Mode 1-2	1, 2	-	19
Cor. 1st	-	2 × 1st	19
Mode 1-4	1, 2, 3, 4	-	23
Cor. 1st, 2nd	-	2 × 1st + 2 × 2nd	23
Mode 1-4, Cor.1st	1, 2, 3, 4	2 × 1st	27
Full model	-	-	177

[1] Correction modes associated to rotational boundary DOFs.
[2] Total number of DOFs for model with fixed joints.

Table 1: Normal modes and correction modes for Substructures 2 and 3.

The computed NRFD values are shown in Figures 6 and 7. As shown in the figures, at least, the first seven free and fixed global modes, respectively, are well-described by all the evaluated reduced models; measured as NRFD < 1 %. However, to increase the precision for higher order modes, the constraint modes in Substructures 2 and 3 need to be complemented by at least four modes. However, increasing the number of fixed-interface normal modes and/or correction modes in the reduction basis result in additional generalized DOFs in the reduced system, hence, increasing the computational cost. Moreover, the accuracy when using correction modes and normal modes are comparably, as long as the same number of modes are included in the reduction basis.

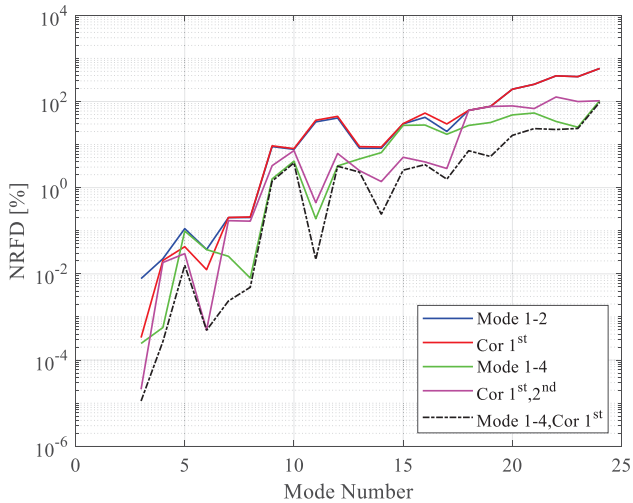

Figure 6: NRFD values for systems with unconstrained rotations at joints.

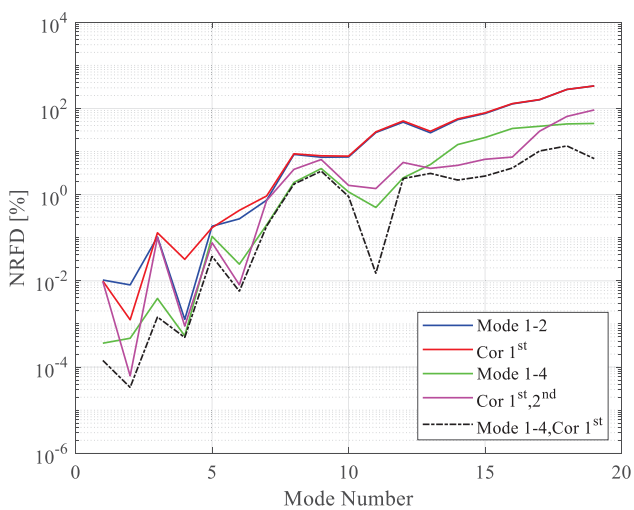

Figure 7: NRFD values for systems with constrained rotations at joints.

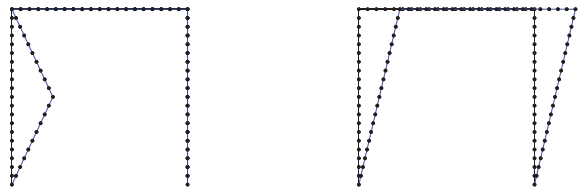

Figure 8: Failure modes spanned by rigid body modes.

Note that the NRFD value is not computed for the first two eigenmodes for the systems with free rotations at the joints. This is due to that the first two modes are rigid body modes with zero frequency. By properly scaling of the rigid body modes, the failure modes, shown in Figure 8, are obtained.

5.2 Dynamic response analysis and results

The dynamic response is computed for the reduced system where the reduction basis for Substructures 2 and 3 includes four normal modes and two first order correction modes. Again, the reduction basis for Substructure 1 includes the normal modes and constraint modes shown in Figures 4 and 5, respectively. The reduced model has a total of 27 DOFs in the initial stage, i.e. when the plastic hinges are fixed, whereas the full model has a total of 177 DOFs. The response is computed using the time-stepping scheme presented in Section 4. Direct time-integration is performed using the Newmark method, with parameters $\beta = 1/12$ and $\gamma = 1/2$ that result in a conditionally stable integration scheme with forth order accuracy [19]. The critical time increment is computed as $dt_{crit} = 2.45/\omega_{max}$. The analysis is performed with a time increment $dt = dt_{crit}/10$ and the analysis time is set to 150 ms.

Snapshots of the deformed shape during the first 50 ms is shown in Figure 9. As shown in the figure, the response of the left column during the first, approximately, 10 ms is similar to that of a fully supported fixed–fixed column due to the inertia of the supporting horizontal beam.

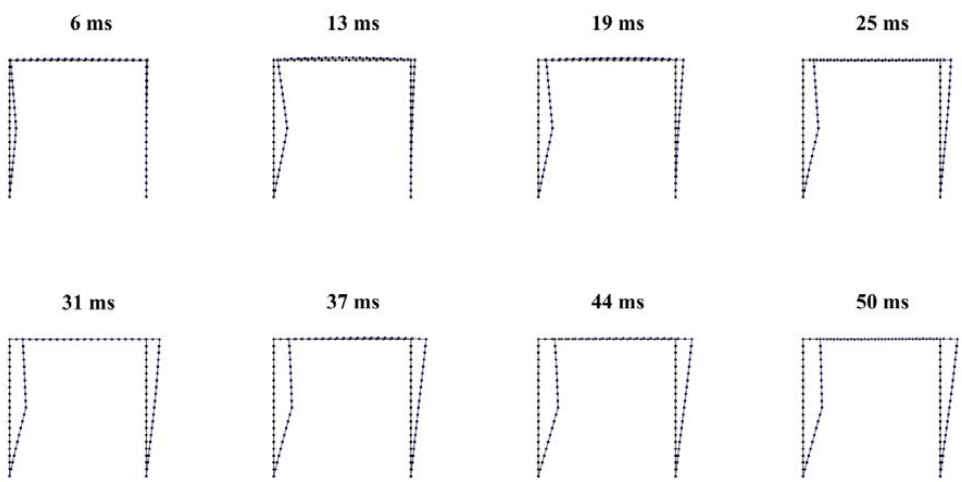

Figure 9: Snapshots of the deformed shape during the first 50 ms. The deformation is scaled by a factor of 15.

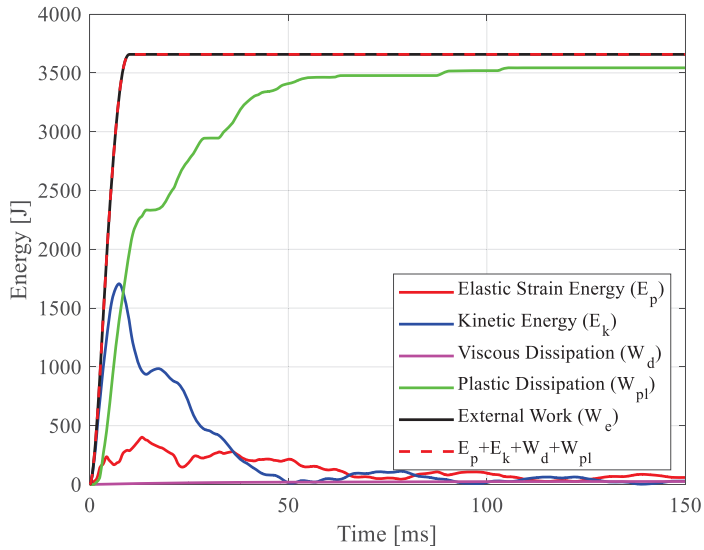

Figure 10: Elastic strain and kinetic energy, plastic and viscous dissipation and external work for the reduced system.

As shown in Figure 10, the energy induced by the external impulse pressure is mainly dissipated by plastic deformations, i.e. by rotation of the predefined plastic hinges. A low Rayleigh beta damping is included in the analysis by setting $\mathbf{C} = 10^{-5} \cdot \mathbf{K}$. As shown in the figure, the viscous dissipation is almost zero.

The relative rotation of the plastic hinges is shown in Figure 11. As shown, most of the plastic dissipation is due to plastic rotation in Joints 1 and 2. The rotation computed with the full model is shown in light gray color. As shown in the figure, the response is almost identical to that of the reduced model. Note that the relative rotation of the plastic hinges is an important parameter in a design calculation, which should not exceed the rotation capacity of the cross-section.

The horizontal displacement at Joints 2 and 4 is shown in Figure 12. The displacement is very close to the displacement computed with the full model. The fundamental eigenfrequency for the non-yielding frame structure is 11.7 Hz, corresponding to a period of 1/11.7 = 85 ms. Clearly, the displacement after approximately 50 ms can essentially be described by the fundamental mode and a plastic displacement.

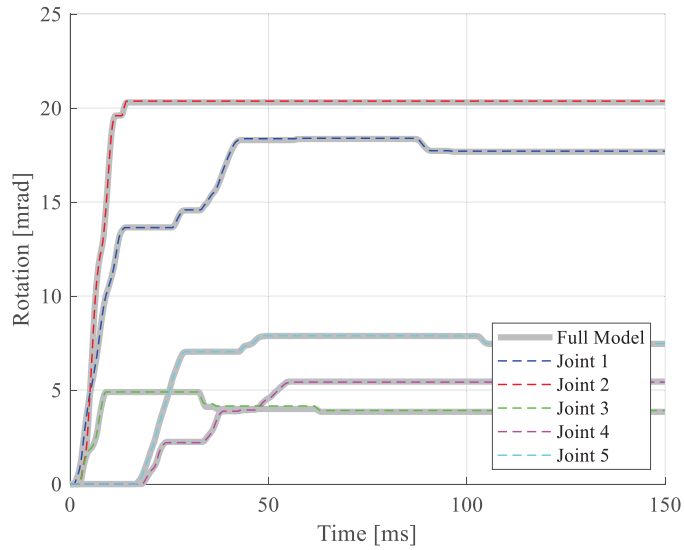

Figure 11: Relative rotations at Joints 1–5, positioned according to Figure 2b.

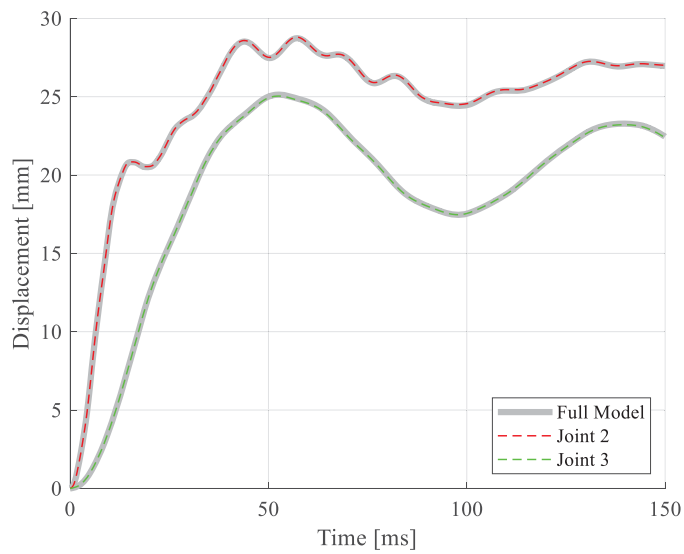

Figure 12: Horizontal displacements at Joints 2 and 3, positioned according to Figure 2b.

If a suitable reduction basis is applied to Substructure 1, to properly describe the application of the external pressure, the global displacements can be well-described by only including two fixed-interface normal modes (or correction modes) for Substructures 2 and 3, as indicated by Figures 11 and 12. However, a more refined reduction basis is needed to properly describe the reaction and interface forces between the substructures. The influence of the reduction basis on the horizontal interface force in Joint 4 is shown in Figure 13. As shown, the constraint modes need to be complemented by at least four modes to obtain a reasonable accurate response. The

accuracy for the models reduced by using fixed-interface normal modes and correction modes, respectively, are comparable. Hence, the correction modes are then the preferred choice since the generation of these modes are less computationally expensive (in this simple example, however, the computational cost of generating either normal modes or corrections modes is negligible).

The critical time increment in a conditionally stable direct time integration method is inversely proportional to the highest eigenfrequency. Consequently, a reduction of a system that removes the high frequency content can result in a more computationally efficient analysis. To get an estimation of how much the eigenfrequency is affected by the reduction bases studied herein, the highest eigenfrequency is computed for the initial state of the reduced systems, i.e. when all joints are fixed.

The highest eigenfrequency of the reduced models including two and four fixed-interface normal modes in the reduction bases for Substructure 2 and 3 is 4.2 kHz and 4.3 kHz, respectively. The highest eigenfrequency when using two and four correction modes is 4.2 kHz and 4.4 kHz, i.e. almost equal to the eigenfrequencies obtained when using normal modes. However, the highest eigenfrequency in the reduced models is in this case most likely governed by Substructure 1, reduced by a more refined reduction basis.

For the reduced model including four fixed-interface normal modes and two first-order correction modes the highest eigenfrequency is 4.7 kHz. In comparison, the highest eigenfrequency of the full model is 74.5 kHz, i.e. a factor of 74.5/4.7 ≈ 16. Furthermore, the highest eigenfrequency for a reduced system where the rigid–perfectly plastic joints are modeled using penalty elements, with a stiffness 10 times the mean stiffness of the corresponding entries in the unreduced stiffness matrix, is 64.4 kHz. Hence, for the model studied herein, the number of time increments can be decreased by a factor 64.4/4.7 ≈ 14 by avoiding penalty elements.

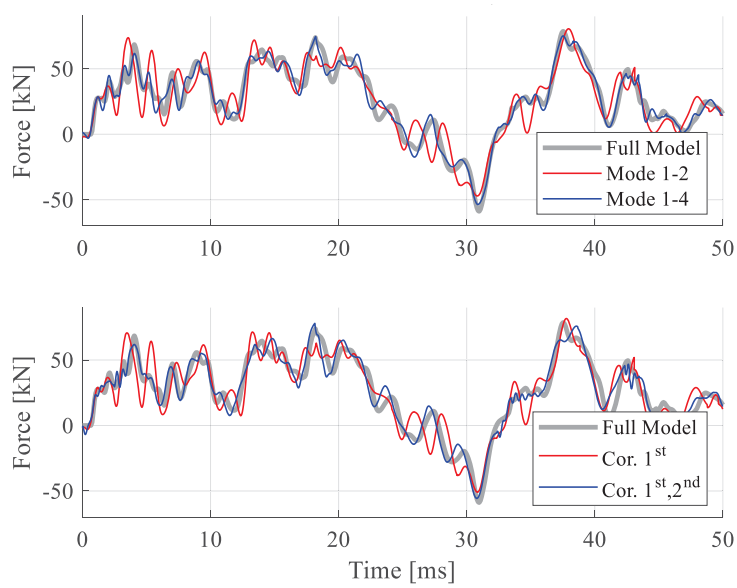

Figure 13: Horizontal interface force at Joint 4.

6 CONCLUSIONS

In the study, strategies are developed to enable time-efficient models for concrete frame structures subjected to blast loading, appropriate for use in a structural design process. Dynamic substructuring is employed to obtain reduced models with localized nonlinearities, such as predefined plastic hinges in a beam–column structure. The parts of the substructures that remains linear elastic are modeled by Ritz-vectors whereas parts with a nonlinear response are retained as physical degrees-of-freedom. Furthermore, a time-stepping scheme is presented that is shown to be suitable for reduced models including local and predefined rigid-plastic behavior.

The proposed methodology is applied and demonstrated in a numerical example of a concrete frame structure. The standard Craig-Bampton method that uses fixed-interface normal modes and constraint modes is evaluated. Furthermore, reduction bases augmented by so-called correction modes are investigated. Various reduction bases are evaluated for the substructures included in the supporting structure, i.e. the substructures that are not subjected to external loading. Two correction modes or two standard fixed-interface normal modes are sufficient to describe the displacement and relative rotations at the plastic hinges. However, to obtain an acceptable accuracy of the interface forces between the substructures, at least four correction modes or four standard fixed-interface modes are needed. For the studied load case, the accuracy when using correction modes and fixed-interface normal modes are comparable.

Moreover, the highest eigenfrequency for the reduced systems, which is related to the critical increment size in conditionally stable direct time integration methods, is evaluated. It is shown that a reduction of the studied model by use of dynamic substructuring can increase the critical time increment by a factor of approximately 16. Furthermore, it is shown that by enforcing a rigid–plastic behavior using the proposed time-stepping scheme, the critical increment size can increase by a factor of approximately 14 compared to a modeling approach where the rigid–plastic behavior is enforced using penalty elements.

The present methodology can be extended further to, for example, consider large deformations and failure, e.g. by considering the rotation capacity of the cross-sections. Furthermore, the methods can be applied and evaluated for larger and more complex structures, e.g. three-dimensional beam–column structures. Also, a more refined modeling approach for frame corners can be investigated, where the corner itself is treated as a separate substructure.

REFERENCES

[1] J.M. Biggs, *Introduction to Structural Dynamics*. McGraw-Hill, New York, 1964.

[2] L. Andersson, P. Persson, P. Austrell, K. Persson, Reduced order modeling for the dynamic analysis of structures with nonlinear interfaces. *Proceedings of the 7th ECCOMAS Thematic Conference on Computational Methods in Structural Dynamics and Earthquake Engineering (COMPDYN 2019)*, Crete, Greece, 24–26 June, 2019.

[3] D. de Klerk, D.J. Rixen, S.N. Voormeeren, General Framework for Dynamic Substructuring: History, Review, and Classification of Techniques, *AIAA Journal*, **46 (5)**, 1169–1181, 2008.

[4] O. Flodén, K. Persson, G. Sandberg, Reduction methods for the dynamic analysis of substructure models of lightweight building structures, *Computers and Structures*, **138**, 49–61, 2014.

[5] Unified Facilities Criteria (UFC), *Structures to Resist the Effects of Accidental Explosions*, U. S. Army Corps of Engineers, Naval Facilities Engineering Command, Air Force Civil Engineer Support Agency, UFC 3-340-02, December 5 2008.

[6] R.J. Guyan, Reduction of Stiffness and Mass Matrices, *AIAA Journal*, **3 (2)**, 380, 1965.

[7] J. O'Callahan, P. Avitabile, R. Riemer, System Equivalent Reduction Expansion Process (SEREP), *Proceedings of the 7th International Modal Analysis Conference*, Las Vegas, Nevada, 1989.

[8] R.R. Craig, M.C.C. Bampton, Coupling of Substructures for Dynamic Analysis, *AIAA Journal*, **6 (7)**, 1313–1319, 1968.

[9] R.H. MacNeal, A Hybrid Method of Component Mode Synthesis, *Computers and Structures*, **1 (4)**, 581–601, 1971.

[10] S. Rubin, Improved Component-Mode Representation for Structural Dynamic Analysis, *AIAA Journal*, **13 (8)**, 995–1006, 1975.

[11] R.R. Craig, C.J. Chang, On the Use of Attachment Modes in Substructure Coupling for Dynamic Analysis. *Proceedings of the 18th Structures, Structural Dynamics and Material Conference*, San Diego, CA, 1977.

[12] D.J. Rixen, A dual Craig–Bampton method for dynamic substructuring, *Journal of Computational and Applied Mathematics*, **168(1–2)**, 383–391, 2004.

[13] F.M. Gruber, M. Gille, D.J. Rixen, Time integration of dual Craig-Bampton reduced systems. *Proceedings of the 6th ECCOMAS Thematic Conference on Computational Methods in Structural Dynamics and Earthquake Engineering (COMPDYN 2017)*, Rhodes Island, Greece, 15–17 June, 2017.

[14] R. Craig, A. Hale, Block-Krylov Component Synthesis Method for Structural Model Reduction. *Journal of Guidance, Control and dynamics, American Institute of Aeronautics and Astronautics*, **11(6)**, 562–570, 1988.

[15] D.J. Rixen, High Order Static Correction Modes for Component Mode Synthesis. *Proceedings of the fifth World Congress on Computational Mechanics*, Vienna, Austria, 7–12 July, 2002.

[16] R.R. Jr. Craig, A.J. Kurdila, *Fundamentals of Structural Dynamics, 2nd Edition*, John Wiley & Sons, New Jersey, 2006.

[17] K. J. Bathe, *Finite element procedures*. Prentice-Hall, 1996.

[18] C. Farhat, L. Crivelli, M. Géradin, Implicit time integration of a class of constrained hybrid formulations—Part I: Spectral stability theory, *Computer Methods in Applied Mechanics and Engineering*, **125 (1–4)**, 71–107, 1995.

[19] M. Geradin, D.J. Rixen, *Mechanical Vibrations: Theory and Applications to Structural Dynamics, Third Edition*. Wiley, New York, 2014.

Paper C

Reduced Order Modeling of Soft-Body Impact on Glass Panels

Linus Andersson[a,*], Marcin Kozłowski[b], Peter Persson[a], Per-Erik Austrell[a] , Kent Persson[a]
[a]Department of Construction Sciences, Lund University, Sweden
[b]Department of Structural Engineering, Silesian University of Technology, Poland
*linus.andersson@construction.lth.se

Abstract

In the paper, strategies for reduced order modeling of glass panels subjected to soft-body impact are developed by means of dynamic substructuring. The aim is to obtain accurate and computationally efficient models for prediction of the pre-failure elastic response. More specifically, a reduction basis for the subsystem representing the glass panel is established using correction modes, being fixed-interface component modes that considers loading on the substructure boundary. The soft-body impactor is effectively modeled by a nonlinear single-degree-of-freedom system, calibrated by experimental data. Furthermore, a simplified and computationally efficient modeling approach is proposed for the contact interaction between the glass panel and the impact body. An experimental campaign was carried out to validate the developed models. In particular, the glass strain was measured on simply supported monolithic glass panels subjected to soft-body impact. Additional impact tests were performed to determine the dynamic characteristics of the impactor. Moreover, a detailed numerical reference model was developed to evaluate the discrepancy between the experimental tests and the results provided by the reduced order models. The developed models show good agreement with the experimental results. For the studied load cases, it is shown that an accurate prediction of the pre-failure glass strain can be obtained by systems including only a few generalized degrees-of-freedom.

Keywords: reduced order model, dynamic substructuring, soft-body impact, structural glass, impact testing, damping, finite element analysis.

1. Introduction

During the last few decades, glass has become an increasingly common building material in modern architecture. Glass is not only used for building enclosures and translucent facades allowing sunlight into the building, but also in load-bearing structures and glazed barriers, such as full-height façades and parapets for balconies or interior level changes.

If the glass barrier constitutes a safety risk for building occupants, building regulations in most countries prescribes that the glazing must be designed to withstand accidental impact of humans. A dynamic verification is then required, usually performed by experimental testing using the standardized soft-body pendulum for glass classification according to the European Standard EN 12600 [1]. The test arrangement used for glass classification, shown in Figure 1, consists of a glass panel fixed in a steel frame and a soft impact body on a pendulum, representing a human body falling towards the glass panel.

Impact tests can be very costly, especially for large and complex glass structures. Furthermore, it can be difficult to set-up a test arrangement that accurately capture the structural behavior of the underlying load-bearing structure. Moreover, a structural verification using tests applied to the real structure can be both costly and requires a re-design of the existing structure if the load-bearing capacity turns out to be inadequate. Therefore, it can be preferable to instead perform the verification by means of dynamic calculation methods. Beside a reduced cost and the possibility to easily evaluate different design concepts, numerical analyses enable an increased insight into the structural behavior and additional control of e.g. structural and material parameters. In a physical impact test, however, the material parameters can vary depending on the specific glass specimen, why several tests are needed to adequately account for statistical variations. The validity of using numerical simulations for strength evaluation of glass structures have been shown by several researchers, see e.g. [3–6].

Static load cases are often verified by means of a commercial finite element (FE) software. For this purpose, a specialized FE tool *ClearSight* [7] has been developed at the Department of Construction Science, Lund University, being streamlined for an interactive and efficient verification of glass panels subjected to static load cases. However, using a FE analysis to calculate the dynamic response due to impact can be time-consuming and computationally expensive. In general, a nonlinear transient response analysis is required, and the FE model should include the glass panel and its fixings, the impactor, and a suitable description of the contact interaction between the impactor and the glass structure. To set up and perform such an analysis can be time-consuming and often requires a relatively advanced FE software and extensive user knowledge.

To enable a more time-efficient and straightforward approach for evaluating dynamic load cases, reduced modeling techniques specialized for glass panels subjected to impact loading have been proposed by several researchers, see e.g. [8–13]. For instance, in [8], reduction bases were successfully constructed using predefined load patterns, employed for reduced modeling of glass panels in a Rayligh-Ritz fashion. In [13], various reduced models of unsupported glass panels subjected to low-velocity impact are investigated. For example, a three degree-of-freedom (DOF) spring-mass model is proposed, constructed by calibrating the system matrices to the strain energies and eigenfrequencies of the fundamental flexural modes of a glass panel in free–free conditions. Thus, the mode shapes

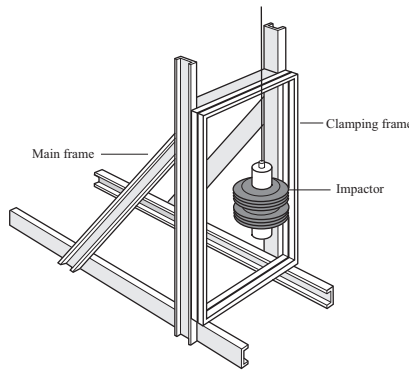

Figure 1: Test frame with impactor according to the European Standard EN 12600 [1].

are used implicitly for identifying eigenfrequencies and energies, which are then employed in a second stage for calibrating the lumped-mass systems. Furthermore, a lumped mass model based on Hertz contact law (see e.g. [14]) is proposed for modeling the impactor. However, the low-velocity impacts studied in [13] were generated using a specialized spherical impactor, particularly suitable for approximation using Hertz law. Further, the reduced models were successfully validated by experimental studies, suggesting that the importance of higher order modes increases for larger glass panels and a stiffer impactor. In [10], a simplified engineering model based on equivalent static loads is presented, which enables a very quick and straightforward verification of impact loading. However, because the response of higher order modes is neglected, it is only applicable for two- and four-sided rectangular, continuously supported glass panels within a limited range of dimensions.

In the present paper, strategies for reduced order modeling of soft-body impact are developed by means of dynamic substructuring (DS). The aim is to achieve an accurate prediction of the pre-failure elastic response while significantly reducing the computational cost. More specifically, a reduction basis for the subsystem representing the glass panel is established using correction modes, being fixed-interface component modes that considers loading on the substructure boundary [15, 16]. Because information related to the loading pattern is considered in the derivation, all the generated correction modes will, by definition, be excited by the applied load. In contrast, a reduced basis established using eigenmodes may include redundant modes, e.g. anti-symmetric modes that cannot be excited by a centric impact. The soft impact body is effectively modeled by a nonlinear viscous single-degree-of-freedom (SDOF) system, calibrated by experimental data. Furthermore, a simplified and computationally efficient modeling approach, assuming a constant contact area, is employed for modeling the contact interaction between the glass panel and the impact body.

An experimental campaign was carried out to validate the developed models. In particular, the glass strain was measured on simply supported monolithic glass panels subjected to impact loading. The test arrangement was similar to the standardized impact test for glass classification described in EN 12600 [1]—the glass panels were mounted in a steel frame and impact loads were generated by releasing the standardized EN 12600 impactor from

various drop heights. Additional impact tests on a very stiff steel column (which was considered rigid) were also performed to determine the dynamic characteristics of the impactor. The test arrangement and the standardized impactor employed in the experimental campaign are shown in Figures 2a and 2b, respectively.

To evaluate the differences between the measured glass strain and the strain provided by the reduced models, a detailed FE model, herein referred to as a reference model, was established using the commercial FE software Abaqus [17]. The reference model includes a penalty contact formulation to consider the interaction between the impactor and the glass panel, geometric nonlinearity, hyperelastic constitutive models for rubber, and a sophisticated modeling of the tire air pressure, aiming to mimic the impact tests. Evaluating the deviation between the response computed with the reduced models, the reference model and the experimental tests makes it possible to distinguish between errors related to modeling abstractions and simplifications employed in the reduced models and other, unknown error-sources.

To summarize, the aim of the paper is to:

- develop accurate reduced order models for computation of the pre-failure glass strain, suitable for implementation in user-friendly design tools,
- validate the developed models by experimental data,
- set up a detailed numerical reference model to get further insight into the structural behavior and to evaluate the discrepancy between measurements and the response computed with the reduced order models.

The paper is structured as follows. In Section 2, reduced modeling concepts for simulating soft-body impact are presented, including techniques for reduced modeling of the impactor, the glass panel, and the contact interaction. In Section 3, a detailed FE model of the standardized impactor is presented, herein referred to as the reference model, being used for calibration as well as validation of the reduced models. Experimental tests are presented and discussed in Section 4—both experiments involving testing of glass panels subjected to soft-body impact as well as tests to characterize the dynamic properties of the impactor. In Section 5, calibrations of the impactor models as well as a validation of the assembled reduced models are presented, both by comparison to experimental results and the response computed with the numerical reference model. Finally, the results are discussed in Section 6 and conclusions are presented in Section 7.

2. Reduced order models for analysis of soft-body impact on glass panels

Upon impact, contact is established between the glass panel and the impactor. Hence, a coupled system is formed consisting of the glass structure and the impacting body. Glass is a brittle material that is essentially linear elastic before failure [2]. Hence, at least if neglecting geometric nonlinearity, the pre-failure structural response of monolithic glass panels can be accurately represented by a linear model. However, a nonlinear model may be required to properly describe the contact interaction between the soft impact body and the glass panel, as well as the nonlinear behavior of the pneumatic tires. Nonetheless, the coupled system can be reduced by means of DS,

(a) (b)

Figure 2: Experimental set-up for glass impact tests (a) and impactor (b).

allowing for a reduction of the linear glass substructure while retaining the physical DOFs interacting with the soft impact body.

Several DS methods have been developed since the late 1960s, extensive reviews can be found in [18–20]. We base our approach on the Craig-Bampton (C-B) method [21], which preserves the physical boundary DOFs of the substructures. However, instead of using the fixed-interface normal modes, employed in the standard C-B method, a reduction basis for the glass substructure is established using correction modes that considers loading on the substructure boundary, see further Section 2.1. Furthermore, the impactor is effectively modeled by a nonlinear single-degree-of-freedom (SDOF) system, see Section 2.2.

Interface reduction is applied, as further discussed in Section 2.3, such that only one boundary DOF is retained for the glass substructure, corresponding to the mean vertical displacement of a group of nodes located at the center of the glass panel. The reduced substructures are then assembled in a standard manner to form a reduced model of the coupled system. Strategies for computing the dynamic response of the assembled system is further discussed in Section 2.4.

2.1. Reduced order modeling of glass panels

A reduction of a system including local nonlinearities, such as the coupled impactor-glass system, necessitates a DS technique that preserves the physical boundary DOFs. For example, the standard C-B method [21] or the MacNeal/Rubin approaches [22, 23], which uses the fixed- and free-interface normal modes, respectively, are suitable methods. The preferred method can be due to both accuracy and computational efficiency, which in turn considers both the computational cost of establishing the reduction basis and the number of variables required in the final system.

In the present study, a DS method that uses fixed-interface correction modes is employed for reducing the glass panel, an approach first proposed in [15] and later extended in [16] to enable a mixed usage of normal modes and correction modes (this method was also employed in [24] for establishing reduced models of concrete frame

structures, where plastic joints were treated as local nonlinearities). For the glass-impactor system, this type of reduction basis turns out to be favorable both regarding the system size and the computational cost related to the computation of the reduction basis vectors. As shown in the derivation below, the correction modes are generated by a sequence of matrix-vector multiplications, whereas the fixed- or free-interface normal modes are computed by solving an eigenvalue problem. Furthermore, information related to loading on the substructure boundary DOFs is considered in the derivation of the correction modes and, consequently, redundant modes that cannot be excited by loads applied on the substructure boundary are automatically excluded. Reduction bases including correction modes, also referred to as block-Krylov subspaces, can be derived in several ways. Following Rixen in [16], but excluding the fixed-interface normal modes in the reduction basis, the derivation is as follows.

Neglecting damping, the equation of motion for the glass substructure in partitioned form can be written as:

$$\begin{bmatrix} \mathbf{M}_{ii} & \mathbf{M}_{ib} \\ \mathbf{M}_{bi} & \mathbf{M}_{bb} \end{bmatrix} \begin{bmatrix} \ddot{\mathbf{u}}_i \\ \ddot{\mathbf{u}}_b \end{bmatrix} + \begin{bmatrix} \mathbf{K}_{ii} & \mathbf{K}_{ib} \\ \mathbf{K}_{bi} & \mathbf{K}_{bb} \end{bmatrix} \begin{bmatrix} \mathbf{u}_i \\ \mathbf{u}_b \end{bmatrix} = \begin{bmatrix} \mathbf{p}_i \\ \mathbf{p}_b \end{bmatrix} \tag{1}$$

where the subscripts i and b denotes the interior and interface boundary DOFs, respectively (the number of interior and boundary DOFs is henceforth denoted n_i and n_b, respectively, and the total number of DOFs is thus $n = n_i + n_b$). Notice that the interface DOFs includes the glass panel DOFs interacting with the impactor model. Furthermore, if the external forces on the interior DOFs are zero, the top row of Eq. 1 can be rewritten as:

$$\mathbf{M}_{ii}\ddot{\mathbf{u}}_i + \mathbf{K}_{ii}\mathbf{u}_i = -\mathbf{M}_{ib}\ddot{\mathbf{u}}_b - \mathbf{K}_{ib}\mathbf{u}_b. \tag{2}$$

Hence, the substructure can be considered excited by imposed displacements on its boundary. Further, the internal displacements can be split into a static part and a dynamic correction

$$\mathbf{u}_i = \mathbf{u}_{i,\,\text{stat}} + \mathbf{y} \tag{3}$$

where $\mathbf{u}_{i,\,\text{stat}} = -\mathbf{K}_{ii}^{-1}\mathbf{K}_{ib}\mathbf{u}_b$ is the quasi-static solution, obtained from Eq. 2 assuming $\ddot{\mathbf{u}}_i$ and $\ddot{\mathbf{u}}_b$ are zero. The dynamic part, $\mathbf{y}$, is added to the quasi-static solution to provide the dynamic response. Further, by inserting Eq. 3 into Eq. 2 and rearranging the terms, the dynamic response of $\mathbf{y}$ can be expressed as

$$\mathbf{M}_{ii}\ddot{\mathbf{y}} + \mathbf{K}_{ii}\mathbf{y} = -\mathbf{M}_{ii}\ddot{\mathbf{u}}_{i,\text{stat}} - \mathbf{M}_{ib}\ddot{\mathbf{u}}_b = \mathbf{Y}\ddot{\mathbf{u}}_b \tag{4}$$

where $\mathbf{Y} = \mathbf{M}_{ii}\mathbf{K}_{ii}^{-1}\mathbf{K}_{ib} - \mathbf{M}_{ib}$ can be interpreted as inertia forces associated to static modes [16]. Thus, the acceleration of the boundary DOFs, the mode shapes and the mass distribution determines the forces applied in Eq. 4. This procedure can be continued by replacing $\mathbf{y}$ with a quasi-static solution and a dynamic correction $\mathbf{z}$:

$$\mathbf{y} = \mathbf{y}_{\text{stat}} + \mathbf{z} \tag{5}$$

where $\mathbf{y}_{\text{stat}} = \mathbf{K}_{ii}^{-1}\mathbf{Y}\ddot{\mathbf{u}}_b$ is the static solution obtained from Eq. 4, assuming $\ddot{\mathbf{y}}$ is zero. By inserting Eq. 5 into

Eq. 4, and rearranging the terms, the dynamic response of $\mathbf{z}$ can be expressed as

$$\mathbf{M}_{ii}\ddot{\mathbf{z}} + \mathbf{K}_{ii}\mathbf{z} = -\mathbf{M}_{ii}\mathbf{K}_{ii}^{-1}\mathbf{Y}\frac{\mathrm{d}^4\mathbf{u}_b}{\mathrm{d}t^4}. \tag{6}$$

Thus, the response of the interior displacements is given by a sequence of quasi-static solutions:

$$\mathbf{u}_i = \mathbf{u}_{i,\,\mathrm{stat}} + \mathbf{y}_{\mathrm{stat}} + \mathbf{z}_{\mathrm{stat}} + \dots \tag{7}$$

where, in a similar manner, $\mathbf{z}_{\mathrm{stat}} = -\mathbf{K}_{ii}^{-1}\mathbf{M}_{ii}\mathbf{K}_{ii}^{-1}\mathbf{Y}\frac{\mathrm{d}^4\mathbf{u}_b}{\mathrm{d}t^4}$ is the quasi-static solution of Eq. 6. Hence, a recursive procedure is obtained, indicating that the dynamic response can be approximated as

$$\mathbf{u}_i \approx -\mathbf{K}_{ii}^{-1}\mathbf{K}_{ib}\mathbf{u}_b + \sum_{j=1}^{l}\left(-\mathbf{K}_{ii}^{-1}\mathbf{M}_{ii}\right)^{j-1}\mathbf{K}_{ii}^{-1}\mathbf{Y}\frac{\mathrm{d}^{2j}\mathbf{u}_b}{\mathrm{d}t^{2j}} \tag{8}$$

where l is the number of static corrections. Furthermore, the higher order derivatives $\frac{d^{2j}u_b}{dt^{2j}}$ can be treated as separate DOFs. Hence, instead of computing a sequence of static corrections, a dynamic response analysis is conducted by means of generalized coordinates representing the amplitudes of the correction modes. The set of j-th order correction modes are then given by:

$$\mathbf{x}_{\mathrm{cor},j} = \left(\mathbf{K}_{ii}^{-1}\mathbf{M}_{ii}\right)^{j-1}\mathbf{K}_{ii}^{-1}\mathbf{Y} \tag{9}$$

where $\mathbf{x}_{\mathrm{cor},j}$ is a $n_i \times n_b$ matrix, containing the correction modes generated in iteration j. Notice that each correction mode is associated to a boundary DOF. Consequently, a large number of boundary DOFs result in a large number of correction modes being generated in each iteration, why this method is best used in combination with an interface reduction technique (see further Section 2.3).

To avoid numerical round-off errors, the correction modes are generated using the modified Gram–Schmidt orthogonalization procedure [25, 26]. Furthermore, the static correction modes are not mutually mass- and stiffness orthogonal. This can e.g. be achieved by solving a small eigenvalue problem:

$$\left(\mathbf{X}_{ik,\mathrm{cor}}^{\top}\mathbf{K}_{ii}\mathbf{X}_{i,\mathrm{cor}}\right)\mathbf{Z} = \left(\mathbf{X}_{i,\mathrm{cor}}^{\top}\mathbf{M}_{ii}\mathbf{X}_{i,\mathrm{cor}}\right)\mathbf{Z}\mathbf{\Lambda} \tag{10}$$

where $\mathbf{X}_{ik,\mathrm{cor}} = \begin{bmatrix} \mathbf{x}_{\mathrm{cor},1} & \mathbf{x}_{\mathrm{cor},2} & \dots & \mathbf{x}_{\mathrm{cor},l} \end{bmatrix}$ is the $n_i \times k$ correction mode matrix, $\mathbf{\Lambda}$ is a diagonal matrix containing pseudo-frequencies and $\mathbf{Z}$ contains the corresponding eigenvectors, which are normalized such that $\mathbf{Z}^{\top}\left(\mathbf{X}_{ik,\mathrm{cor}}^{\top}\mathbf{M}\mathbf{X}_{ik,\mathrm{cor}}\right)\mathbf{Z} = \mathbf{I}$. An orthonormal basis of the correction modes is then provided by $\tilde{\mathbf{X}}_{ik,\mathrm{cor}} = \mathbf{X}_{ik,\mathrm{cor}}\mathbf{Z}$, and the relation between the substructure physical DOFs and the generalized coordinates $\mathbf{q}$ is given by

$$\begin{bmatrix} \mathbf{u}_i \\ \mathbf{u}_b \end{bmatrix} = \begin{bmatrix} \tilde{\mathbf{X}}_{ik,\mathrm{cor}} & \mathbf{\Psi}_{ib} \\ \mathbf{0}_{bk} & \mathbf{I}_{bb} \end{bmatrix}\begin{bmatrix} \mathbf{q}_k \\ \mathbf{u}_b \end{bmatrix} = \mathbf{T}_{\mathrm{C-B,cor}}\mathbf{q} \tag{11}$$

where $\mathbf{q}_k$ is the amplitudes of the (orthonormal) correction modes and $\mathbf{\Psi}_{ib} = -\mathbf{K}_{ii}^{-1}\mathbf{K}_{ib}$ is the internal part of the constraint modes, corresponding to the static displacement of a unit displacement on a boundary node while the other boundary nodes are held fixed. Using the transformation matrix $\mathbf{T}_{\mathrm{C-B,cor}}$, the system equations for the

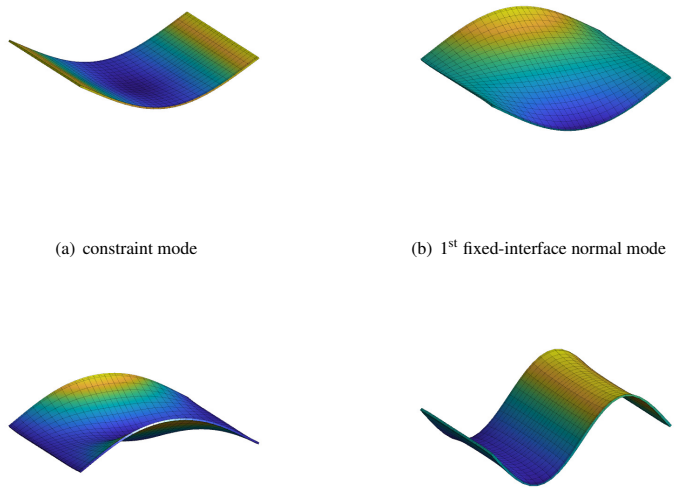

(a) constraint mode

(b) 1st fixed-interface normal mode

(c) 2nd fixed-interface normal mode

(d) 3rd fixed-interface normal mode

Figure 3: Constraint mode and first three fixed-interface normal modes.

un-reduced substructure are projected onto the reduction basis in a standard manner, see e.g. [20]. Further, the reduction basis is established using a reduced set of generalized coordinates, i.e. $k \ll n$.

Notice that the generated correction modes are in fact forming a Krylov sequence [26], why these are also referred to as Krylov modes. As indicated by Eq. 9, the modes can be generated by matrix–vector multiplications. Furthermore, the generated modes, as derived above, are force dependent in the sense that the substructure is considered loaded by imposed displacements on its boundary.

An example is presented in Figure 3 showing the constraint mode and the first three fixed-interface normal modes for a simply supported 1000 mm $\times$ 800 mm glass panel. Further, Figure 4 shows the constraint mode and the first three correction modes. One boundary DOF is considered, corresponding to the mean vertical displacement of a group of nodes positioned at the center of the glass panel. As shown in Figure 3, two of the fixed-interface normal modes are anti-symmetric and cannot be excited by a vertical force applied at the center of the panel. On the contrary, all the correction modes will, by definition, be excited.

2.2. Reduced order modeling of the impactor

The standardized impactor, described in EN 12600 [1], consist of two pneumatic rubber tires and steel weights, as shown in Figure 2b. The impactor mass is almost entirely concentrated to two rigid solids (i.e. the steel weights), positioned symmetrically around the impactor centroid. Consequently, the impactor can, when in contact with the glass panel, be well-represented by a generalized SDOF system. Hence, the impactor mass is lumped to a

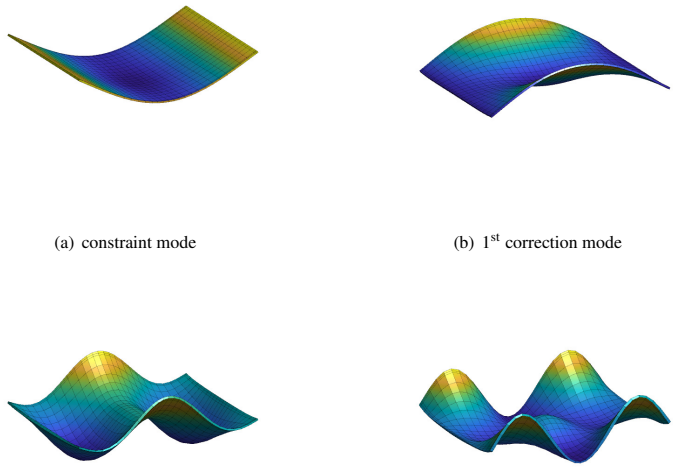

(a) constraint mode

(b) 1st correction mode

(c) 2nd correction mode

(d) 3rd correction mode

Figure 4: Constraint mode and first three correction modes.

single DOF. However, due to the contact interaction between the tire and the glass panel, and the behavior of the pneumatic tires, the SDOF model can be expected to be nonlinear.

With inspiration from Hertz contact law [14], a nonlinear load–displacement relation of the following form was assumed:

$$f_s(u) = k_0 u + k_1 u^{\alpha} \tag{12}$$

Hence, a SDOF model consisting of a linear spring in parallel with a nonlinear spring. Furthermore, a stiffness-proportional viscous damping model was adopted, such that the damping force f_d is proportional to the secant stiffness, i.e.:

$$f_d(u, \dot{u}) = \left(\beta_0 k_0 + \beta_1 k_1 u^{\alpha-1}\right) \dot{u} \tag{13}$$

where β_0 and β_1 are factors that determines the amount of damping (i.e. a nonlinear Rayleigh β-damping). The damping factors and the unknown factors k_0, k_1, and α were calibrated using experimental data as well as results provided by the numerical reference model, see further Sections 4 and 5.

Notice that a linear dashpot model, independent of the displacement, result in an unrealistic damping force having its peak value just upon impact, when the impactor mass velocity has its peak value. Nonetheless, it is of interest to investigate the accuracy of a linear approximate model for the impactor, which enables the use of computationally efficient analysis techniques. Approximate linear models representing the impactor are further

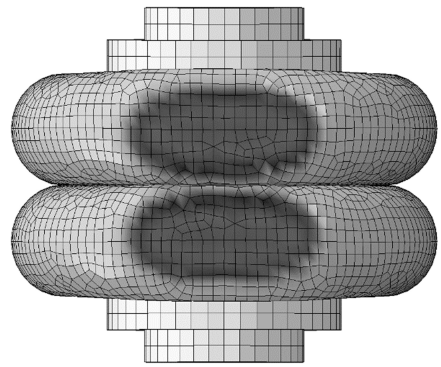

Figure 5: Example of contact area, shown in dark-gray color, provided by the reference models.

discussed in Section 5.1.

2.3. Coupling procedures and interface reduction

The impactor is modeled by a SDOF system, thus, only one DOF is to be connected to the glass panel substructure. Furthermore, the nonlinearity introduced due to contact between the impactor and the glass panel is partly integrated in the nonlinear impactor model, as described in Section 2.2. However, the distribution of the contact stresses determines which DOFs on the glass panel that should be included in the coupling.

Upon impact, contact is established and a small contact area is formed which gradually increases when the impactor kinetic energy is transformed into strain energy (and damping energy dissipation). Consequently, the contact area varies significantly during impact. Nonetheless, an approximate modeling approach assuming a constant contact area can be reasonably accurate, as e.g. shown in [8]. Hence, instead of including a full description of the contact interaction the contact stress distribution $\theta(x, y)$ is assumed constant while the total contact force $F_c(t)$ varies through time, i.e.

$$F_c(t) = \int \sigma_c(t, x, y) dA = F_c(t) \int \theta(x, y) dA \tag{14}$$

where σ_c is the contact stress and $\int \theta(x, y) dA = 1$.

Furthermore, it is reasonable to assume that an approximation that underestimates the contact area in general overestimates the peak-strain in the glass panel, since the contact pressure can then be expected to be larger. Accordingly, a more realistic peak-strain can be obtained if a somewhat larger "best-estimate" contact area is chosen, assuming that the peak-strain occur at a point in time when the contact area is relatively large.

An example of the shape and size of the contact area computed with the numerical reference model (see further Section 3.1) is shown in dark-gray color in Figure 5. Based on the results provided by the reference model, the contact area in the reduced models is assumed to have the shape of two ellipses, shown with purple dashed lines in Figure 6. The major and minor radius of the ellipses is set to 90 mm and 50 mm, respectively. These values are assumed to correspond to the contact area developed when the glass strain reaches a peak value. However, the

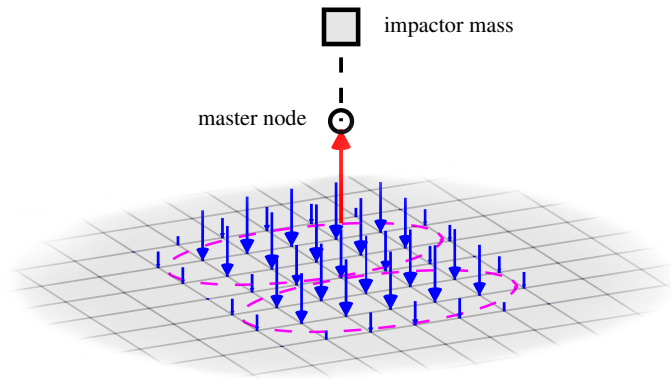

Figure 6: Distributed coupling between a master node and the glass panel slave nodes. The interface forces acting on the slave nodes and the master node are shown in blue and red color, respectively. The SDOF system representing the impactor is shown by the black dashed line. Note that the arrow length is not to scale.

contact area varies both in time and for different load cases, thus, the specified values should only be regarded as rough estimations. Furthermore, a uniform contact stress is assumed within the predefined contact area.

The simplified modeling approach described above was implemented by means of a multi-point constraint (MPC) where the interface forces between a master DOF and a group of slave DOFs are controlled using weight factors. This type of constraint can e.g. be found in Abaqus [17], where it is referred to as a *distributed coupling*. However, since no detailed information describing the implementation have been found, a proposal of how to enforce such a MPC constraint is presented herein. For simplicity, and the fact that only one master DOF is present, a one-dimensional MPC is considered (i.e. only interface forces perpendicular to the glass panel are considered). The MPC constraint, as described below, was implemented in Matlab.

The basis in the MPC method is the requirement that the sum of the interface forces acting on the slave DOFs is equal to the interface force acting on the master DOF, cf. Figure 6. This requirement is not that restrictive and can in principle be fulfilled by any interface force distribution, as long as equilibrium is maintained. As shown further below, this is also why this method allows for customized interface force distributions.

Assume that a set of weight factors w_i, related to the MPC slave DOFs, are normalized such that

$$\widehat{w}_i = \frac{w_i}{\Sigma_{j=1}^{k} w_j} \tag{15}$$

where k is the number of slave DOFs (which should be distinguished from k used in the previous sections, denoting the number generalized coordinates). Further, the constraint is enforced so that the displacement of the master DOF

is the weighted mean value of the slave DOFs [17], i.e.:

$$u^{(m)} = \sum_{j=1}^{k} \hat{w}_j u_j^{(s)} \tag{16}$$

which implies that the displacement associated to slave DOF i can be expressed as:

$$u_i^{(s)} = \frac{1}{\hat{w}_i} \left(u^{(m)} - \sum_{j=1, j\neq i}^{k} \widehat{w}_j u_j^{(s)} \right). \tag{17}$$

Hence, one DOF is redundant and can be calculated based on the displacements of the other DOFs included in the MPC. Further, Eq. 17 can be expressed in matrix form

$$\mathbf{B}\mathbf{u} = 0 \tag{18}$$

where $\mathbf{B}$ is a vector containing the normalized weight factors $\widehat{w}_i$ at entries corresponding to slave DOFs, a negative one at the entry corresponding to the master DOF and zeros in the remaining entries. The size of $\mathbf{B}$ is $1 \times \tilde{n}$, where $\tilde{n} = n + 1$ (thus, one master DOF is added to the glass panel substructure having n DOFs).

The displacement can be partitioned in a set of unique $\mathbf{u}_u$ and redundant $\mathbf{u}_r$ DOFs [18]. If slave DOF k is chosen as the redundant DOF, then $\mathbf{u}_r = u_k^{(s)}$ and $\mathbf{u}_u = \begin{bmatrix} \mathbf{0} & u^{(m)} & u_1^{(s)} & \dots & u_{k-1}^{(s)} \end{bmatrix}$. Hence,

$$\mathbf{B} = \begin{bmatrix} \mathbf{B}_u & \mathbf{B}_r \end{bmatrix} \begin{bmatrix} \mathbf{u}_u \\ \mathbf{u}_r \end{bmatrix} = 0 \tag{19}$$

where $\mathbf{B}_u = \begin{bmatrix} \mathbf{0} & -1 & \widehat{w}_1 & \dots & \widehat{w}_{k-1} \end{bmatrix}$ and $\mathbf{B}_r = \widehat{w}_k$. By rewriting Eq. 19, the redundant displacement can be expressed as

$$\mathbf{u}_r = -\mathbf{B}_r^{-1}\mathbf{B}_u\mathbf{u}_u \tag{20}$$

Thus, the displacement vector can be expressed in terms of the unique displacements,

$$\begin{bmatrix} \mathbf{u}_u \\ \mathbf{u}_r \end{bmatrix} = \begin{bmatrix} \mathbf{I}_{uu} \\ -\mathbf{B}_r^{-1}\mathbf{B}_u \end{bmatrix} \mathbf{u}_u = \mathbf{L}\mathbf{u}_u \tag{21}$$

where $\mathbf{L}$ is a $\tilde{n} \times n$ transformation matrix.

The equation of motion for a linear system, including the redundant DOFs, can be written as:

$$\mathbf{M}\ddot{\mathbf{u}} + \mathbf{C}\dot{\mathbf{u}} + \mathbf{K}\mathbf{u} = \mathbf{f} + \mathbf{g} \tag{22}$$

where $\mathbf{M}$, $\mathbf{C}$ and $\mathbf{K}$ are the $\tilde{n} \times \tilde{n}$ mass, damping and stiffness matrix, $\mathbf{u}$ is the $\tilde{n} \times 1$ displacement vector, $\mathbf{f}$ is the $\tilde{n} \times 1$ external force vector and $\mathbf{g}$ is a $\tilde{n} \times 1$ interface force vector, which is included due to the presence of MPCs. Now, inserting the transformation according to Eq. 21 in Eq. 22 and pre-multiplying with $\mathbf{L}^\top$ yields:

$$\mathbf{L}^\top\mathbf{M}\mathbf{L}\ddot{\mathbf{u}}_u + \mathbf{L}^\top\mathbf{C}\mathbf{L}\dot{\mathbf{u}}_u + \mathbf{L}^\top\mathbf{K}\mathbf{L}\mathbf{u}_u = \mathbf{L}^\top\mathbf{f} \tag{23}$$

thus,

$$\mathbf{L}^\top \mathbf{g} = \begin{bmatrix} \mathbf{I} & \mathbf{0} & \mathbf{0} & \cdots & \mathbf{0} & \mathbf{0} \\ \mathbf{0} & 1 & 0 & \cdots & 0 & \frac{1}{\widehat{w}_k} \\ \mathbf{0} & 0 & 1 & \cdots & 0 & -\frac{\widehat{w}_1}{\widehat{w}_k} \\ \vdots & \vdots & \vdots & \ddots & \vdots & \vdots \\ \mathbf{0} & 0 & 0 & \cdots & 1 & -\frac{\widehat{w}_{k-1}}{\widehat{w}_k} \end{bmatrix} \begin{bmatrix} \mathbf{0} \\ g^{(m)} \\ g_1^{(s)} \\ \vdots \\ g_{k-1}^{(s)} \\ g_k^{(s)} \end{bmatrix} = \mathbf{0} \tag{24}$$

where we use that $-\mathbf{B}_r^{-1}\mathbf{B}_u = -\frac{1}{\widehat{w}_k}\begin{bmatrix} \mathbf{0} & -1 & \widehat{w}_1 & \dots & \widehat{w}_{k-1} \end{bmatrix}$.

As indicated by Eq. 24, the weight factors control the distribution of the interface forces acting on the slave DOFs. For example, Eq. 24 implies that $g_k^{(s)} = -\widehat{w}_k g^{(m)}, g_1^{(s)} = \frac{\widehat{w}_1}{\widehat{w}_k} g_k^{(s)} = -\widehat{w}_1 g^{(m)}$ and, in general, $g_i^{(s)} = \frac{\widehat{w}_i}{\widehat{w}_k} g_k^{(s)} = -\widehat{w}_i g^{(m)}$. Further, according to Eq. 15, the weight factors are normalized, which implies that

$$\sum_{j=1}^{k} g_j^{(s)} = \sum_{j=1}^{k} g^{(m)} \widehat{w}_j = g^{(m)} \sum_{j=1}^{k} \widehat{w}_j = g^{(m)}. \tag{25}$$

Hence, equilibrium is maintained. Moreover, it should be noted that the above formulation allows for arbitrary weight factors, e.g. to consider a non-uniform interface force distribution or a non-uniform element mesh.

2.4. Dynamic response analysis

In the experimental tests, the pendulum impactor is released from a specific drop height and starts a swing motion until, at its lowest point, impact with the glass panel. The numerical analyses are initiated just upon impact. Thus, the dynamic response of the impactor-glass system is obtained by solving an initial value problem—the external forces are zero and an initial velocity is prescribed to the impactor. The initial velocity $\dot{u}_{0,\text{imp}}$ is computed based on the pendulum drop height:

$$\dot{u}_{0,\text{imp}} = \sqrt{2gh} \tag{26}$$

where g is the gravitational acceleration and h is the drop height. Solution methods for both linear and nonlinear systems are investigated. Furthermore, only the first phase, when there is contact between the impactor and the glass panel, is considered.

2.4.1. Linear systems with nonclassical damping

If the coupled impactor–glass structure is approximated using a linear model with classical damping, a closed-form solution is straightforward to obtain by means of modal expansion techniques applied to the assembled system [25]. However, this approach is in general not feasible for systems with non-classical (also referred to as non-proportional) damping since a projection of the system equations onto a modal basis would then not result in a diagonal damping matrix. According to Section 5.1, the damping ratio of a linear impactor model can be estimated to be about 5%, whereas the damping ratio of the simply supported glass panels is approximately 1.7%, as discussed further in Section 4. Thus, the damping of the assembled system is indeed non-proportional and, consequently, a traditional modal analysis cannot be utilized. Nonetheless, a closed-form solution can be achieved.

For example, by means of the complex damped eigenmodes using a state space formulation (see e.g. [27]) or by use of the so-called modal strain energy (MSE) method, which is an approximate method to account for non-proportional damping [28, 29]. An advantage using the MSE method compared to a state space formulation is that the number of system variables are halved and that imaginary variables can be avoided. Furthermore, the numerical investigations presented in [28] suggests that the MSE method is accurate for systems with damping less than approximately 20%, thus, it can be assumed sufficiently accurate for the studied glass-impactor system.

The damping ratio of a SDOF system representing a modal coordinate can be expressed as:

$$\zeta = \frac{E_D}{4\pi E_S} \tag{27}$$

where E_D is is the one-cycle modal energy loss due to viscous damping and E_S is the modal strain energy amplitude, given by:

$$E_S = \frac{1}{2}\boldsymbol{\phi}_j^\top \hat{\mathbf{K}} \boldsymbol{\phi}_j \tag{28}$$

where $\hat{\mathbf{K}}$ is the $\hat{m} \times \hat{m}$ global stiffness matrix, representing the coupled impactor–glass system, and $\boldsymbol{\phi}_j$ is the eigenvector for mode j, obtained by solving the generalized eigenvalue problem:

$$\left(\hat{\mathbf{K}} - \omega_j^2 \hat{\mathbf{M}}\right) \phi_j = 0 \tag{29}$$

where ω_j is the corresponding eigenfrequency. Notice that the elements of the eigenvectors includes physical as well as generalized DOFs.

In accordance with the MSE method, the modal energy loss is computed as:

$$E_D = \pi \omega_j \boldsymbol{\phi}_j^\top \hat{\mathbf{C}} \boldsymbol{\phi}_j \tag{30}$$

where ω_j is the eigenfrequency for mode j and $\hat{\mathbf{C}}$ is the $\hat{m} \times \hat{m}$ global damping matrix, containing the damping submatrices related to the glass and impactor, respectively. It follows that the modal damping ratio for mode j can be computed as:

$$\zeta_j = \frac{\boldsymbol{\phi}_j^\top \hat{\mathbf{C}} \boldsymbol{\phi}_j}{2\omega_j \boldsymbol{\phi}_j^\top \hat{\mathbf{M}} \boldsymbol{\phi}_j} \tag{31}$$

where $\hat{\mathbf{M}}$ is the $\hat{m} \times \hat{m}$ global mass matrix.

As in a traditional modal decomposition applied to systems expressed in terms of physical DOFs, a linear system reduced by means of DS can be expressed in modal coordinates:

$$\mathbf{q} = \sum_j \boldsymbol{\phi}_j \eta_j \tag{32}$$

where η_j is the modal coordinate for mode j.

If neglecting damping, the system equations can be diagonalized by projecting the system onto the modal basis:

$$\boldsymbol{\Phi}^\top \hat{\mathbf{M}} \boldsymbol{\Phi} \ddot{\eta} + \boldsymbol{\Phi}^\top \hat{\mathbf{K}} \boldsymbol{\Phi} \eta = \boldsymbol{\Phi}^\top \tilde{\mathbf{p}} \tag{33}$$

where $\mathbf{\Phi} = \begin{bmatrix} \boldsymbol{\phi}_1 & \boldsymbol{\phi}_2 & \dots & \boldsymbol{\phi}_{\hat{m}} \end{bmatrix}$ is the modal matrix and $\eta = \begin{bmatrix} \eta_1 & \eta_2 & \dots & \eta_{\hat{m}} \end{bmatrix}^\top$ is the modal amplitudes. Hence, a set of $\hat{m}$ uncoupled differential equations, which can be solved independently, is obtained.

Now, by introducing the modal damping ratios determined by means of the MSE method, and assuming that the external force is zero, each modal response is given by:

$$\eta_j(t) = e^{-\zeta_j \omega_j t} \left(\eta_j(0) \cos(\omega_{jD} t)) + \frac{\dot{\eta_j}(0) + \zeta_j \omega_j \eta_j(0)}{\omega_{jD}} \sin(\omega_{jD} t) \right) \tag{34}$$

where ζ_j is the damping ratio for mode j and $\omega_{jD} = \omega_j \sqrt{1 - \zeta_j^2}$ is the jth natural frequency with damping [25]. In contrast to a traditional modal response analysis, which commonly uses a truncated modal basis, it is in this case reasonable to include all $\hat{m}$ modes in the modal basis because a reduction has already been performed on the substructure level. Hence, the modal analysis is primarily employed for diagonalizing the system matrices, not for reducing the system size.

In a standard modal analysis, the modal damping matrix is in general constructed directly in the modal domain by means of modal damping ratios, e.g. provided by experimental tests. However, using the MSE method, the global damping matrix $\hat{\mathbf{C}}$, containing the damping submatrices, is required. The SDOF model representing the impactor uses stiffness-proportional damping, as discussed in Section 2.2. Hence, if considering a linear impactor model, viscous damping is modeled by a ordinary dashpot. The damping matrix related to the glass panel is constructed by means of Rayleigh-damping, i.e.

$$\mathbf{C} = \alpha \mathbf{M} + \beta \mathbf{K} \tag{35}$$

where α and β are the Rayleigh damping parameters [25]. The glass panel damping is further investigated in Section 4 and the calibration of the Rayleigh parameters are discussed in Section 5.

By using the above methodology, a closed-form solution is obtained for initial value problems of linear systems even though non-proportional damping is present. Notice, however, that the above procedure is indeed an approximation due to that possible off-diagonal terms is not considered in the modal damping matrix given by $\mathbf{\Phi}^\top \hat{\mathbf{C}} \mathbf{\Phi}$.

2.4.2. Direct time-integration of nonlinear systems

The dynamic response of the nonlinear systems is solved using implicit direct time-integration. For the reduced models, direct time-integration is performed using Newmark's method [25]. The Newmark parameters are set to $\beta = \frac{1}{4}$ and $\gamma = \frac{1}{2}$ resulting in a unconditionally stable system, which is convenient when solving a nonlinear system. Further, force equilibrium in each time increment is established by means of Newton-Raphson iterations [25].

3. Numerical reference model

A detailed FE model of the impactor was established using the commercial FE analysis software Abaqus [17]. The response computed with the reference model complements the experimental results in a validation of the

reduced models (see further Section 5.3). Furthermore, the FE model provides insight into the impactor structural behavior and its interaction with the glass panel, which is vital knowledge in the process of deriving and evaluating a reduced model.

Furthermore, a FE model of the glass panel was developed, employed both in the Abaqus analyses including the impactor reference model and for generating system matrices, which are necessary in the process of establishing reduced models representing the glass panel. The FE model of the glass panel was modeled in Abaqus. However, to get full access to the FE procedures a separate, but in practice equivalent, FE model was made using Matlab.

3.1. Impactor

The impactor rubber tires are pneumatic bias-ply tires which consist of rubber reinforced by nylon ply-cords, usually in an angle $\pm$ 30°–40° from the direction of travel, with each additional ply positioned in opposite direction [6].

In Abaqus, the nearly incompressible rubber material was modeled using a hyperelastic model. The strains in the rubber turns out to be relatively small ($<$ 20 %), why a Neo-Hooke model, with parameters according to Table 1, is judged to be sufficiently accurate. The rubber tires were modelled by four-node shell elements and the nylon cords were modelled using so-called rebar layers, a feature in Abaqus that allows for specifying orthogonal or skew reinforcement embedded in shell or membrane elements. Hence, the nylon cords are not modeled by separate elements, but is rather modeled as a smeared rebar layer positioned at the shell element reference surface. The cords diameter was set to 0.45 mm with a spacing 1.6 mm, in accordance with [5]. By an optical investigation of a cut of a tire, the thickness of the rubber was estimated to 5 mm.

An accurate model of the stiffness distribution of the nylon ply-cords is important for a realistic behavior of the tire model. The pressure exerted by the contained air is mainly balanced by tensile stresses in the nylon cords having a stiffness several order of magnitude larger than the rubber (even when considering the difference in cross-section area). Therefore, the stiffness of the inflated tires is primarily due to prestressing of the nylon ply-cords and, consequently, the angle of the nylon cords have a relatively large effect on the structural behavior. However, data for the nylon cord angle for the specific tires used in this study was not available. Instead, the angle was determined by comparison of the deformed shape of the actual tire, when inflated and non-inflated, with the deformed shape given by a quasi-static analysis of the tire inflation. Based on this comparison, the angle was estimated to be 40°.

The tire air pressure was modeled using a feature in Abaqus denoted *fluid cavity*, which considers the coupling between the deformation of the tire structure and the pressure exerted by the contained air. Using this modeling approach, only the quasi-static air pressure is considered, whereas the dynamic pressure is ignored. An overpressure of 4.07 bar was prescribed in the undeformed configuration to obtain an air pressure of 3.5 bar in the deformed configuration.

The steel weights, rims, and the screw spindle (the axis connecting the two weights) were modeled using linear elastic material properties according to Table 1. In principle, the weights can be modeled as rigid bodies since these are much stiffer than the tires. However, the deformation of the rim and the screw spindle might not be negligible. Also, the off-center location of the weights causes the screw spindle to bend, which in turn effects the deformation

Table 1: Material models employed in the reference model.

Material	Material model	Material parameters
Rubber	Hyperelastic, Neo-Hookean	$G = 1.2$ MPa, $K = 2$ GPa, $\rho = 1100$ kg/m^3 [5, 6]
Nylon	Linear elastic	$E = 3$ GPa, $\nu = 0.3$, $\rho = 1100$ kg/m^3 [5, 30]
Steel	Linear elastic	$E = 210$ GPa, $\nu = 0.3$, $\rho = 7830$ kg/m^3 [5]
Glass	Linear elastic	$E = 72$ GPa, $\nu = 0.23$, $\rho = 2500$ kg/m^3 [31]

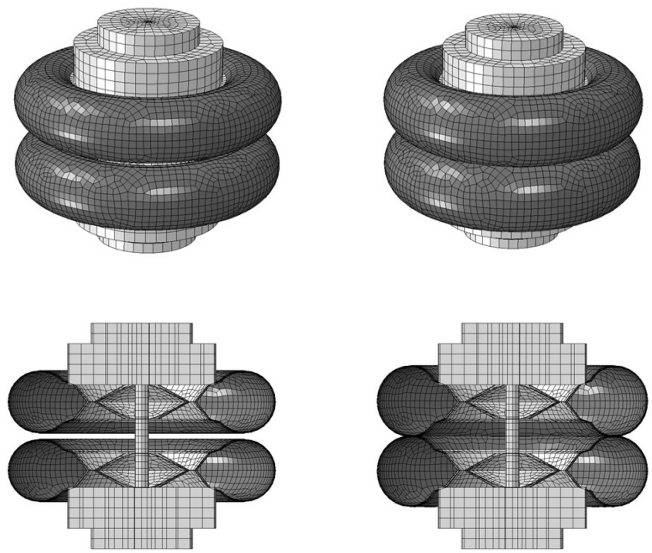

Figure 7: Undeformed (left) and inflated (right) configuration. The rubber/nylon and steel are shown in dark-gray and gray color, respectively.

of the tires. To consider a possible influence of these effects the steel weights and the screw spindle were modeled by eight-node solid elements, whereas the rim was modeled with four-node shell elements. The impactor model mesh, for both the un-inflated and inflated configuration, is shown in Figure 7.

A viscous stiffness-proportional damping was calibrated to the energy loss measured in the impact tests, as discussed in Sections 4 and 5.1. Moreover, a contact interaction was prescribed between the tires, with a friction coefficient of $\mu = 0.7$ in accordance with [6].

3.2. Glass panel

The glass panel was modeled with solid shell elements, which uses an assumed strain distribution for an enhanced modeling of bending [32]. An advantage using these elements compared to conventional shell elements is that no special treatment is needed to consider offsets of loads or prescribed boundary conditions. An evaluation of using solid shells for modeling glass panels is e.g. presented in [33].

The supporting steel frame was assumed rigid and the EPDM rubber strips positioned between the glass and the steel were modeled by linear elastic spring beds. In the experimental set-up, the rubber along the supports

(a) (b)

Figure 8: Soft-body impact test set-up (a) and strain gauge on the rear side of the glass panel (b).

were prestressed due to bolting of the glass panels, which affect the rubber stiffness. Therefore, the stiffness of the spring beds were calibrated based on the fundamental frequencies as measured for the 8, 10 and 12 mm, respectively, simply supported glass panels. Using this approach, the stiffness of the rubber strips was estimated to 10 MPa (the glass geometry, density, and stiffness, which also affect the fundamental periods, are thus regarded as relatively well-known parameters). The in-plane stiffness of the rubber strips was modeled in a similar manner using elastic springs.

In accordance with the measurements discussed in Section 4, a damping ratio of 1.7% was assumed for the glass panels being modeled by means of Rayleigh α- and β-damping. The derivation of the Rayleigh parameters is further discussed in Section 5 and the prescribed values are presented in Table 4.

4. Experimental testing

Experimental tests were performed to validate the reduced models. In particular, the strain was measured on simply supported monolithic glass panels with dimensions $1000\ \text{mm} \times 800\ \text{mm}$, made of regular soda-lime silicate toughened glass. The glass panel impact tests were part of an experimental campaign summarized in [34, 35], which includes additional tests of glass panels mounted with various fixing methods, such as linear clamps, local clamp fixings and point fixings. Moreover, glass with different heat treatment as well as glass laminated with different materials were also tested.

Additional measurements were performed to identify the dynamic characteristics of the impactor. The dynamic properties of the impactor, such as the dynamic stiffness and damping turn out to have a large impact on the dynamic behavior of the coupled impactor–glass system. Also, an increased insight into the structural behavior is essential in the process of developing reduced models, to ensure that no significant characteristics of the system are lost in the reduction process.

Table 2: Impactor rigid impact energy loss.

Test No	Drop height (h_0) [mm]	Height diff. ($\Delta h = h_0 - h_1$) [mm]	Energy loss ($\Delta \frac{h}{h_0}$)[%]	Mean [%]
1	100	20	20	20
2	100	20	20	
3	200	55	27.5	28
4	200	55	27.5	
5	300	80	26.7	27
6	300	80	26.7	
7	450	140	31.1	30
8	450	130	28.8	
9	700	230	32.9	32
10	700	220	31.4	

4.1. Dynamic characteristics of impactor

The impactor design is described in [1], where the impactor parts are specified in detail. The tires should be of the type 3.50-R8 4PR (by Vredestein) or tires that are demonstrated equivalent. In the present study, two Michelin 3.50-S83 tires were used (see Figure 8 b), which were also used in the experimental tests presented in [5]. The inflation pressure is 3.5 bar and the total weight of the impactor is 50 kg.

The impactor damping and stiffness were evaluated based on impact with a very stiff steel column, which can be considered rigid. The impactor acceleration was measured at several locations on the impactor weights, as shown in Figure 2b. Similar tests were also performed in [5]. However, the tests performed in the present study also included an estimation of the impactor damping. More specifically, the difference between the maximum height of the impactor after impact h_1 and the initial drop height h_0 was measured. Hence, the energy loss during impact (ΔE) was estimated as

$$\Delta E = mg\left(h_0 - h_1\right). \tag{36}$$

The measurement of the impactor position was performed by recording the impact sequence on video at a frame rate of 240 frames per second, sufficiently high to enable a smooth slow-motion video. Before the impact tests were performed, a physical measurement-grid was positioned in the plane of the pendulum, filmed at the same angle and position as the impact tests. This measurement grid was then used to calibrate the measurements performed directly in the slow-motion videos. Tests were preformed with an impactor drop height of 100, 200, 300, 450 and 700 mm, respectively.

The estimated energy loss, which in turn determines the damping, is presented in Table 3. Notice that the experimental methodology implies that the mass of the impactor weights can be assumed sufficiently large so that the system can be well-represented by a SDOF system when in contact with the rigid wall and a rigid mass floating in space when contact is not established.

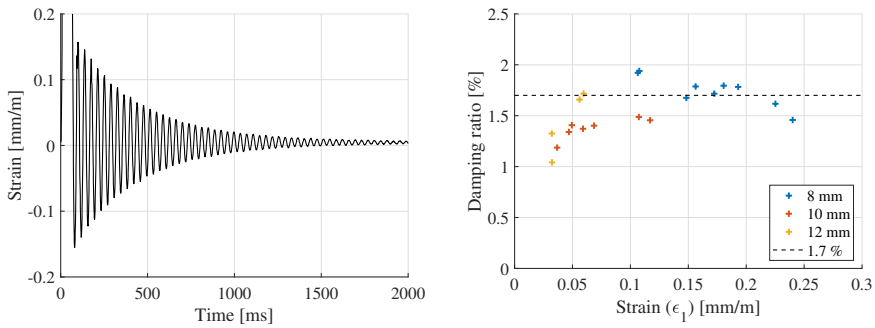

(a) Horizontal strain measured on rear side of glass

(b) Damping ratios estimated for various glass thicknesses

Figure 9: Decay of motion in terms of glass strain for test with a drop height of 500 mm and a glass thickness of 10 mm (a) and estimated damping ratios (b). The strain ϵ_1 is the strain measured at cylce i, corresponding to u_i in Eq. 37. The mean damping ratio for measurements with $\epsilon_1 > 0.1$ mm/m is equal to 1.7% and is shown by the black dashed line.

4.2. Soft-body impact on glass panels

Experimental results from impact tests of two-sided simply supported glass panels, as shown in Figure 8a, was used for validation of the reduced order models. The glass panels consist of toughened monolithic glass with nominal thickness 8, 10 and 12 mm, respectively. As described in [35], the horizontal strain was measured by a strain gauge bonded at the rear side (tensile side) of the glass panels at the point of impact, see Figure 8b. Impact tests were conducted with a drop height of 100, 200, 300, 400 and 500 mm, respectively.

The signal from the strain gauge was logged at a frequency of 600 Hz for a few seconds. However, the impactor contact time is typically less than 80 milliseconds. Hence, the logged strain data includes the decay of motion after impact, which was utilized for estimating the damping of the glass panels and its fixings. An example of the logged strain data is shown in Figure 9a. Further, the logarithmic decrement is given by:

$$\delta = \frac{1}{n} \ln \left(\frac{u_i}{u_{i+n}} \right) = \frac{2\pi\zeta}{\sqrt{1-\zeta^2}} \tag{37}$$

where u_i is the amplitude measured at cycle i, n is the number of cycles between the measured amplitudes and ζ is the damping ratio. If assuming linear elasticity, the displacement amplitudes in Eq. 37 can be replaced by the measured strain amplitude. The estimated damping for some of the tests is presented in Figure 9b. The x-axis denotes the strain amplitude measured at cylce i, corresponding to u_i in Eq. 37. As shown in the figure, the damping ratio does not vary much with neither the glass thickness nor the amplitude. However, it should be noted that the strain amplitude is fairly low in all the measurements, i.e. less than 0.25 mm/m. Based on the data from the impact tests, the damping ratio of the glass and its fixings was estimated to 1.7 %. This is slightly larger than the damping ratios reported in e.g. [36, 37] where, however, different test arrangements were used.

In addition to the estimation of the glass panel damping ratio, the measured strain due to free vibration after impact was used for estimation of the fundamental periods of the simply supported glass panels. Note that the glass strain, which is measured in the center of the glass panel, is mainly due to vibration of the fundamental mode. For glass panels with thickness 8, 10 and 12 mm, respectively, the fundamental period was estimated to 46, 37 and 31

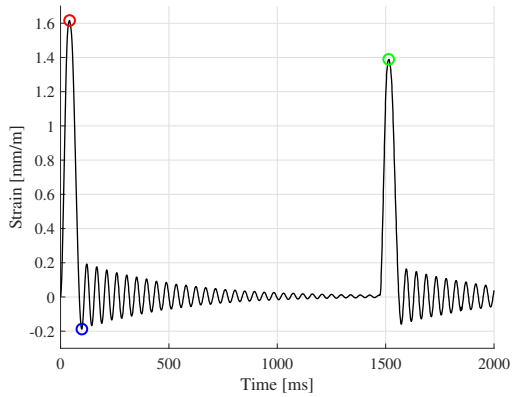

Figure 10: Horizontal strain measured on the rear side of the glass panel with thickness 8 mm for the double impact test. The initial drop height was 200 mm.

milliseconds, respectively.

Finally, the strain was measured for a double impact test, as shown in Figure 10. This was done for one impact test: the 8 mm glass panel subjected to an impact corresponding to a drop height of 200 mm. The measured strain was exploited to implicitly estimate the energy loss during impact for the whole system. This includes energy dissipation due to deformation of the impactor (e.g. frictional or viscous damping), through frictional effects due to contact, and deformation of the glass panel and its fixings.

If assuming linear elastic behavior, the response can be obtained by solving an initial value problem of a linear system. As implied by Eqs. 32 and 34, the displacements of such a system is linearly dependent on the initial velocity. Accordingly, the displacements are quadratically dependent on the initial kinetic energy of the impact body $E_{K,0}$, given by

$$E_{K,0} = \frac{m_{\text{imp}} \dot{u}_{0,\text{imp}}^2}{2}. \tag{38}$$

It follows that the square of the ratio between the peak strain in the first and second impact is proportional to the ratio between the kinetic energies induced in the system upon the first and second impact, respectively. Hence,

$$\left(\frac{\epsilon^{(2)}}{\epsilon^{(1)}} \right)^2 = \frac{{E_{K,0}}^{(2)}}{{E_{K,0}}^{(1)}} \tag{39}$$

where $\epsilon^{(1)}$ and $\epsilon^{(2)}$ are the strains measured for the first and second impact, and ${E_{K,0}}^{(1)}$ and ${E_{K,0}}^{(2)}$ are the kinetic energy just before the first and second impact, respectively. From the measured peak strains according to Figure 10 (red and green circle), the ratio between the kinetic energy in the first and second impact can be estimated to $(1.386/1.616)^2 = 0.74$. Thus, the energy induced in the system upon the second impact is 74% of the impact energy in the first impact and, accordingly, the energy loss is approximately 26%. This is fairly close to the energy loss measured in the rigid impact tests, shown in Table 3, which may indicate that the energy dissipation related to the deformation of the glass panel is fairly small. However, it should be noted that the energy loss computed

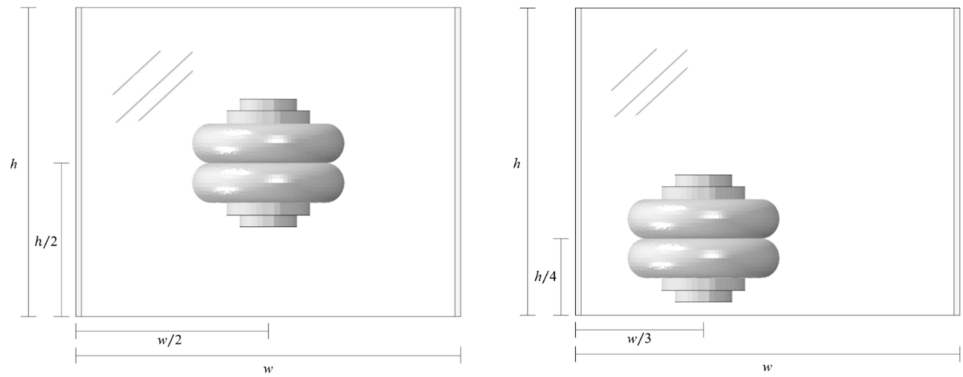

(a) Load Case A (b) Load Case B

Figure 11: Position of impactor in load case A and B. The glass panel dimensions are h = 1000 mm and w = 800 mm. Spring beds are applied on the parts of the glass panels marked with light gray color.

from a double impact test using the above procedure is in principle only valid for linear systems, why it should only be regarded as a rough estimate. Moreover, some of the induced energy is not dissipated during the impact but instead causes the glass panel to oscillate after impact. The glass panel strain energy is related to the square of the glass strain. Accordingly, a strain energy ratio can be estimated based on the peak strain during impact and the peak strain after impact. Using the measured strains according to Figure 10 for the first impact (red and blue circle), the strain energy ratio is $(0.1925/1.616)^2 = 1\%$, which principally is negligible.

5. Model validation

In order to validate the reduced models, the computed response is compared to both experimental results and the response provided by the reference model. Two load cases are evaluated where the point of impact is centric (load case A) and eccentric (load case B), respectively. In both load cases impact loading of a two-sided continuously supported monolithic glass panel, with width 1000 mm and height 800 mm, is studied. The position of the impactor for load case A and B, respectively, is shown in Figure 11.

Calibrations of the impactor reference model and the developed SDOF models, representing the impactor, are presented in Section 5.1. In Section 5.2, the response computed with the reference model and the reduced models are compared and evaluated based on load case A and B. Furthermore, in Section 5.3, a validation based on experimental results is presented for load case A.

5.1. Calibration of impactor models

A calibration of the numerical reference Abaqus model of the impactor was conducted based on the rigid impact tests discussed in Section 4. Numerical analyses of impact with a rigid surface was performed to simulate the experimental tests. The analyses were initiated just upon impact by prescribing an initial velocity to the impactor. The model was calibrated in the sense that a stiffness-proportional viscous damping was prescribed

Table 3: Impactor energy loss due to impact with rigid beam.

Drop height [mm]	Experiment [%]	FE model[1] [%]	SDOF model [%]
100	20	24	22
200	28	26	25
300	27	28	27
450	30	30	30
700	32	32	32

[1] Viscous dissipation and frictional damping due to contact interaction.

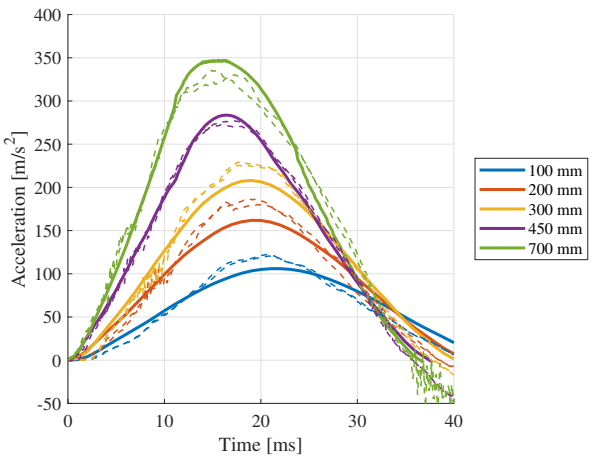

Figure 12: Comparison of impactor acceleration according to reference model (solid line) and experiments (dashed line).

to match the energy loss obtained in the experimental tests, see Table 3. Based on this calibration, a damping parameter of $\beta = 0.022$ was prescribed to the rubber, proportional to the strain-free elastic stiffness. The other material parameters was set according to Table 1.

The impactor acceleration is shown in Figure 12 for a drop height of 100, 200, 300, 450, and 700 mm, respectively. The dashed lines are the accelerations measured in the impact tests and the solid lines are the accelerations provided by the numerical simulations, extracted from a node close to the position of the accelerometer in the experimental test. As shown in the figure, the computed accelerations show good agreement with the experimental results for drop heights 450 and 700 mm. However, the measured peak acceleration is higher, and the measured pulse time is shorter for drop heights 100, 200, and 300 mm. It may be that some of the discrepancy is due to that the damping of the impactor is in fact frictional rather than viscous for lower amplitudes; a coulomb type damping would result in an unsymmetrical and shorter acceleration pulse with a larger peak acceleration. Notice that even though friction is considered in the contact interactions in the reference model, this has a small impact on the total energy dissipation, which is mainly due to viscous damping.

The nonlinear SDOF model, presented in Section 2.2, was calibrated to the impactor reference model. More specifically, a hysteresis loop, representing the behavior of a generalized SDOF system, was obtained from the reference model by plotting the movement of the impactor mass centroid and the total contact force between the

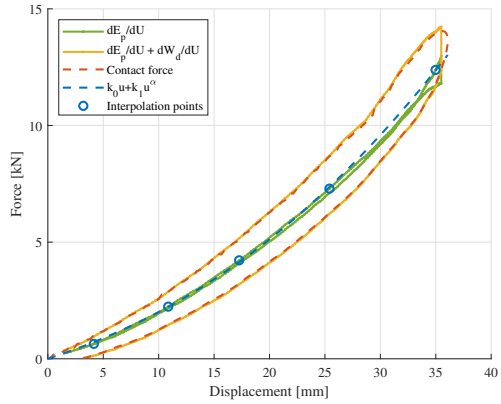

Figure 13: Example of calibration of nonlinear SDOF model from the hysteresis loop provided by the reference model.

impactor and the rigid surface. The total contact force is equal (but with opposite sign) to the sum of the impactor damping force and elastic force. To distinguish the total elastic force from the total internal force, the elastic force was approximated as the derivative of the total strain energy with respect to the displacement of the impactor mass centroid, as shown by the green curve in Figure 13. In a similar manner, the damping force was estimated as the derivative of the viscous dissipation. Hence, the sum of the derivatives, shown by the yellow curve in Figure 13, represent the total internal force, which is very close to the total contact force shown by the dashed red curve. The unknown stiffness factors in the generalized SDOF model (i.e. k_0, k_1 and α in Eq. 12) was then computed from the load–displacement curve in a least-square sense. More specifically, the factors k_0, k_1 were determined by a least-squares problem for a given α value. By traversing a sequence of α values, a best estimate was obtained. For instance, the blue dashed curve in Figure 13 correspond to the nonlinear SDOF model calibrated to the data pairs marked by blue circles. Note that the derivatives are ill-conditioned close to the peak displacement, why these are only computed for displacements less than approximately 35 mm.

The acceleration given by the nonlinear SDOF model, with factors calibrated to $k_0 = 1.59{\cdot}10^5$, $k_1 = 1.25{\cdot}10^7$, and $\alpha = 2.242$, respectively, is shown for various drop heights in Figure 14a. The damping parameters in Eq. 13 were calibrated to $\beta_0 = 8{\cdot}10^{-4}$ and $\beta_1 = 4{\cdot}10^{-3}$, respectively, based on the shape of the hysteresis loop provided by the reference model and the measured energy loss, presented in Table 3. The hysteresis loop for various drop heights are shown in Figure 15, computed with the reference model and the nonlinear SDOF system, respectively.

As discussed in Section 2.4, a linear system can be solved using modal expansion techniques and, in particular, a closed-form solution can be achieved for initial value problems. A linear model of the assemble system implies the use of a linear impactor model. However, as shown in Figure 12, the pulse time vary with the impact energy, which is expected for a nonlinear system. The system appears stiffer, i.e. the pulse time is shorter, for an increasing drop height, which is also consistent with the nonlinear system discussed above. Nonetheless, a simplified approximate model can be derived using the measured pulse time.

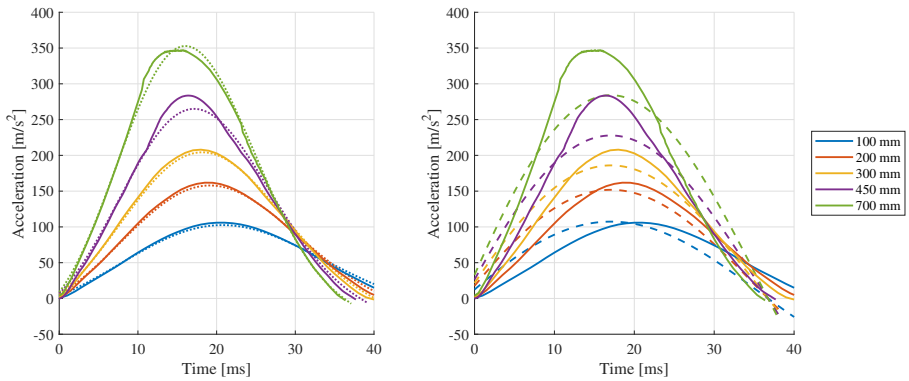

(a) Reference model / Nonlinear SDOF (b) Reference model / Linear SDOF

Figure 14: Comparison of impactor acceleration according to reference model (solid), nonlinear (dotted) and linear (dashed) SDOF model.

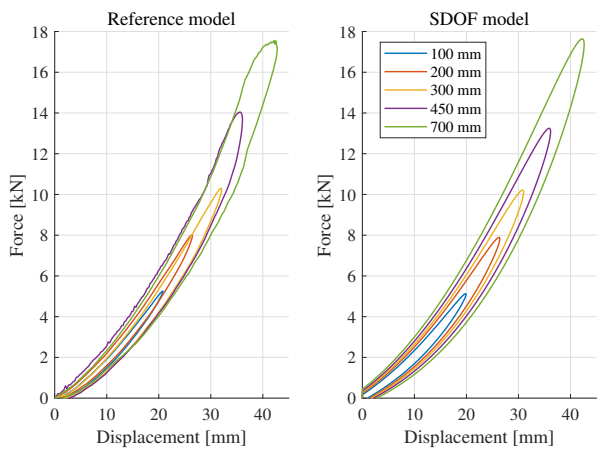

Figure 15: Comparison of total contact force and centroid displacement computed using the reference model and SDOF system, respectively.

When contact is established, the movement of the impactor mass centroid can be represented by a SDOF system subjected to free vibration. It then follows that the pulse time, which corresponds to half the natural period of the system, can be employed for estimating a linear stiffness. Using this approach, a pulse time of 38 ms was considered for estimating an approximate stiffness, which is close to the pulse time measured for a drop height of 450 mm. Hence, the natural period of the system can be approximated as $T = 2 \cdot 38 = 76$ ms, corresponding to an angular frequency of $\omega = 82.7$ rad/s. Accordingly, the stiffness is given by $k = m\omega^2 = 342$ kN/m. Similar to the nonlinear system, a stiffness-proportional damping was considered (i.e. a ordinary dashpot) with a damping coefficient calibrated to $c = 445$ Ns/m (corresponding to a damping ratio of $\zeta = 5.4\%$). The acceleration computed with the linear SDOF model is shown in Figure 14b. Notice that there is an instantaneous acceleration in the acceleration curves, which is a consequence of the initial damping force being linearly proportional to the

Table 4: Rayleigh parameters for the glass panel substructure and natural periods and damping ratios for the assembled system.

Glass thickness	α	β	T_1 [ms]	T_2 [ms]	ζ_1[1][%]	ζ_2[1][%]
8 mm	1.25	$1.21 \cdot 10^{-4}$	144.8	26.6	1	9.4
10 mm	1.49	$1.14 \cdot 10^{-4}$	117.6	25.7	1.6	9.1
12 mm	1.67	$1.07 \cdot 10^{-4}$	103.1	24.5	2.3	8.1

[1] Damping ratio computed by means of the MSE method, as described in Section 2.4.

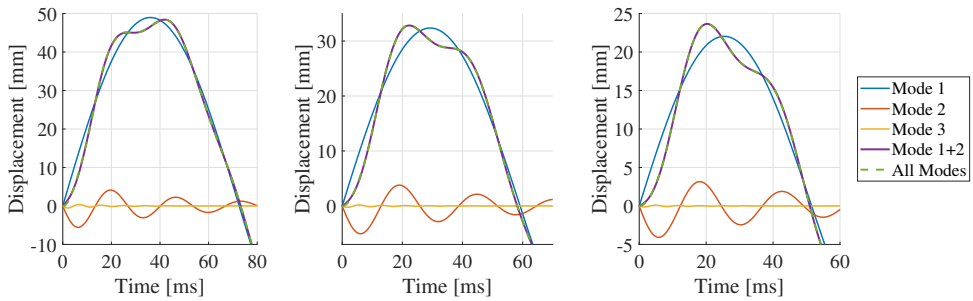

(a) h = 500 mm, t = 8 mm (b) h = 500 mm, t = 10 mm (c) h = 500 mm, t = 12 mm

Figure 16: Displacement of glass panel mid-point computed with the linear model. The modal contributions for the first three global modes are plotted separately.

prescribed initial velocity. Also, the computed pulse time is, as expected for a linear system, not dependent on the impact energy.

5.2. Evaluation of reduced order models

One of the benefits of the reduced linear model is the possibility to perform a modal decomposition of the coupled system. Beside the possibility to perform computationally efficient modal analyses, the eigenfrequencies, eigenmodes, and modal responses can be investigating to get further insight into the structural behavior. Moreover, the eigenfrequencies of the global system can be used for calibrating the Rayleigh damping model employed for constructing a damping matrix for the glass panel substructure. The Rayleigh damping parameters can then be utilized in the linear as well as the nonlinear analyses.

Figure 16 shows the glass panel mid-point displacement provided by the linear reduced order model, including six component modes in the glass panel reduction basis. Furthermore, the mid-point displacement has been decomposed into the contributions from the first three global modes, shown by separate curves in the figure. As shown, the response can be almost entirely represented by the first two modes, this is true for all the thicknesses studied. In the fundamental global mode, the displacement of the impactor DOF and the glass panel have the same sign, i.e. they are oscillating in-phase as shown in Figure 18. The second mode, however, is an "out-of-phase"-mode, where the displacement of the impactor and the glass panel have opposite signs. For higher order modes, it turns out that the impactor deformation is very small. This is due to that the impactor mass is large compared to the effective mass in the out-of-plane direction for higher order modes—for anti-symmetric modes the effective mass is zero, and for symmetric modes the effective mass decreases rapidly with the mode order.

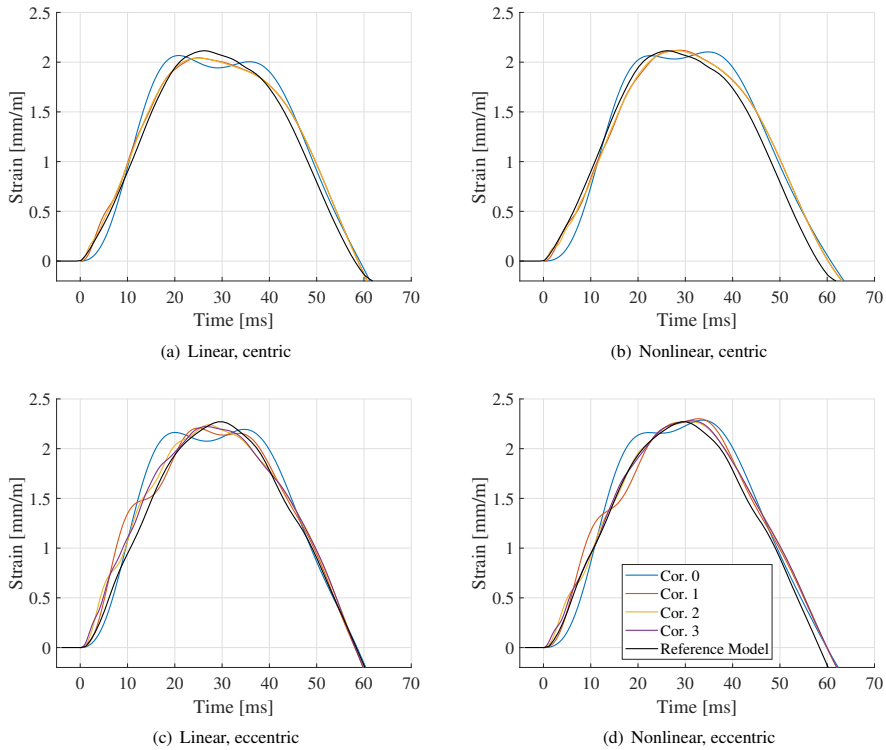

(a) Linear, centric (b) Nonlinear, centric

(c) Linear, eccentric (d) Nonlinear, eccentric

Figure 17: Horizontal strain computed with the linear and nonlinear reduced order models for various reduction basis. The label "Cor. i" denotes the order of the correction modes, where $i = 0$ implies that only constraint modes are considered.

The Rayleigh damping parameters for the glass panel were calibrated to match a "best-estimate" damping of 1.7% (c.f. Section 4) for the eigenfrequency of the first and second global mode, respectively [25]. The damping parameters, the corresponding natural periods, and the modal damping ratios are presented in Table 4. Notice that the modal damping ratios for the assembled system, computed by means of the MSE method, considers both the Rayleigh-damping prescribed to the glass panel substructure as well as the viscous damping model employed in the impactor SDOF model, which is linearly proportional to the frequency. Consequently, the computed global damping ratios will be frequency dependent, as shown in Table 4.

As further discussed in Section 4, the energy loss of the impactor-glass system was estimated to be around 26% for a glass panel thickness of 8 mm and a drop height of 200 mm. The corresponding energy loss provided by the linear model is approximately 18%, indicating that the damping prescribed to the assembled system is somewhat low. However, as discussed in Section 4, the energy loss estimated based on a double impact test should be regarded as a rough estimation due to limitations in the experimental methodology; for example, energy loss related to the motion of the pendulum is not considered, and a linear elastic behavior is assumed.

Figure 17 shows the horizontal strain on the rear side of the glass panel at the point of impact for various

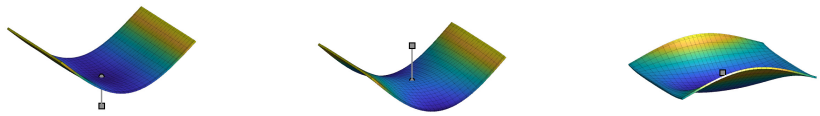

(a) Global Mode 1 (b) Global Mode 2 (c) Global Mode 3

(d) Global Mode 4 (e) Global Mode 5

Figure 18: First five global modes for assembled reduced system consisting of a linear impactor SDOF model and a reduction basis for the glass panel including a total of six component modes. The impactor mass is shown by the black square.

reduction bases applied to the glass substructure. As shown in the figure, the peak-strain is similar for all the models. However, a refined reduction basis is required for the glass substructure to capture the shape of the strain curve, in particular for the eccentric load case. Notice that the reduction basis employed for reducing the glass substructure should be sufficiently large so that the deformed shape of the glass panel for the important global modes can be resolved. Hence, the number of component modes required may be larger than the number of global modes needed for an accurate representation of the global response.

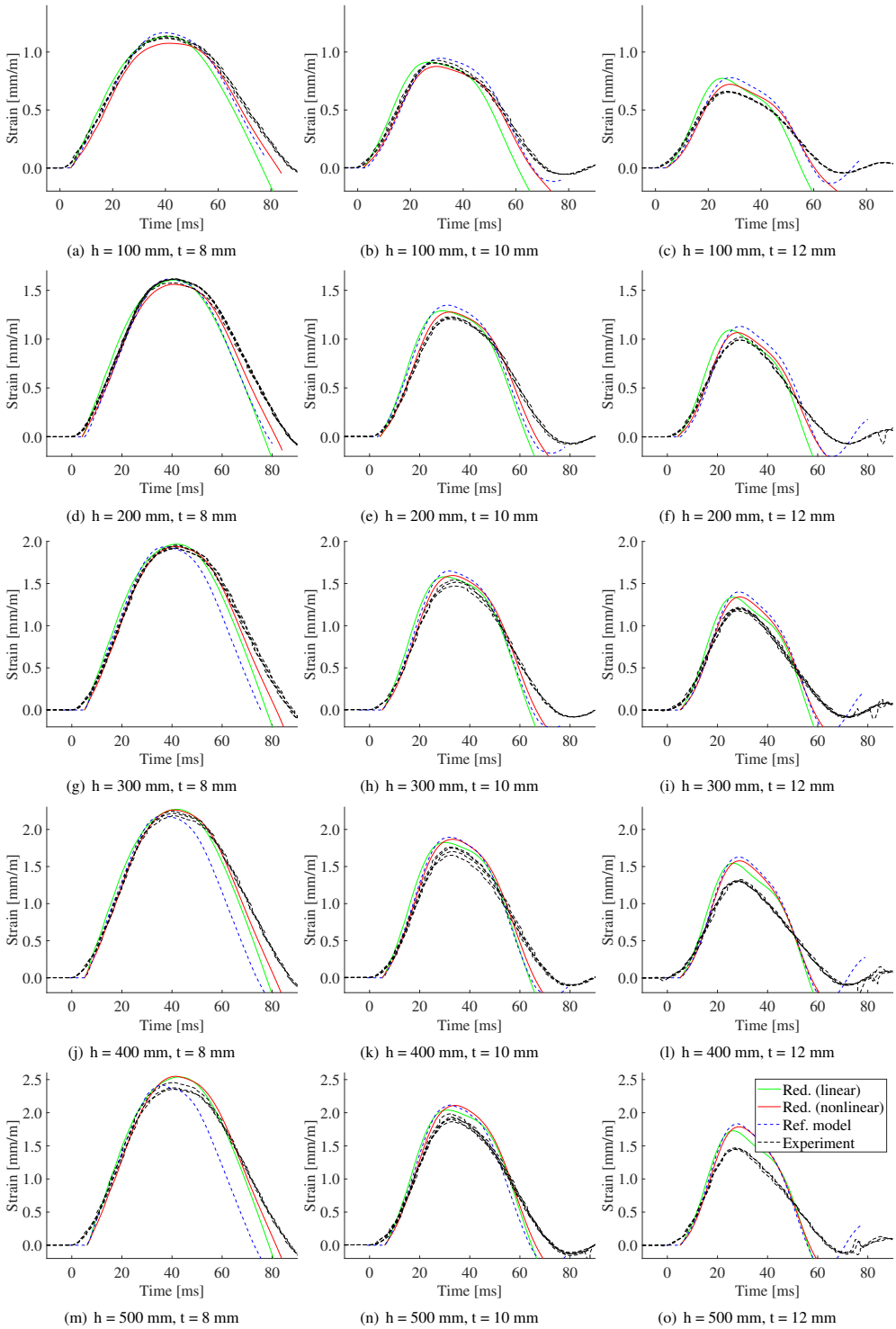

(a) h = 100 mm, t = 8 mm (b) h = 100 mm, t = 10 mm (c) h = 100 mm, t = 12 mm

(d) h = 200 mm, t = 8 mm (e) h = 200 mm, t = 10 mm (f) h = 200 mm, t = 12 mm

(g) h = 300 mm, t = 8 mm (h) h = 300 mm, t = 10 mm (i) h = 300 mm, t = 12 mm

(j) h = 400 mm, t = 8 mm (k) h = 400 mm, t = 10 mm (l) h = 400 mm, t = 12 mm

(m) h = 500 mm, t = 8 mm (n) h = 500 mm, t = 10 mm (o) h = 500 mm, t = 12 mm

Figure 19: Comparison between the measured and computed glass strain on the rear side of the glass panel at the center of impact. The impactor drop height, h, is 100 to 500 mm and the glass panel thickness is 8, 10 and 12 mm, respectively.

5.3. Validation of numerical models using experimental data

The measured horizontal strain on the rear side of the glass panels are shown for various drop heights and glass thicknesses in Figure 19, together with the corresponding strain given by the reference model and the reduced linear and nonlinear model, respectively. In the reduced models, the glass panel was reduced using six component modes (i.e. five fixed-interface correction modes and a constraint mode). As shown in the figure, the strain computed with the reference model and the reduced nonlinear model corresponds well to the measured strains for impact tests with a drop height 100 mm. However, the differences are amplified for impact tests with an increasing drop height. The deviation is especially pronounced for the glass panels with thickness 12 mm. Furthermore, it is of interest to evaluate not only the peak strain (even though this, in general, is the governing parameter in a design calculation) but also the shape of the strain curves indicating how well the models capture the structural behavior. As shown in the figure, the shape of the strain curves is relatively close for glass panels with thickness 8 mm, whereas the shape of the computed strain curves somewhat differ for glass panels with larger thickness.

The strain provided by the linear model is very close to the response computed with the nonlinear reduced model for the cases with a drop height of 500 mm. This is due to that the stiffness prescribed to the linear model fits better for larger amplitudes, as manifested by the acceleration curves in Figure 14. Accordingly, the pulse time is slightly underestimated by the linear model for lower drop heights .

6. Discussion

When verifying the load-bearing capacity of glass structures subjected to impact loading, time efficient and user-friendly design tools can be of great utility, allowing for an interactive design process where alternative designs may be tested. In the present study, an approach using DS have been employed for developing reduced order models that are computationally efficient while providing an accurate prediction of the pre-failure elastic response. For the studied load cases, the coupled impactor-glass system can be well-represented by only two global modes. However, it should be noted that the influence of higher order modes might not be negligible for larger glass panels or panels with other boundary conditions. Moreover, it was shown that up to four component modes may be required to resolve the displacement of the glass panel in the global modes.

A reduction basis for the glass panel was constructed using correction modes, as further discussed in Section 2.1. An alternative could be to construct a reduction basis by means of the traditional C-B or Rubin approaches, that uses the fixed- and free-interface normal modes, respectively. However, not much would be gained if these methods were applied to linear systems, i.e. where linear subsystems are used for modeling the glass panel as well as the impactor. The assembled system includes m + 1 DOFs, i.e. the glass panel has a total of m DOFs and an additional DOF is added representing the displacement of the lumped impactor mass. Clearly, the computational cost for generating a set of component normal modes or global eigenmodes is in practice identical. On the contrary, an approach using correction modes replaces the eigenvalue problem by a number of matrix-vector multiplications. Furthermore, the set of correction modes, by definition, excludes redundant modes, which cannot be excited by

loading on the substructure boundary. Accordingly, there are no anti-symmetric mode shapes in the global modal basis, as shown in Figure 18.

As discussed in Section 2.4, linear systems can be solved by means of modal dynamics, which in turn enables a closed-form solution for initial value problems. However, a time discretization is required for identifying the peak glass strain during impact. Moreover, the generalized coordinates must be transformed to physical displacements in each time increment, which in turn can be used for computing the glass strain. Consequently, the post-processing of the dynamic response can become computationally expensive. An approach using modal summation techniques can be employed to overcome this problem. For example, a conservative evaluation can be made by means of an absolute summation of the modal responses. Since only one set of data needs to be evaluated in the physical domain the computational effort in the post-processing stage is reduced significantly. However, it should be noted that the modal phase information is lost in a modal summation, why an absolute summation may be too conservative in some applications.

In general, the developed models show good agreement with the experimental results. However, there are some discrepancies, which are especially pronounced for glass panels with a nominal thickness of 12 mm (see Figure 19). The deviation can be due to errors/imperfections in the experimental set-up and/or inadequate modeling abstractions, such as the assumption of a constant contact area, neglection of geometric nonlinearity (i.e. membrane action), and an assumed viscous damping model. Notice, however, that the glass strain curves provided by the reduced models and the numerical reference model are very similar, suggesting that the deviations are due to simplifications made in both models. Recall that both the reduced models and the numerical reference model uses a viscous damping model (in contrast to e.g. a frictional modal) and, furthermore, ignores the dynamic air pressure in the impactor tires. One can thereby assume that these simplifications, or other unknown errors, are the reason for the deviations.

The damping matrix of the glass substructure was constructed by means of Rayleigh-damping, using both mass- and stiffness-proportional damping. This damping model is convenient since it can be utilized in the physical as well as the modal domain. Notice, however, that a damping model being proportional to the structure mass is clearly unphysical (see e.g. [25]). A more refined damping model may be developed. Moreover, by means of further experimental studies, the frequency dependency of the glass panel as well as the impactor damping can be investigated.

For the glass panel with thickness 8 mm, the shape of the strain curve given by the numerical reference model deviates from the curves obtained with the other models. The pulse is shorter whereas the peak strain is fairly close to the peak strain of the other curves. Since the deviation is pronounced for the 8 mm glass panel, having a bending stiffness considerably lower than the thicker panels, it is reasonable to claim that this discrepancy is due to membrane action being manifested by a stiffer response (i.e. shorter pulse). Recall that geometric nonlinearity is considered in the numerical reference model, while these effects are ignored in the reduced order models. However, one would then expect the measured strains to be closer to the strain provided by the reference model, which is not what the experimental data suggests. Nonetheless, the influence of membrane action can still be one of the

reasons for the discrepancy. The stiffness of the rubber strips along the supports, modeled by means of elastic spring beds, affects the influence of membrane action. The stiffness of the rubber strips (and the in-plane stiffness, in particular) can be regarded as a particularly uncertain parameter, which is influenced by the prestressing force due to bolting of the glass panels. Hence, the influence of membrane action might not be accurately captured by the reference model, even though geometric nonlinearity is considered. Furthermore, it is plausible that the stiffness of the rubber strips are in fact nonlinear, e.g. due to friction between the rubber and the glass/steel surface.

7. Conclusions

The paper presents strategies for reduced order modeling of glass panels subjected to soft-body impact. The aim was to develop accurate reduced order models for computation of the pre-failure elastic response, suitable for implementation in user-friendly interactive design tools. Concepts for reduced modeling of the glass panel, the impactor and the contact interaction between the glass panel and the impact body were investigated. In particular, a methodology is proposed for calibrating a nonlinear SDOF model representing the impactor. Furthermore, a model validation was performed based on experimental tests and a detailed numerical reference model. Moreover, a fixed-interface DS method that uses correction modes was successfully employed for developing computationally efficient models of the coupled impactor–glass system. The following conclusions can be drawn:

- The measured glass strains and the strains provided by the numerical models are fairly close. The discrepancy is similar for the reduced models and the reference model, suggesting that the deviations are due to inadequate modeling abstractions applied in both models.
- The impactor acceleration measured during impact with a very stiff steel column (which can be considered rigid) is close the the acceleration provided by the numerical reference model.
- A nonlinear SDOF model representing the impactor was successfully calibrated to the reference model. In particular, the acceleration computed for impact with a rigid surface with the nonlinear SDOF model showed very good agreement with the acceleration provided by the numerical reference model.
- The evaluation of the reduced order models suggests that a simplified modeling approach assuming a constant contact area is fairly accurate.
- Reduction bases including correction modes turn out to be particularly suitable for implementation in design tools, such as *ClearSight*, where a manual selection of component modes should be avoided. The set of correction modes automatically excludes redundant modes that cannot be excited by loading on the substructure boundary.
- If the impactor is approximated by a linear modal, a closed-form solution can be obtained by means of the modal strain energy method, which enables the use of modal expansion techniques for lightly damped systems with non-proportional damping. For the studied load cases, the coupled impactor-glass system can be well-represented by only two global modes.

- A very computationally efficient approximate evaluation of the glass strain can be obtained if a closed-form modal solution is combined with a modal summation technique, e.g. an absolute summation of the peak modal responses. Using this approach, a time discretization in the physical domain is avoided.

Acknowledgments

Financial support from the RecoNcile project, a part of the EU program Interreg IVA, and the Swedish glass associations; Glasbranschföreningen, Svensk Planglasförening and Balkongföreningen i Norden is gratefully acknowledged. ÅForsk Foundation is acknowledged for financing the part with the experimental campaign, grant ref. no. 18-510.

References

[1] SS-EN-12600. Glass in building-pendulum test-impact test method and classification for flat glass. Swedish Standards Institute, 2003.

[2] M. Feldman, R. Kaspar, B. Abeln, A. Gessler, K. Langosch, J. Beyer, et al.,*Guidance for European structural design of glass components*, Publications Office of the European Union, 2014.

[3] K. Persson, B. Doepker, Glass panes subjected to dynamic impact loads, *Proceedings of the XXIV A.T.I.V. conference*, Parma, Italy, 2009.

[4] M. Timmel, S. Kolling, P. Osterrieder, P. Du Bois, A finite element model for impact simulation with laminated glass. *Int J Impact Eng*, **34(8)**, 1465–78, 2007.

[5] M. Kozłowski, Experimental and numerical assessment of structural behaviour of glass balustrade subjected to soft body impact, *Composite Structures*, **229**, 111380, 2019.

[6] J. Pelfrene, S. V. Dam, J. Kuntsche, W. V. Paepegem, Numerical simulation of the EN 12600 pendulum test for structural glass, *Challenging Glass 5*, Ghent, Ghent University, 2016.

[7] ClearSight, Computer Software, Department of Construction Science, Lund University.

[8] M. Fröling, K. Persson, P.-E. Austrell, A reduced model for the design of glass structures subjected to dynamic impulse load, *Engineering Structures*, **80**, 53–60, 2014.

[9] L. Viviani, A. Consolaro, M. Maffeis, G. Royer-Carfagni, Engineered modelling of the soft-body impact test on glazed surfaces, *Engineering Structures*, **226**, 111315, 2021.

[10] J. Schneider, S. Schula, Simulating soft body impact on glass structures. *Proceedings of the Institution of Civil Engineers: Structures and Buildings*, **169(6)**, 416–31, 2016.

[11] J. Alonso, J. Parra, A. Pacios, M. Huerta, Similarity index: A procedure for comparing impact time histories validated with soft impact test, *Eng Struct*, 198:109513, 2019.

[12] J. Parra, J. Alonso, A. Pacios, M. Huerta, Effective energy applied to a glass plate during an impact test, *Int J Impact Eng*, 130:11–8, 2019.

[13] T. Janda, J. Schmidt, P. Hála, P. Konrád, A. Zemanová, R. Sovják, J. Zeman, M. Šejnoha, Reduced order models of elastic glass plate under low velocity impact, *Computers and Structures*, **244**, 106430, 2020.

[14] V.L. Popov, M. Heß, E. Willert, *Handbook of contact mechanics*, Springer, Berlin Heidelberg, 2019.

[15] R. Craig, A. Hale, Block-Krylov Component Synthesis Method for Structural Model Reduction. *Journal of Guidance, Control and dynamics, American Institute of Aeronautics and Astronautics*, **11(6)**, 562–570, 1988.

[16] D.J. Rixen, High Order Static Correction Modes for Component Mode Synthesis. *Proceedings of the fifth World Congress on Computational Mechanics*, Vienna, Austria, 7–12 July, 2002.

[17] Simulia, ABAQUS v. 6.14, Computer Software and Online Documentation, Dassault Systems, Providence, RI, USA.

[18] D. de Klerk, D.J. Rixen, S.N. Voormeeren, General Framework for Dynamic Substructuring: History, Review, and Classification of Techniques, *AIAA Journal*, **46 (5)**, 1169–1181, 2008.

[19] O. Flodén, K. Persson, G. Sandberg, Reduction methods for the dynamic analysis of substructure models of lightweight building structures, *Computers and Structures*, **138**, 49–61, 2014.

[20] R.R. Jr. Craig, A.J. Kurdila, *Fundamentals of Structural Dynamics, 2nd Edition*, John Wiley & Sons, New Jersey, 2006.

[21] R.R. Craig, M.C.C. Bampton, Coupling of Substructures for Dynamic Analysis, *AIAA Journal*, **6 (7)**, 1313–1319, 1968.

[22] R.H. MacNeal, A Hybrid Method of Component Mode Synthesis, *Computers and Structures*, **1 (4)**, 581–601, 1971.

[23] S. Rubin, Improved Component-Mode Representation for Structural Dynamic Analysis, *AIAA Journal*, **13 (8)**, 995–1006, 1975.

[24] L. Andersson, P. Persson, K. Persson, Model Reduction for Structures Subjected to Blast Loading by use of Dynamic Substructuring, *Proceedings of EURODYN 2020, XI International Conference on Structural dynamics*, Streamed from Athens, Greece, 23–26 November 2020.

[25] A. K. Chopra, *Dynamics of Structures. Theory and Applications to Earthquake Engineering. 5th Edition.* Prentice Hall, NJ, 2016.

[26] L.N. Trefethen, D. Bau III, *Numerical Linear Algebra*, SIAM, Philadelphia, 1997.

[27] C. Hoen, An Engineering Interpretation of the Complex Eigensolution of Linear Dynamic Systems, *IMAC XXIII*, Orlando, USA, 2005.

[28] M.-H. Tsai, K.-C. Chang, A study of the modal strain energy method for viscoelastically damped structures, *Journal of the Chinese Institute of Engineers*, **24:3**, 311–320, 2001.

[29] Q. Jiang, Z. Zhou, W. Huang, Investigation on the Modal Strain Energy for Dynamic Analysis of Steel-Concrete Vertically Mixed Structures, *Journal of Asian Architecture and Building Engineering*, **14:3**, 671–678, 2015.

[30] E O Bolarinwa , O A Olatunbosun, Finite element simulation of the tire burst test. *Proceedings of the institution of mechanical engineers*, Birmingham, England, 2004.

[31] E. Björklund, A. Christoffersson, *Computational Modeling and Experimental Verification of Soft-Body Impact on Glass Structures*, Master's thesis, Report TVSM-5246 Lund University, Lund, 2020.

[32] R. P. R. Cardoso, J. W. Yoon, M. Mahardika, S. Choudhry, R. J. Alves de Sousa, R. A. Fontes Valente, Enhanced assumed strain (EAS) and assumed natural strain (ANS) methods for one-point quadrature solid-shell elements, *International Journal for Numerical Methods in Engineering*, **75(2)**, 156–187, 2008.

[33] M. Fröling, K. Persson, Computational methods for laminated glass. *Journal of Engineering Mechanics*, **139(7)**, 780–90, 2013.

[34] M. Kozłowski, K. Persson, D. Honfi, N. W. Portal, Structural Behaviour of Glass Panels Under Soft-body Impact, *Challenging Glass 7*, Ghent, Ghent University, 2020.

[35] M. Kozłowski, *Structural Safty of Glass Components*, Report TVSM-7169 Lund University, Sweden, 2020.

[36] C. Bedon, M. Fasan, C. Amadio, Vibration Analysis and Dynamic Characterization of Structural Glass Elements with Different Restraints Based on Operational Modal Analysis, *Buildings*, 9, 13, 2019.

[37] A. Ramos, F. Pelayo, M.J. Lamela, A. Fernández Canteli, Evaluation of damping properties of structural glass panes under impact loading, *Proceedings of COST Action TU0905, Mid-term Conference on Structural Glass*, Poreč, Croatia, 2013.